UNIVERSITÀ DEGLI STUDI DI PADOVA

Dipartimento di Fisica e Astronomia "Galileo Galilei"

Master Degree in Physics

Final Dissertation

Dark Matter Phenomenology with Vector Portals

Thesis supervisor

Prof. Francesco D'eramo

Thesis co-supervisor

Dr. Natascia Vignaroli

Candidate

Mattia Cavallo

Academic Year 2022/2023

Contents

Introduction

The study of the universe has begun ever since men looked up to the sky to recognize the different stars that slowly moved around them, trying to understand what those tiny light spots were. Many years and many men passed since those days, while the basis of what we now call astronomy, astrophysics and cosmology were being built over time. Today we can say that we have a fairly good understanding of what lies outside our planet: we know what is a star, how it was born and how it dies; we know how large is the universe, and most of the history behind it; and we know how the universe is filled up, although not as good as we would like to think.

The last claim, in particular, has been one of the main topics of discussion for the last 50 years in cosmology, astrophysics and even particle physics: almost a century ago, a Swiss astronomer called Zwicky noted a discrepancy between the mass inferred by gravitational interactions and the visible mass in a cluster of galaxies; he attributed this discrepancy to some undefined "Dark Matter", which interacts gravitationally with other masses but doesn't interact with light. Only 40 years later his idea was recovered because of the observations of galaxy rotation curves by Vera Rubin; from then on, papers referring to the "Dark Matter problem" began to raise exponentially.

The idea that Dark Matter is made up of a new type of particle, with unknown but non-vanishing interactions with ordinary matter, appeared shortly after. More recent developments in observational cosmology have almost ruled out any other possible explanation for the origin of Dark Matter, therefore its particle nature is widely accepted in the scientific community. However, the features of this Dark Matter particle are still largely obscure. For this reason, a rich variety of experimental strategies has been employed to look for this elusive particle: direct searches try to detect the interaction between dark and ordinary matter, indirect searches look for Dark Matter annihilation products coming on the Earth, colliders look for Dark Matter production in high-energy reactions. No signal has been observed yet, but these experiments are useful to put bounds on the theoretical models we can produce.

Among all the models in the literature, one of the most popular ones is given

by WIMPs (Weakly Interacting Massive Particles): their popularity is mainly due to the so-called "WIMP miracle", a surprising accordance between the typical cross section for weak interactions and the resulting relic density via freeze-out mechanism for a weakly interacting particle (which would match the observed one). Moreover, the mass range of WIMPs coincides with the mass scale required for new physics to appear to solve the gauge hierarchy problem, thus making them alluring also from a theoretical point of view.

This thesis is structured as follows: in Chapter 1, we recall all the evidence gathered until now for the existence of Dark Matter; we also give a quick overview on the different particle candidates existing in the literature. In Chapter 2 we provide a detailed description of the WIMP paradigm, illustrating the close relation between the decoupling from the primordial bath and the final relic density; moreover, we describe the different experimental strategies employed for Dark Matter searches and the main bounds given by the most recent experiments. In Chapter 3 we focus on a specific type of WIMP framework: we suppose that WIMPs interact with the Standard Model particles via a neutral massive gauge boson, associated with a new $U(1)$ gauge symmetry; we discuss the main theoretical features of this model, with emphasis on anomaly cancellation. In Chapter 4 there is the original contribution of this work: we analyze the phenomenology of one particular model, comparing it with the most recent experimental limits available. Finally, in Chapter 5 we summarize our conclusions. The two ending appendices are a useful syllabus for Standard Model notation and a quick re-derivation of the Boltzmann equation.

Chapter 1

Evidence for Dark Matter

To begin our discussion, first, let's take a look at Fig. 1.1: it shows the cosmic pie, the current energy content of the universe. Visible matter constitutes just 5 percent of the total energy budget. Although we claim to know well this part, there are still many unanswered questions in this small sector. Anyway, the feature that catches the eye when looking at the cosmic pie is that striking 95 percent dark component: the vast majority of our universe is of completely unknown origin and composition. That's the reason why so much effort and paperwork have been poured into the study of the dark side of the universe in the last 50 years.

In this work, we will focus on the Dark Matter (DM) slice of the pie [1, 2, 3, 4]: DM represents an intensive and prolific research field, both for its astrophysical (and cosmological) relevance and its theoretical appeal. In fact, many problems in particle physics can find a solution if we introduce new particle species, and DM could just be one of them, that we have not recognized yet.

However, before diving into the landscape of particle theories, we present a summary of the evidence collected until now for the existence of DM. Its presence has been inferred mainly through its gravitational interaction with visible matter: stars and galaxies were not moving right, and it turns out that the missing piece is very large.

One caveat here is necessary: although the zoology of particle models trying to explain DM is very rich, its existence is still debated: various theories in the literature try to explain the experimental anomalies observed since 1933 without recurring to DM. Among them, the most successful one is the "MOdified Newtonian Dynamics" (MOND, [5, 6]), introduced in 1983, whose basic idea is a modification of Newton's second law: $F = ma$ turns into $F = \mu(a)ma$, where $\mu(a)$ deviates from unity only for very small accelerations. Anyway, it has been proven that MOND is not enough at scales larger than galactic scales, and a new type of matter is required in any case [7].

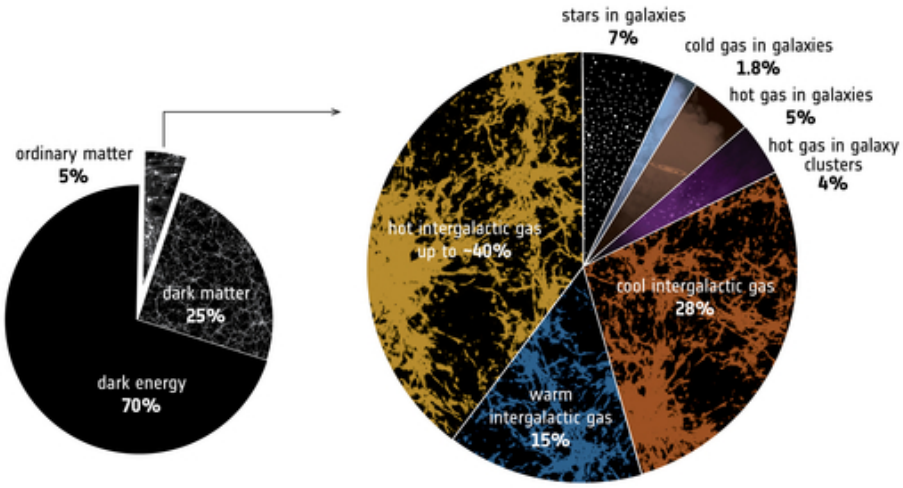

Figure 1.1: On the left, the cosmic pie for our universe. On the right, the cosmic pie for ordinary matter. It's interesting to note that stars make up only a small percentage of the whole baryonic matter.

1.1 Galaxy scale

The first robust clue of DM existence can be found at the galactic scale, in particular from **galactic rotation curves**, which represent the orbital speed of visible stars as a function of their distance from the galactic center. In spiral galaxies, most of the visible matter is gathered around the bulge and the disk. The stars present in these structures are collisionless, so they move only according to the gravity they feel: this feature makes them excellent DM tracers. In fact, studying the galactic rotation curves of nearby galaxies, some anomalies were spotted since the '70s [8].

In fact, from a simple Newtonian analysis, a star at a distance r from the center of the galaxy (assuming spherical symmetry) moves with a velocity:

$$v(r) = \sqrt{\frac{GM(r)}{r}} \tag{1.1}$$

Where $M(r)$ is the total mass contained in the sphere of radius r. Most of the visible matter of a galaxy is concentrated around the bulge: then, at large radii, we can consider $M(r) \simeq const$, so we expect a behavior like $v(r) \propto r^{-1/2}$. Instead, what we actually see is reported in Fig. 1.2: a $v(r) \simeq const$ behavior at large radii,

that seems to be common to all spiral galaxies [9]. The conclusion we draw is that, apart from the visible matter, galaxies have an invisible component that extends beyond the limit of the disk, in the form of a dark halo. From the galactic rotation curves, we can also infer its mass density distribution:

$$M(r) \propto r \quad \rightarrow \quad \rho_{DM}(r) \sim \frac{1}{r^2} \tag{1.2}$$

The characteristics of the DM halos are still very unclear. For reference, an order of magnitude estimate of the Milky Way DM halo mass and size scale can be given by [11]:

$$\begin{cases} M_{halo} \sim 10^{12}\, M_{\odot} \\ R_{halo} \sim 100\,\text{kpc} \end{cases} \tag{1.3}$$

Both the mass and the radius of the DM halo are one order of magnitude larger than their baryonic counterparts. However, a precise analysis of the DM halo density profiles is not so easy, since in most galaxies it is difficult to disentangle the dark and the visible contribution to the rotation curve. From this point of view, a convenient analysis can be performed on Low Surface Brightness galaxies, which are DM-dominated objects, and, for this reason, they are perfectly suited to study the different properties of DM density profile [12].

Further help is provided by numerical simulations [13]: we simulate the structure formation from the original density fluctuation (which we talk about in Section 1.3), including DM as a gas of collisionless particles, interacting only via the gravitational force. The output suggests the existence of a universal DM density profile for any mass scale [14], however there is still debate its shape; the following distributions are the most used in the literature:

Navarro-Frank-White [15]:
$$\rho_{NFW}(r) = \frac{\rho_0}{(r/r_s)(1+r/r_s)^2} \tag{1.4}$$

Einasto [16]:
$$\rho_{Ein}(r) = \rho_0 \exp\left[-\frac{2}{\gamma}\left(\left(\frac{r}{r_s}\right)^{\gamma} - 1\right)\right] \tag{1.5}$$

Burkert [17]:
$$\rho_{Bur}(r) = \frac{\rho_0}{(1+r/r_s)(1+(r/r_s)^2} \tag{1.6}$$

The parameters ρ_0, r_s and γ depend on the galaxy under consideration (in Table 1.1 the parameters for the Milky Way are reported).

One of the major problem for these simulations is that they are not in total agreement with observations. In particular, at the galactic scale, the problem is related to the galactic center: while most of the simulations depict a (more or less) cuspy density profile towards the innermost galactic regions, observations suggest a flat inner core. This tension is mainly due to the low length resolution of the

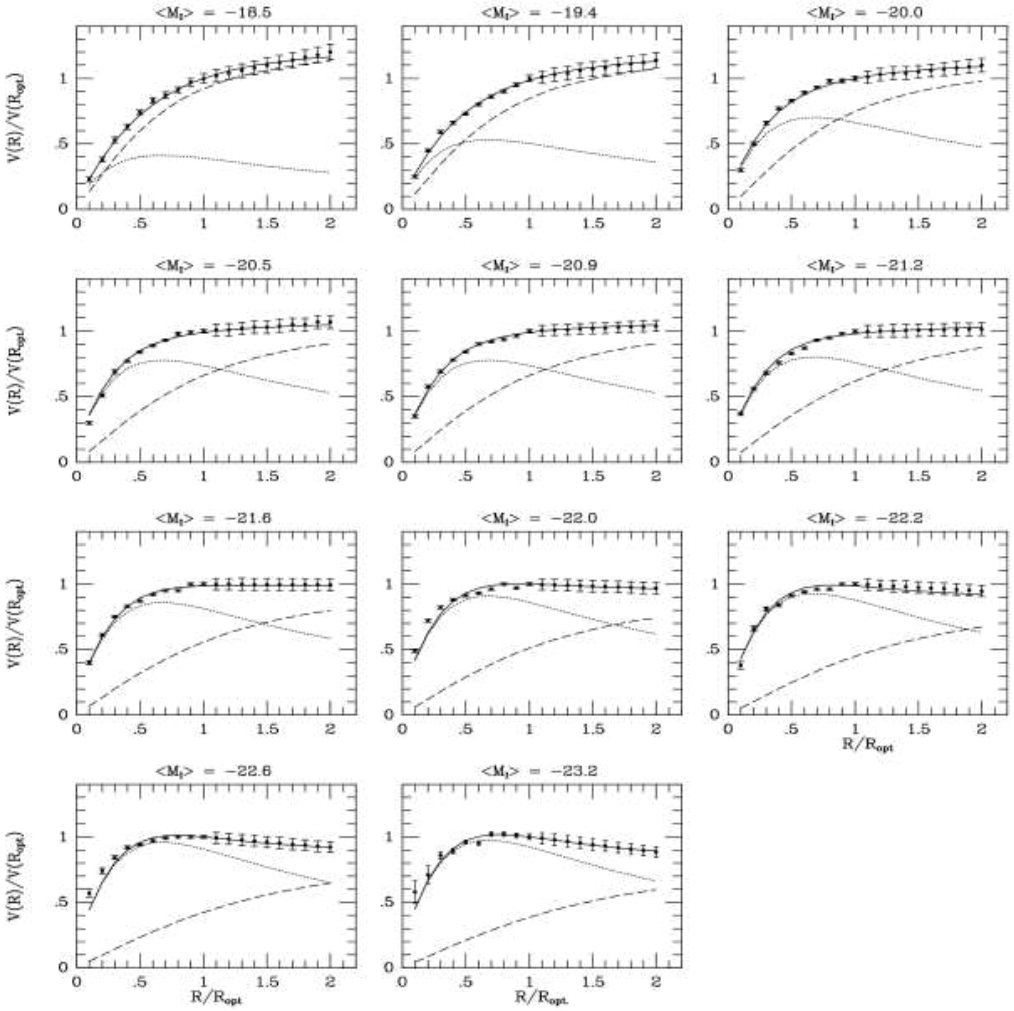

Figure 1.2: Rotation curves of spiral galaxies for different luminosities. The dotted line represents the contribution from the baryon disk, while the dashed line is the contribution from the halo. From [10].

	ρ_0 (GeV cm^{-3})	r_s (kpc)	γ
NFW	0.32	19.6	
Einasto	0.11	16.07	0.22
Burkert	1.57	9.26	

Table 1.1: Values of different distribution parameters for the Milky Way. The references are [18] for NFW, [19] for Einasto and [20] for Burkert.

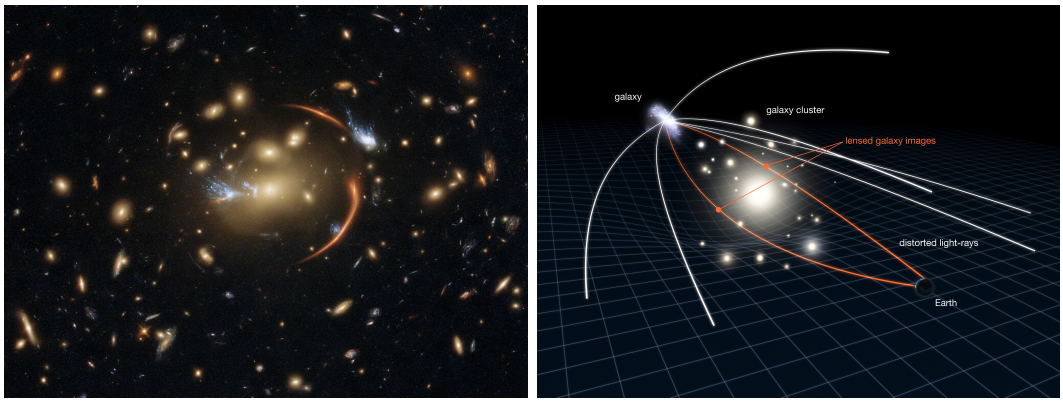

Figure 1.3: On the left: an amazing example of strong gravitational lensing from the galaxy cluster MACSJ0138.0-2155 (Credit:ESA/Hubble & NASA, A. Newman, M. Akhshik, K. Whitaker) On the right: schematic explanation of gravitational lensing (Credit:NASA, ESA & L. Calçada)

simulations and to the difficulties associated with the galactic center, a region that is not fully resolved even accounting only for baryons. Moreover, non-trivial interactions between the baryonic disk and the DM halo may be crucial [21, 22].

Besides its distribution, one of the most important parameters for experiments is the local value of the DM density: it is fundamental to know how much DM we are surrounded by when we try to observe its scattering (direct detection, Section 2.3.1) and, in general, it is useful to understand better the local shape of the Milky Way's halo. The local DM density, despite the large uncertainties it suffers, is believed to be around [23]:

$$\rho_{DM}^{(local)} \simeq (0.3 \pm 0.1)\,\text{GeV cm}^{-3} \tag{1.7}$$

1.2 Cluster scale

We now turn our attention to galaxy clusters. These objects are huge structures that contain a very large number of galaxies, bound together by gravity. Historically, they gave the first hint of DM existence: indeed, when Zwicky in 1933 [24] was observing the Coma cluster, he noted that galaxies were moving too fast with respect to the total mass inferred from luminous matter (the velocity dispersion and the mass of the cluster are related by the virial theorem); the discrepancy factor was about 400, so clearly something was missing from the picture.

Nowadays we have multiple ways to measure the total mass of a cluster in order to find its dark matter component. For example, we can study the gases contained in the intergalactic medium: these gases, which represent the largest fraction of the visible mass of a cluster, can be accelerated by the strong gravitational fields, emitting X-rays via thermal bremsstrahlung. By measuring this emission, it's possible to reconstruct the gas density profile, which in turn gives us information about the total mass of the cluster. The equation for hydrostatic equilibrium for the gas reads:

$$\frac{dp(r)}{dr} = -\frac{G_N M(r)\rho(r)}{r^2}, \tag{1.8}$$

where p, ρ are respectively the pressure and density of the gas at radius r, G_N is Newton's gravitational constant and $M(r)$ is the mass of the cluster enclosed within the radius r. Assuming the gas to be ideal, we can relate its pressure to its temperature and density; we obtain:

$$M(r) = -\frac{rT}{\mu m_p G_N}\left[\frac{d\log\rho}{d\log r} + \frac{d\log T}{d\log r}\right], \tag{1.9}$$

where $\mu \simeq 0.6$ is the average molecular weight (the gas is almost entirely made of protons) and m_p is the proton mass. Using this relation, we then find that the temperature should obey:

$$T \approx (1.3 - 1.8)\,\mathrm{keV}\left(\frac{M(r)}{10^{14}M_\odot}\right)\left(\frac{1Mpc}{r}\right) \tag{1.10}$$

If we identify $M(r) = M_{baryons}$, the prediction is in disagreement with the observed temperature $T \approx 10$ keV; in fact, galaxy clusters are dominated by their DM component, which usually makes up 90% of their total mass.

However, the most powerful tool we have at our disposal to infer the presence of non visible mass is provided by General Relativity: the **gravitational lensing**. This effect refers to the distortion of light rays that pass near a massive object (that we call gravitational lens); the distortion can either be a simple deformation of the image of the source, in which case we talk about *weak gravitational lensing*

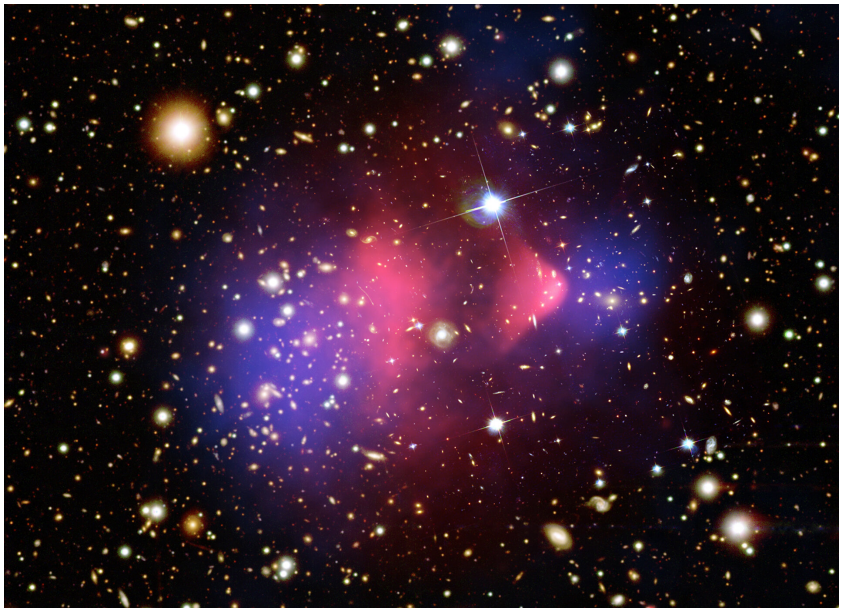

Figure 1.4: The Bullet Cluster. While the gas in the red region experienced a drag force due to the collision, acquiring the characteristic bullet shape, the 2 dark matter halos have crossed each other apparently without interacting at all. Credit:NASA/CXC/CfA/M. Markevitch et al.; NASA/STScI; Magellan/U.Arizona/D. Clowe et al.; NASA/STScI; ESO WFI.

[25], or it can be so strong to produce multiple images spread on the so called Einstein ring (Fig. 1.3); in this case, we talk about *strong gravitational lensing* (see, for example, [26]).

Through the study of the distorted image of the source, it's possible to infer the total mass of the lens: in this way, we can weigh not only large and massive objects, on which the strong gravitational effect takes place (mainly galaxy clusters), but also smaller objects like galaxies.

One of the best uses of this technique, in synergy with the X-ray emission analysis, is given by the study of the Bullet Cluster [27]: this cluster is made up of two different clusters that have crossed each other. In Fig. 1.4 it's possible to appreciate the two different components: the bullet-shaped red region corresponds to the hot interacting gas, that has been heated up by the collision; the blue regions instead correspond to the gravitational wells inferred by gravitational lensing. It's clear that the largest matter component is separated from the baryonic gas, and this provides one of the greatest evidence for DM existence. This feature can also be taken as a disproof for theories like MOND, since the behavior of the cluster can hardly be explained with unknown gravitational effects, without introducing at least some DM component.

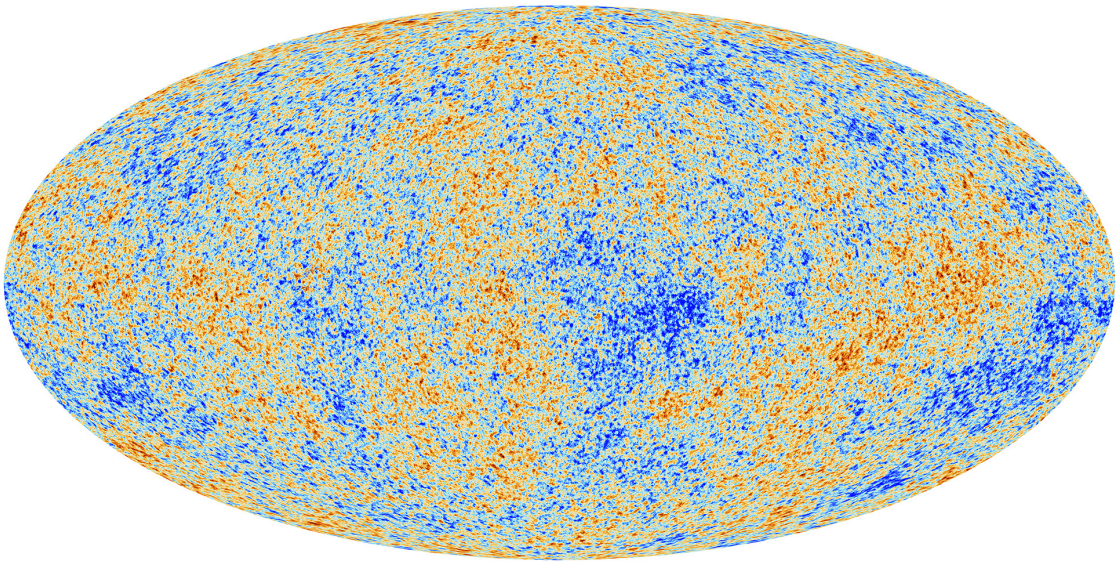

Figure 1.5: The CMB temperature fluctuations measured by Planck.

1.3 Cosmological scale

Last but not least, we discuss now the evidence we gathered at the cosmological scale. This evidence is the result of the analysis of the Cosmic Microwave Background (CMB, Fig. 1.5), that provides not only one of the most important proofs for the need for non-baryonic matter, but it also gives the most precise determination of the total amount of DM in the universe.

Before discussing in detail how the analysis of CMB anisotropies can give us precious information about cosmological parameters, it's instructive to think about what happens if we remove DM from the cosmos equation: Would the universe evolve in the same way as we know it? Luckily, the CMB gives us a very clear picture of the universe as it was shortly after the Big Bang, so we can use it as a starting point. The main difference we see when we look at the CMB with respect to our current universe is its homogeneity: the CMB is the same everywhere, except for the very small perturbations, on the scale of 10^{-5}. Our universe, instead, is highly inhomogeneous (for example, the density difference between our galaxy and the surrounding intergalactic space is on the order of 10^5); then, the immediate conclusion we draw is that the initial tiny perturbations grew up under the influence of gravity.

We can try to give an estimate of this behavior: in the early universe we can consider $\rho = \rho_{crit}$, and the time evolution is governed by the Friedmann equation:

$$H^2 - \frac{8}{3}\pi G\rho = 0 \tag{1.11}$$

A slightly denser region $\rho' > \rho$ will evolve instead as:

$$H^2 - \frac{8}{3}\pi G\rho' = -\frac{k}{a^2} \tag{1.12}$$

Subtracting the two equations, we get:

$$-\frac{8}{3}\pi G(\rho' - \rho) = -\frac{k}{a^2} \tag{1.13}$$

Thus, the perturbation δ evolve like:

$$\delta = \frac{\rho' - \rho}{\rho} = -\frac{3k}{8\pi G\rho a^2} \tag{1.14}$$

At the time of CMB emission, baryons and photons were tightly bound together, so the photon perturbations we see on the CMB are the same for the baryon fluid. At this stage, the universe is in a matter dominated regime for which we know that $\rho \propto a^{-3}$: therefore, the evolution for the perturbations is $\delta \propto a$. If we fast forward to the present, we find:

$$\delta_{today} \simeq \delta_{CMB}\frac{a_0}{a_{CMB}} \simeq 10^{-5} \times 10^3 = 10^{-2} \tag{1.15}$$

The result is off of 7 orders of magnitude! This is a crucial evidence for the need of non-baryonic matter: before recombination, in fact, baryon perturbations cannot grow because of the interaction with photons. DM, instead, is only gravity-driven, so it can pile up in order to form gravitational wells. After CMB, baryons fall inside these already existing potential wells, allowing much faster growth of the density perturbation.

But the CMB is much more than a simple proof of the existence of DM: it holds a lot of information for the study of many fundamental cosmological parameters, and for this reason, it is one of the most important constraints for any cosmological model. This information is stored inside the CMB anisotropies: we just need to learn how to read them.

The temperature anisotropies are usually expanded in spherical harmonics:

$$\delta T(\theta, \phi) = \sum_{l=2}^{+\infty} \sum_{m=-l}^{l} a_{lm} Y_{lm}(\theta, \phi) \tag{1.16}$$

Larger values of l correspond to smaller angular scales, so the largest value of l in the sum is set by the resolution of the experiment ($l_{max} \simeq \pi/\theta_{res}$). The first two multipole terms are not present in the sum: the monopole $l = 0$ simply set the scale of the CMB temperature, while the dipole contribution $l = 1$ is due to the

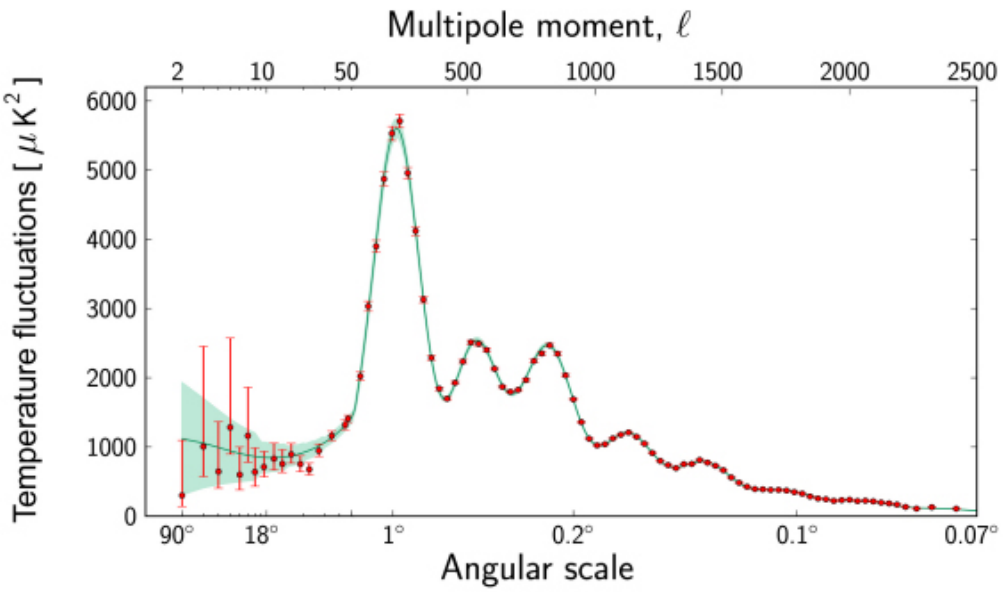

Figure 1.6: The CMB power spectrum. The red dots correspond to Planck data, with their own error bars. At lower multipoles, there are less independent measurements to average, so the uncertainty increases. The green curve is the best fit for the Standard Cosmological Model.

Earth motion with respect to the CMB rest frame. If the fluctuations are assumed to be Gaussian, a very good approximation for the CMB, then all the information is encoded in the **power spectrum**:

$$C_l = \langle |a_{lm}|^2 \rangle = \frac{1}{2l+1} \sum_{m=-l}^{l} |a_{lm}|^2 \tag{1.17}$$

Here, we can give a qualitative explanation on how the power spectrum in Fig. 1.6 is formed, and how we can extract information from it.

At the end of the inflationary period, the whole universe was highly homogeneous, except for the tiny fluctuations in density and temperature produced by the inflation itself; these fluctuations are the original seeds for the large structures we see nowadays (galaxies, clusters, superclusters). We can study how they evolve and what effect they had on the different particle species that populated the universe at that time.

We focus on the particle species that will be relevant for the CMB formation: protons and electrons, photons and DM. DM is the easiest one: as already said, it interacts only through gravity, so it will simply flow towards the higher density perturbations. Protons, electrons and photons have to be treated together, since

they form a very tightly bound plasma, because of Coulomb and Thompson processes. At first, protons and electrons follow the same behavior of DM, gathering around the same denser spots; in these overdense regions, however, the photon gas gets heated up, causing the radiation pressure to rise. Ordinary matter gets pushed apart towards the underdense regions, where gravity takes the upper hand again, and the same process repeats. The net result is an oscillatory motion, whose speed is set by the speed of sound of the plasma (for a photon gas, $c_s = c/\sqrt{3}$). This oscillatory motion goes on until the photons are set free, namely when CMB occurs: the final result of this process is caught up by the power spectrum.

The peaks correspond to the perturbation scales that were at the maximum compression at the time of CMB. These peaks are influenced by the amount of both baryonic matter and DM: the baryonic matter lowers the speed of the sound of the plasma, influencing the position of the peaks. On the other hand, DM creates deeper and deeper potential wells from which escaping is increasingly difficult: this affects the relative strength between the different peaks. Putting all of this together, the Planck Collaboration found [28]:

$$\begin{aligned} \Omega_m &= 0.3111 \pm 0.0056 \\ \Omega_b h^2 &= 0.02242 \pm 0.00014 \\ \Omega_{DM} h^2 &= 0.11933 \pm 0.00091 \end{aligned} \tag{1.18}$$

The results are clear: DM is 5 times more abundant than baryonic matter, and the evidence at all scales agrees on this.

1.4 Known features

After all the collected evidence, we can now summarize all the properties that any particle physics model of DM must satisfy. All the following properties are totally model-independent.

Stability We know that DM existed at the time of CMB, and it exists still today, holding galaxies and clusters together. This suggests that it is composed of stable particles, or, at most, its lifetime is greater than the age of the universe:

$$\tau_{DM} \gg t_U \simeq 14\,\mathrm{Gyr} \tag{1.19}$$

This seems a pretty tough constraint to overcome for massive particle models, since more massive particles decay quicker. In this case, one usually introduces a new discrete symmetry, so that only reactions with an even number of DM particles are allowed (in this way, decays are forbidden [29]). For example, the conservation of the R-parity in supersymmetry implies that the lightest supersymmetric particle is stable.

Charge neutrality DM is not observed to interact with light at any frequency [30]: this means that it is very likely neutral, maybe with a small electric or magnetic dipole moment [31]. For example, models of millicharged DM exist in the literature [32], in which DM couples to the photon through an admixture of the usual $U(1)_{em}$ gauge group with a new dark $U'(1)$ gauge symmetry.

Mass The mass of the major component of DM has been constrained only within 80 orders of magnitude. The upper limit comes from the unsuccessful searches for MACHOs (Massive Astrophysical Compact Halo Objects) in the dark halo of our galaxy using gravitational microlensing. This type of gravitational lensing involves much smaller objects with respect to its strong and weak version: if a massive compact object passes near the line of sight of a background source, the source flux gets magnified for a brief period. Among the best candidates for MACHOs, there are primordial black holes [33]; however, these objects are increasingly less likely to be the only DM component [34]. The limit reads:

$$m_{DM} < 10^{48}\,\text{GeV} \tag{1.20}$$

The lower limit, instead, is set by the smallest DM structures we can observe (which are dwarf galaxies of size $R_{halo} \simeq 1\,kpc$): DM must be able to localize in such small structures. For bosons, we impose this condition on the De Broglie wavelength:

$$\lambda_{DM} = \frac{h}{p} = \frac{2\pi}{m_{DM} v_0} < R_{halo} \quad \rightarrow \quad m_{DM}^{(boson)} \gtrsim 10^{-22}\,\text{eV} \tag{1.21}$$

For fermions, instead, we must account for the Pauli exclusion principle; if the ground state is totally filled, the energy density is:

$$\rho_{DM} = m_{DM} n_{DM} = m_{DM} \int \frac{d^3p}{(2\pi)^3} = g \frac{m_{DM}^4 v_F^3}{6\pi^2} \tag{1.22}$$

At this point, supposing a spherical distribution of mass ($M_{halo} = \frac{4\pi}{3}\rho R_{halo}^3$), we impose the Fermi velocity to be smaller than the escape velocity v_{esc}:

$$v_F = \left(\frac{9\pi}{2g}\frac{M_{halo}}{m_{DM} R_{halo}^3}\right)^{1/3} < \left(\frac{2GM_{halo}}{R_{halo}}\right)^{1/2} = v_{esc} \tag{1.23}$$

We find what is known as the Tremaine-Gunn bound:

$$m_{DM}^{(fermion)} \gtrsim (G^3 M_{halo} R_{halo}^3)^{-1/8} \simeq 0.7\,\text{keV} \tag{1.24}$$

Self-interactions The fact that DM forms spherical halos around the galaxy, without collapsing into a disk as baryons do, tells us that DM must be dissipationless (although scenarios that provide the existence of a DM disk exist in the literature [35]). Moreover, DM is also assumed to be collisionless, and the best upper limits for its self-interactions come from the Bullet Cluster [27]. Anyway, the limit is actually quite mild:

$$\frac{\sigma_{self}}{m} \leq 1\,\mathrm{cm}^2\,\mathrm{g}^{-1} \simeq 10^{-24}\,\mathrm{cm}^2\,\mathrm{TeV}^{-1} \tag{1.25}$$

However, simulations performed with collisionless DM predict the formation of several massive subhaloes in the Milky Way that are "too big to fail" to produce stars and thus be visible [36]. Such a problem could be alleviated if we suppose Self-Interacting DM: these models assume a velocity-dependent scattering cross section, that is able to reduce the central densities of galaxies thus leading to simulations compatible with observations [37].

Coldness DM is classified as hot or cold based on how fast it was when it decoupled from the primordial plasma: hot DM decoupled when it was still relativistic, while cold DM decoupled in a non-relativistic regime. This is a very important property, that determines the major features of the large scale structures in the universe: in fact, when DM decouples, it experiences collisionless damping, washing out perturbations on a characteristic cutoff scale. This cutoff scale sets the smallest DM structures we can see nowadays.

From this analysis, we see that DM must be non-relativistic when the universe had a temperature $T \simeq 3.6\,\mathrm{keV}$ [38]. Interestingly enough, this is the reason why neutrinos, the only suitable candidate for DM within the SM, can only constitute a small contribution for the observed abundance of DM: decoupling at a temperature of $T \simeq 1\,\mathrm{MeV}$, with a mass lower than 1 eV, they are considered hot DM; thus, they would lead to a much different evolution of the universe, where big structures form first, while the smaller ones are formed later through fragmentation (contrary to actual observations, that suggest a bottom-up formation of structures, where smaller structures form first and are later pulled together by gravity).

1.5 Overview on particle candidates

The great amount of evidence presented in the previous sections led many physicists to start thinking about what DM could possibly be made of. However, very little clue is given about the microscopic properties of DM: the limits presented in Section 1.4 are very loose, and they do not help to narrow down the landscape

of possible particle models. This can be considered a consequence of the universality of gravity, which doesn't carry any information about the microphysics of a system. Nevertheless, particle physics can give us a helping hand.

Currently, many problems still arise in the Standard Model (SM) of particle physics. To address these problems, many theoretical frameworks require the introduction of new particles; and many times, these particles just happen to be excellent DM candidates.

We use to divide DM candidates based on their production mechanism:

- The *thermal relics* are particles produced via interactions with the thermal bath; this means that, in the early universe, they were in equilibrium with the thermal bath, and then decoupled. The decoupling (or freeze-out) process is very important, because it sets the relic density that we oserve today;
- The *non-thermal relics* include all the other models that never got the chance to be in thermal equilibrium with the thermal bath. The production mechanism for these relics include freeze-in models [39] and decay products of primordial fields during phase transitions.

In the following, we list some of the most studied DM candidates, with particular focus on their link with particle physics.

1.5.1 WIMPs

Weakly Interacting Massive Particles (WIMPs) have been regarded as the best candidates for DM for many years now. From the particle physics point of view, they arise as a solution for the gauge hierarchy problem: the mass of the Higgs boson can be written as $m_h^2 = m_{h,0}^2 + \Delta m_h^2$, where $m_{h,0}^2$ is the tree-level mass and

$$\Delta m_h^2 \sim \frac{\lambda^2}{16\pi^2} \int^{\Lambda} \frac{d^4p}{p^2} \sim \frac{\lambda^2}{16\pi^2}\Lambda^2 \tag{1.26}$$

is the quantum corrections resulting from loop-level diagrams; λ is an $\mathcal{O}(1)$ dimensionless coupling and Λ is the energy scale at which the SM in no longer valid. In the SM $\Lambda \sim M_{Pl}$ ($\approx 10^{19}\,\text{GeV}$), and this causes Δm_h^2 to be 36 orders of magnitude bigger than the mass of the Higgs boson m_h ($\simeq 125\,\text{GeV}$), thus requiring a fine tuning between $m_{h,0}^2$ and Δm_h^2 which seems highly unnatural. This problem may be solved introducing new physics at the TeV scale, namely WIMPs. We will discuss deeply about this candidate in Chapter 2.

1.5.2 Axions

In the contest of QCD, the strong-CP problem is connected to the unnatural cancellation of CP-violating terms in the QCD Lagrangian. The QCD Lagrangian

can be written as:

$$\mathcal{L}_{QCD} = -\frac{1}{4}G^{A,\mu\nu}G^{A}_{\mu\nu} + \overline{\psi}i\not{D}\psi + \theta\frac{g_s^2}{32\pi^2}G^{A,\mu\nu}\tilde{G}^{A}_{\mu\nu} \tag{1.27}$$

The last term, which involve the dual of the gluon field strength $\tilde{G}_{\mu\nu} = \frac{1}{2}\epsilon^{\mu\nu\rho\sigma}G_{\rho\sigma}$, is a non-perturbative term (it can be written as a divergence of a current) which is connected to the chiral anomaly of QCD, and it is the source of CP violation in the color sector of the SM. Such term would produce observables like an electric dipole moment of the neutron, that however have still not been observed (the current limit requires $|\theta| \leq 10^{-10}$ [40]). The vanishing of the parameter θ is a fine-tuning problem that probably hides some new physics behind it.

The Peccei-Quinn solution of this problem promotes θ to a dynamical field whose vacuum energy naturally leads to $\theta = 0$. This is accomplished by the introduction of a $U(1)_{PQ}$ global symmetry spontaneously broken at some large energy scale f_a;moreover, this new symmetry suffers from a chiral anomaly which generates an effective term in the Lagrangian:

$$\mathcal{L}_{\phi} = \frac{1}{2}\partial^{\mu}a\partial_{\mu}a + \frac{g_s^2}{32\pi^2}\frac{a}{f_a}G^{A,\mu\nu}\tilde{G}^{A}_{\mu\nu} \tag{1.28}$$

a is a new scalar field, which we call the **axion**. The vacuum energy of the axion is at minimum when $a = -f_a\theta$: in this way, the CP-violating terms vanish and the strong-CP problem is solved.

As a consequence of the chiral anomaly, the axion acquires a mass of the order $m_a \sim \Lambda^2_{QCD}/f$, where $\Lambda_{QCD} \approx 200\,\text{MeV}$: the Supernova 1987a already pushes the mass limit below 10 meV [41], making the axion an extremely light particle. Despite this, the axion can still be regarded as a good DM candidate, but only if its production mechanism is non-thermal: a thermal production, in fact, would mean that axions are hot relics (they are relativistic at decoupling), which cannot account for the majority of the DM abundance we see in the universe.

A non-thermal production mechanism, instead, is able to produce a relic density compatible with observation; the details of this process are somewhat involved, but a nice review can be found in [42].

1.5.3 Sterile neutrinos

The neutrino flavor oscillation is an observed phenomenon that is possible only if neutrinos have a mass. This is a problem in the SM, where neutrinos appear only as left-handed fields, and are thus not allowed to possess a Dirac mass term (Appendix A). One elegant solution to this problem is given by the so-called seesaw

mechanism: we introduce in the Lagrangian a certain number of right-handed neutrinos N_R with a Majorana mass term:

$$\mathcal{L}_\nu = -\sum_{i,j}\left[y_{ij}^{(\nu)}\overline{L}_L^i\tilde{\varphi}N_R^j + \frac{1}{2}M_{ij}\overline{N}_R^{c,i}N_R^j + h.c.\right] \tag{1.29}$$

The first term is the Yukawa interaction between the two neutrino chiralities, while the second term is the Majorana mass term for right-handed neutrinos (which involves the charge conjugated field of N_R). After the spontaneous symmetry breaking of the electroweak symmetry, the Yukawa interaction brings the usual Dirac mass term for neutrinos ($m_{ij}^{(\nu)} = y_{ij}^{(\nu)}v/\sqrt{2}$), that, together with the Majorana one, forms the following mass matrix:

$$m_\nu = \begin{pmatrix} 0 & m^{(\nu)} \\ m^{(\nu)} & M \end{pmatrix} \tag{1.30}$$

If we suppose $M \gg v$, then the eigenstates with a dominant contribution of left-handed neutrinos (which we call active neutrinos) will be almost massless (since their mass is inversely proportional to M). Eigenstates with a dominant contribution of right-handed neutrinos (which we call **sterile neutrinos**) will, instead, have mass almost equal to M. In this way, the seesaw mechanism is able to explain why the left-handed neutrino mass is so small and why we have not yet observed the right-handed neutrinos.

Sterile neutrinos could be produced by the oscillations of active neutrinos at high temperature in the thermal plasma [43]: the predictions can then be compared to astrophysical observations, in order to find constraints on the mass and mixing angle. The results for the simplest model of three sterile neutrinos require the mass of the lighter one to be $m_\nu < 3.5\,\text{keV}$ [44] to account for all the DM density, though this limit is in conflict with observations from cosmological structures [45]. The relic abundance, however, could be enhanced by a cosmological lepton number asymmetry [46], so that it matches the observed DM density even for small neutrino masses.

1.5.4 Supersymmetric candidates

The theory of supersymmetry was born to put on equal footing the two fundamentally different types of particles we know: bosons and fermions. In the SM, bosons play the role of force carriers, while fermions are the constituents of matter; supersymmetry provides a partner of the opposite class (a fermion corresponds to a boson and vice versa) to each particle. Besides its symmetric appeal, this theory is studied for several reasons, like the ability to solve the gauge hierarchy problem

(which we mentioned before) and its natural connection to a Grand Unified Theory (GUT). Unfortunately, the main weakness of supersymmetry is that there is still no experimental evidence for it. For a full discussion on the theory, we refer to [47, 48].

It seems clear that, even in the contest of the Minimal Supersymmetric Standard Model (MSSM), the simplest supersymmetric theory which comprehends all the particles we already know, a lot of new particles need to be added [1, 3]: this is a prolific field to search for DM candidates, but we need to satisfy the constraints listed in Section 1.4, in particular the stability requirement. We can do that by introducing a new Z_2 discrete symmetry (the R-parity) which associates a positive charge to SM particles and negative charge to their supersymmetric partners; in this way, if R-parity is conserved, the lightest supersymmetric particle cannot decay into light SM particles, and as a result it is stable.

Among the supersymmetric candidates for DM, it's worth citing:

- Neutralino [3]: neutralinos are the four mass eigenstates resulting from the mixing of four neutral Majorana fermions (2 Higgsino, zino, photino), the superpartners of the neutral bosons of the SM (Higgs bosons, Z boson and photon).
- Gravitino [49, 50]: spin 3/2 superpartner of the graviton.

Chapter 2

The WIMP paradigm

The rest of this thesis is devoted to the study of WIMPs. Actually, "WIMP" is a very broad definition, which includes various particles coming from very different theoretical backgrounds. In this chapter we will review their common features, why they have been considered the best DM candidates and what experimental strategies are employed to find them.

2.1 Freeze-out

The evolution of the WIMP relic density can be studied by means of the Boltzmann equation. This is a fundamental tool for the physics of the early universe, that describes the evolution of the phase space distribution $f(\vec{x}, \vec{p}, t)$ of a particle species in an expanding universe (we present a detailed derivation of the Boltzmann equation in Appendix B). If we suppose that the DM particles χ interact via annihilation reactions like:

$$\chi\chi \to \psi\psi \tag{2.1}$$

where ψ is a SM particle in equilibrium with the thermal bath, then the Boltzmann equation will read:

$$\dot{n} + 3Hn = \langle\sigma v\rangle\left(n_{eq}^2 - n^2\right) \tag{2.2}$$

Here, n is the number density of DM, $H = \dot{a}/a$ is the Hubble parameter, $\langle\sigma v\rangle$ is the annihilation cross section and n_{eq} is the equilibrium number density. At this point, it's useful to introduce a new variable, the *comoving number density*:

$$Y_i = \frac{n_i}{s} \tag{2.3}$$

The advantage of this variable is that it scales out the effect of the expansion of the universe. In fact, both the number density n_i and the entropy density s scale like

a^{-3} (the entropy $S = sa^3$ is constant). This can be directly seen in the left-hand side of the Boltzmann equation:

$$\frac{dY}{dt} = \frac{d}{dt}\left(\frac{n}{s}\right) = \frac{d}{dt}\left(\frac{na^3}{S}\right) = \frac{1}{S}\frac{d(na^3)}{dt} = \frac{1}{s}\left(\frac{dn}{dt} + 3Hn\right) \tag{2.4}$$

We can rewrite the Eq. (2.2) in terms of the variable $x = m/T$, in order to obtain (remembering that $Ta = cost$):

$$\frac{dY}{dx} = -\frac{\langle\sigma v\rangle s}{Hx}(Y^2 - Y_{eq}^2) \tag{2.5}$$

We can manipulate this equation to get the form ($\Gamma_A = n_{eq}\langle\sigma v\rangle$ is the annihilation rate):

$$\frac{x}{Y_{eq}}\frac{dY}{dx} = -\frac{\Gamma_A}{H}\left[\left(\frac{Y}{Y_{eq}}\right)^2 - 1\right] \tag{2.6}$$

From this equation, we can note an interesting detail: when $\Gamma_A \ll H$, $dY/dx \simeq 0$. This condition has a clear physical meaning: the number-changing processes for DM are efficient at maintaining equilibrium as long as the reactions can keep up with the expansion of the universe. Eventually, the universe will become so large that DM particles will not find each other to annihilate, and, at this point, the comoving number density will not change anymore. This moment in time is called *freeze-out*, and it is defined by:

$$\Gamma_A(T_{FO}) = H(T_{FO}) \tag{2.7}$$

WIMPs are classified as cold relics; this means that they decouple when they are non-relativistic:

$$m_\chi > T_{FO} \tag{2.8}$$

The freeze-out temperature is very important for the final relic density; the reason for this can be seen in the equilibrium distribution, which, for a non-relativistic particle, can be approximated by the Maxwell-Boltzmann one:

$$n_{eq} \simeq g\left(\frac{mT}{2\pi}\right)^{\frac{3}{2}} \exp\left(-\frac{m-\mu}{T}\right) \tag{2.9}$$

When $m > T$, particles start to feel the Maxwell-Boltzmann suppression, as we can see from Fig. 2.1; the suppression is effective until the decoupling, at which point the comoving number density gets frozen. A later decoupling translates into a greater suppression, so in a lower relic density today.

After freeze-out, the DM is no longer in chemical equilibrium, but it remains in thermal equilibrium with the surrounding plasma because of elastic scattering

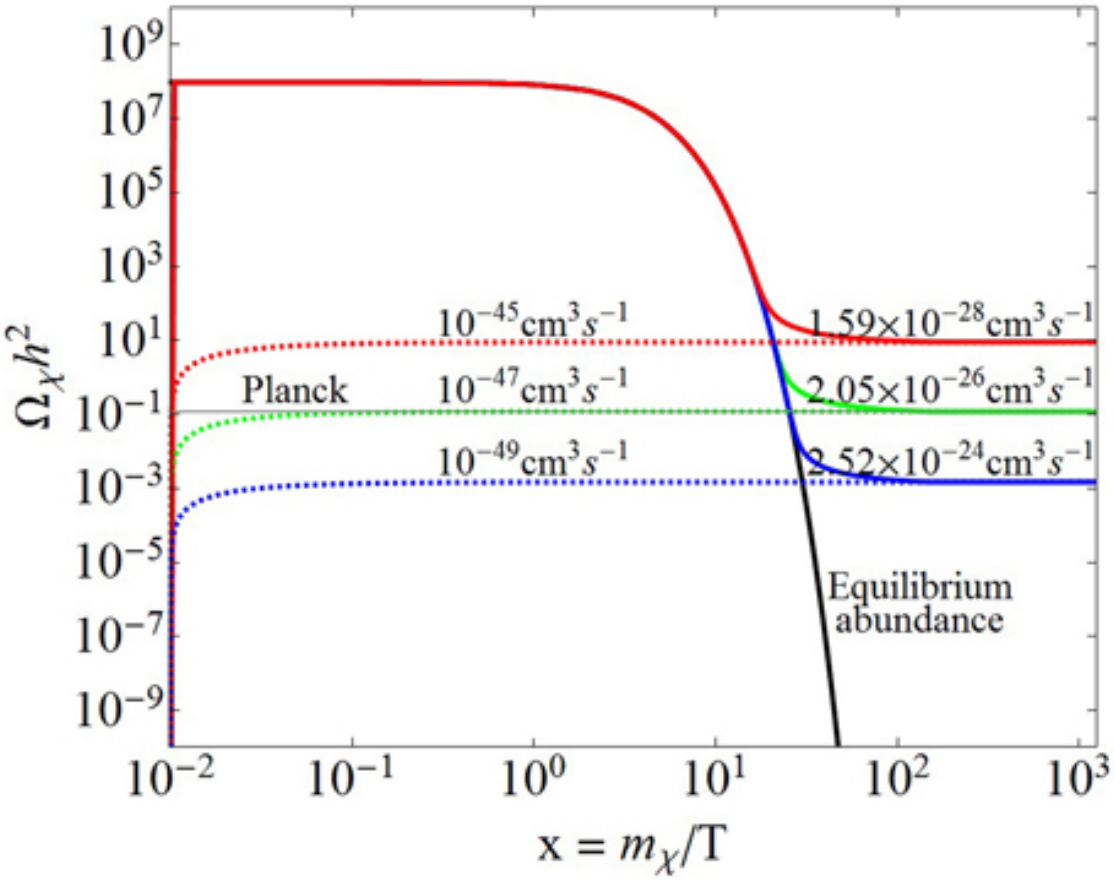

Figure 2.1: The relic density evolution for cold dark matter. The different solid lines correspond to different annihilation cross sections: for higher cross sections, the freeze-out happens at later times, so the Maxwell-Boltzmann suppression is more effective. The dashed lines illustrate the evolution for freeze-in models, which are not treated in this thesis. The horizontal band gives the observed relic density from Planck data. From [51]

($\chi\,\mathrm{SM} \to \chi\,\mathrm{SM}$). This process is still effective because there are a lot of targets: SM particles are still relativistic, so their number density is not Maxwell-Boltzmann suppressed. This scattering allows the DM fluid to share the same temperature with the thermal bath, at least until the kinetic decoupling, which, as for the chemical decoupling, is marked by the condition:

$$\Gamma_{elastic}(T_{KD}) = H(T_{KD}) \tag{2.10}$$

For cold relics, the kinetic decoupling happens much later than the chemical decoupling: during this time, perturbations are damped by friction between the DM

fluid and the photon bath, and this phenomenon affects the formation of the smallest DM structures. This effect directly competes with the collisionless damping happening after the kinetic decoupling, during the free-streaming, and they both must be taken into account when constraining the DM mass.

2.2 The WIMP miracle

To study the evolution of the comoving number density, the use of the Boltzmann equation is mandatory; however, the equation (2.5) can only be solved numerically. Nevertheless, a semi-analytical solution can be found in the two limiting cases $x \ll x_{FO}$ and $x \gg x_{FO}$.

First of all, we need to find the value of x_{FO}. From the condition (2.7):

$$\frac{\exp(x_{FO})}{x_{FO}^{1/2}} \sim \frac{g_\chi}{g_*^{1/2}} m_\chi M_{Pl} \langle \sigma v \rangle \tag{2.11}$$

Given that x_{FO} appears in the exponential, its dependence on m_χ and $\langle \sigma v \rangle$ is actually quite weak. We can solve Eq. (2.11) by iteration, plugging in some typical values for WIMPs:

$$\begin{aligned} m_{WIMP} &\simeq 100\,\text{GeV} \\ \langle \sigma v \rangle &\simeq 1\,\text{pb} \end{aligned} \tag{2.12}$$

finding $x_{FO} \simeq 25$. This value is consistent with the assumption that we are dealing with cold dark matter ($x_{FO} \gg 1$).

We can explicit the dependence on x of the Hubble parameter and the entropy density (we are neglecting the temperature dependence of g_* and g_{*s}):

$$\begin{cases} H(x) = H(x=1)x^{-2} \\ s(x) = s(x=1)x^{-3} \end{cases} \tag{2.13}$$

In the non-relativistic limit, the cross section can be expanded as:

$$\langle \sigma v \rangle = \sigma_0 x^{-n} \tag{2.14}$$

$n = 0$ corresponds to the s-wave process, $n = 1$ to the p-wave process and so on. Thus, we can rewrite the Boltzmann equation as ($' = \frac{d}{dx}$):

$$Y' = -\frac{\lambda}{x^{2+n}}\left(Y^2 - Y_{eq}^2\right), \qquad \lambda = \frac{s(x=1)\sigma_0}{H(x=1)} \tag{2.15}$$

And, defining the variable $\Delta = Y - Y_{eq}$:

$$\Delta' = -Y'_{eq} - \frac{\lambda}{x^{2+n}}(\Delta^2 + 2\Delta Y_{eq}) \tag{2.16}$$

When $x \ll x_{FO}$, the number density is well approximated by the equilibrium density; we can impose $d\Delta/dx = 0$ to find:

$$\Delta \simeq -\frac{x^{2+n}}{\lambda}\frac{Y'_{eq}}{\Delta + 2Y_{eq}} \tag{2.17}$$

For $x \gg x_{FO}$, instead, the equilibrium density is heavily suppressed; this means that we can neglect Y and Y', so that $\Delta \simeq Y$, to obtain:

$$\Delta' \simeq -\frac{\lambda}{x^{2+n}}\Delta^2 \quad \Rightarrow \quad Y(x) \simeq \Delta(x) = \left(\int_{x_{FO}}^{x} dx\, \frac{\lambda}{x^{2+n}}\right)^{-1} \tag{2.18}$$

From the above equation, we can get the current value of the comoving number density taking the limit $x \to \infty$:

$$Y(t_0) \propto \frac{z_{FO}^{n+1}}{\lambda} \tag{2.19}$$

Plugging in the parameters in (2.12) we can finally find today's WIMP relic density:

$$\Omega_\chi = \frac{m_\chi s(t_0) Y(t_0)}{\rho_{crit}} \to \Omega_\chi h^2 \simeq 0.12 \left(\frac{106.75}{g_*(T_{FO})}\right)^{1/2} \left(\frac{0.7\,\text{pb}}{\langle\sigma v\rangle}\right) \tag{2.20}$$

In Eq. (2.20) we can appreciate the most interesting feature of WIMPs: supposing a mass around the GeV-TeV scale, with the typical cross section expected for a weak-scale interaction, we get a relic density very similar to the DM abundance we observe in the universe. This remarkable conclusion is referred to as the "WIMP miracle", and it is the reason why WIMPs are so appealing as DM candidates.

Another feature we can note from Eq. (2.20) is that the relic density is inversely proportional to the cross section: this means that the current upper bound on DM density translates into a lower bound for the annihilation cross section. If DM is made up of WIMP, then they must have some small, yet non-vanishing interactions with SM particles, interactions that we might be able to detect.

2.3 Experiments

WIMPs have been the focus of most of the experimental effort invested for the search of DM [52]. The experimental strategies are exemplified in Fig. 2.2:

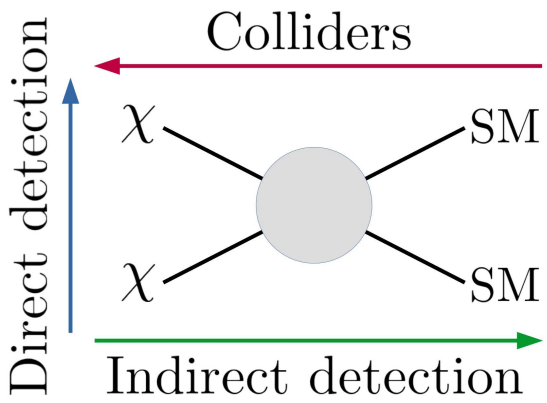

Figure 2.2: Schematic representation of the different types of DM searches.

Direct detection We look for elastic scattering between the WIMPs and SM particles. Because DM interacts so weakly with SM particles, one of the main challenges for this type of experiment is to kill all the background that may spoil the measurements; for this reason, these experiments are usually performed in underground facilities (where they are shielded from cosmic rays).

Indirect detection DM annihilations are fundamental for thermal relics to get in equilibrium with the primordial plasma in the early universe; nowadays, these reactions may leave a distinct signature in the sky, in terms of different stable SM particles (like photons or neutrinos). This signature is actively searched for in indirect detection experiments.

Collider searches DM can also be produced via energetic collisions of SM particles, which happen at particle colliders.

2.3.1 Direct detection

Direct detection experiments are the simplest strategy we can think of when we search for DM signals: we simply wait that some DM particle interacts with ordinary matter and hope to record the event. Unfortunately, this is much easier said than done. From the dark halo model of our galaxy, we expect to be surrounded by DM particles, whose velocity distribution is given in Eq. (2.25): a Gaussian distribution in the galactic reference frame. The Earth, however, together with the solar system, is not at rest in this reference frame: this means that, from our point of view, our planet is constantly hit by a wind of DM particles; for WIMPs

of mass around 100 GeV and relative velocity of 200 km s^{-1} we expect a flux:

$$\Phi_{WIMP} \simeq 9 \times 10^4 \,\mathrm{cm}^{-2}\,\mathrm{s}^{-1} \tag{2.21}$$

This flux can be compared, for example, with the expected flux of solar neutrinos, which have the same behavior from an experimental point of view: both WIMPs and neutrinos have an extremely low cross section, so what we do is build large tanks of specific material chosen to maximize the interaction probability, and we try to detect the recoil energy E_R of the scattered particle. The solar neutrinos flux, however, is many orders of magnitude larger than the expected WIMP flux: if neutrinos were already very hard to observe, WIMPs will be even harder.

One of the main problems when dealing with these weakly interacting particles is given by the background. The signal expected from an interaction between a WIMP and the detector can be originated also by many other sources, primarily cosmic rays, and at a much higher rate: in this way, a possible signal coming from a WIMP would be impossible to distinguish over the noise. This is the reason why direct detection experiments are usually placed in underground facilities (like the INFN laboratories under the Gran Sasso mountain): in this way, even the most penetrating particles are stopped by the thick layer of rock. Additional lead shielding around the detector provides protection against environmental radioactivity: in this way, the background is almost reduced to zero.

The quantitative analysis for the expected number of events requires input from different research fields:

- Astrophysics: the flux of DM particles must be accurately computed from the known local density distribution and local velocity distribution. Unfortunately, these phenomenological parameters are still affected by large uncertainties (cfr. Eq. (1.7));

- Particle physics: the choice of a particular DM particle model heavily influences the expected outcome of an experiment. For example, a heavier DM particle will generate more energetic scattering, making them easier to be seen; on the other hand, the number density will get smaller, so fewer interactions will occur;

- Nuclear physics: the material chosen for the detector plays a very important role. Its spin, in particular, is important to test spin-dependent cross sections, and other properties like the mass and the density (and, of course, the cost) must also be taken into account.

For an elastic scattering between a WIMP with mass m_χ and velocity v and a nucleus with mass $m_\mathcal{N}$ the maximum recoil energy is ($\mu^2_{\chi\mathcal{N}} = \frac{m_\chi m_\mathcal{N}}{m_\chi + m_\mathcal{N}}$ is the reduced

mass):

$$E_R^{max} = \frac{2\mu_{\chi\mathcal{N}}^2 v^2}{m_{\mathcal{N}}} \simeq 50\,\mathrm{keV}\left(\frac{m_\chi}{100\,\mathrm{GeV}}\right)^2\left(\frac{100\,\mathrm{GeV}}{m_{\mathcal{N}}}\right) \tag{2.22}$$

We can see that the typical scattering energies (order of keV) are much lower than the typical nuclear binding energies (order of MeV), so we can model the scattering by treating the nucleus as a whole.

The differential reaction rate is then:

$$\frac{d\Gamma}{dE_R} = N_T n_\chi \langle v \frac{d\sigma_{\chi\mathcal{N}}}{dE_R}\rangle \tag{2.23}$$

where N_T is the number of targets in the detector, $n_\chi = \rho_\chi/m_\chi$ is the WIMP number density and $\sigma_{\chi\mathcal{N}}$ is the WIMP-nucleon cross section. We can rewrite this reaction rate as:

$$\frac{d\Gamma}{dE_R} = 2\pi \frac{N_T n_\chi m_{\mathcal{N}}}{\mu_{\chi\mathcal{N}}} \int_{v_{min}}^{v_{max}} dv \frac{f(v,t)}{v} \frac{d\sigma_{\chi\mathcal{N}}}{d\Omega_*} \tag{2.24}$$

The integral is performed over the relative velocity v. The velocity distribution $f(v,t)$ is assumed to be a truncated Gaussian distribution in the galactic reference frame [53]:

$$f_G(\mathbf{v}) = \begin{cases} \frac{1}{N_{esc}}\left(\frac{1}{2\pi\sigma_v^2}\right)\exp\left(-\frac{|\mathbf{v}|^2}{2\sigma_v^2}\right) & |\mathbf{v}| < v_{esc} \\ 0 & |\mathbf{v}| > v_{esc} \end{cases} \tag{2.25}$$

where σ_v is the velocity dispersion, $v_0 = \sqrt{2}\sigma_v \approx 220\,\mathrm{km\,s^{-1}}$ is the value of the asymptotically flat rotation curve, $v_{esc} \approx 544\,\mathrm{km\,s^{-1}}$ is the galactic escape velocity and N_{esc} is a renormalization factor. To get the velocity distribution with respect to the Earth, we have to account for the motion of the Earth itself $\mathbf{v}_\oplus(t)$ and the motion of the Sun $v_\odot \simeq 232\,\mathrm{km\,s^{-1}}$ around the galaxy:

$$f(\mathbf{v},t) = f_G(\mathbf{v} + \mathbf{v}_\odot + \mathbf{v}_\oplus(t)) \tag{2.26}$$

In Eq. (2.24) v_{max} is set by the galactic escape velocity; v_{min} is related to the sensitivity of our experiment: namely, every experiment has a lower energy threshold E_{th} below which no signal can be detected. Thus, v_{min} represents the minimum velocity needed to produce a scattering that can be observed.

$$v_{min} = \sqrt{\frac{m_{\mathcal{N}} E_{th}}{2\mu_{\chi\mathcal{N}}^2}} = \begin{cases} \sqrt{\frac{m_{\mathcal{N}} E_{th}}{2m_\chi^2}} & m_\chi \ll m_{\mathcal{N}} \\ \sqrt{\frac{E_{th}}{2m_{\mathcal{N}}}} & m_\chi \gg m_{\mathcal{N}} \end{cases} \tag{2.27}$$

For lower masses, the required minimum velocity is very large (eventually overcoming the escape velocity), so direct searches are not well suited for light DM

particles. For heavier masses, instead, the minimum velocity is set by experimental parameters, but the number density is of course decreased, so we expect less statistics.

The only quantity left to discuss, which is also the most important one, is the cross section $\sigma_{\chi\mathcal{N}}$: how does a WIMP interact with our detector? First of all, we can make the following important distinction:

Spin-independent scattering The scattering amplitudes between the WIMP and the nucleons in the target nucleus interfere constructively, resulting in the magnification of the WIMP-nucleus cross section and the subsequent increase of the reaction rate. This means that spin-independent scattering can be tested at best by heavier nuclei targets.

Spin-dependent scattering This type of scattering results from axial-vector coupling, leading to a dependence of the cross section on the spin of the target nucleus.

For example, we can look at the explicit form of the spin-independent scattering cross section:

$$\sigma_{\chi\mathcal{N}}^{(SI)} = \frac{[Zf_p + (A-Z)f_n]^2}{16\pi(m_\chi + m_\mathcal{N})^2} F(E_R)^2 = \sigma_{\chi\mathcal{N}}^{(SI)}\Big|_{E_R=0} F(E_R)^2 \tag{2.28}$$

Here, Z and A are the atomic and mass number of the target nucleus, f_p and f_n are the scattering amplitudes with a proton and a neutron and $F(E_R)$ is the nuclear form factor ($F(0) = 1$).

The current limits on the WIMP-nucleon cross section are reported in Fig. 2.3 and 2.4. A review of the different techniques for direct detection experiments can be found in [54]. No signal has been found yet, but the sensitivity of the experiments is improving generation after generation. There is, however, a natural endpoint to this program: the neutrino floor (yellow region in Fig. 2.3). This is a limit below which our experiment is able to see the scattering produced by neutrinos, which represent an unkillable background. Some future experiments (like DARWIN [55]) are already planning to reach the neutrino floor.

The last thing worth mentioning about direct searches regards the annual modulation of the rate due to the Earth's motion. In Eq. (2.24) the velocity distribution is a time-dependent function: the time dependence is precisely due to the variation of the velocity of the WIMP wind as the Earth rotates around the Sun. This means that the WIMP flux is higher at the beginning of the summer, when the Earth is moving in the opposite direction with respect to the wind, compared to

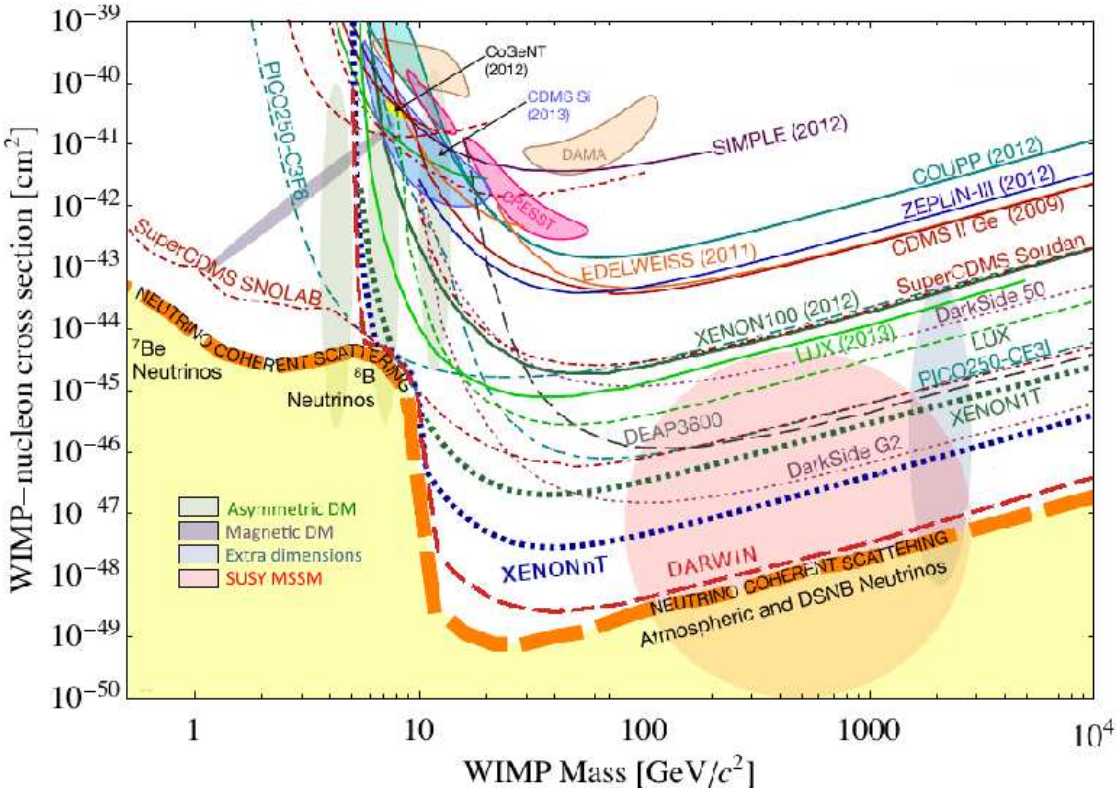

Figure 2.3: Summary for spin-independent WIMP-nucleon scattering cross section. The solid lines are the limits coming from different experiments, shaded closed contours indicate claimed DM signals, while the dotted lines are projections for future experiments. Shaded regions point out the interesting parameter space for different WIMP models. The yellow region is the parameter space dominated by the neutrino background. From [56]

the winter, and this should lead to an increased number of recorded events in June. This excess of observed events has actually been claimed by the DAMA collaboration for several years now [58], however the observations pinpoint a parameter space that is excluded by other experiments. This is the reason why a similar experiment is currently being built in Australia, where the seasonal background is reversed with respect to the northern hemisphere and the eventual observation of the same annual modulation signal would leave no doubt about its astrophysical origin.

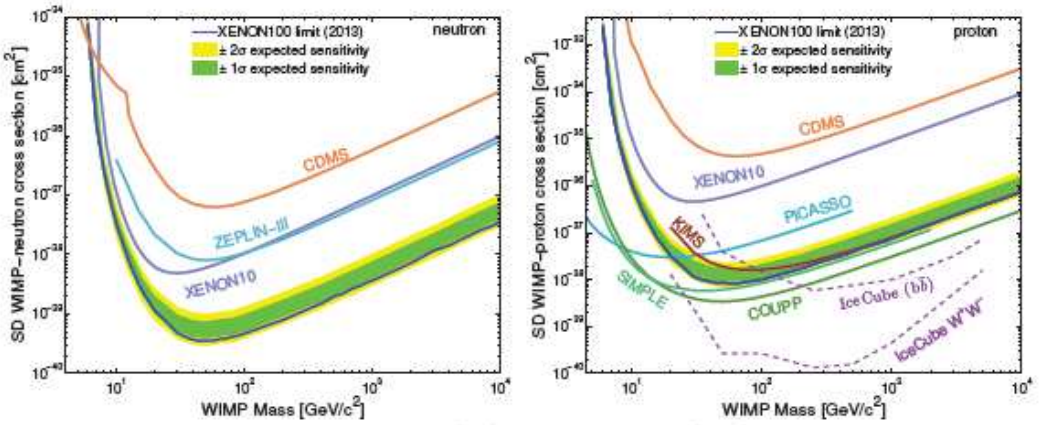

Figure 2.4: Spin-dependent WIMP-neutron (left) and WIMP-proton (right) cross section limits. From [57].

2.3.2 Indirect detection

Annihilations were fundamental to keep DM particles in thermal equilibrium with the primordial plasma; despite being immensely suppressed due to the expansion of the universe, these annihilations may still be going on in some regions of the universe, producing some characteristic signal: the detection of this signal is the aim of indirect detection experiments.

The annihilation rate Γ_A is proportional to the square of the DM density, $\Gamma_A \propto \rho_{DM}^2$: therefore, we have to focus observations in regions where DM is denser (these regions are called *amplifiers*). In our neighborhood, the Sun and the Earth may be regarded as amplifiers, since WIMPs could lose energy through scattering with SM particles inside them and be trapped in their gravitational well. On the galactic scale, instead, we should look at the galactic nucleus, where simulations predict a peak in the DM distribution, or dwarf galaxies, which are DM-dominated structures. The relevance of an astrophysical amplifier can be quantified in the J-factor:

$$J = \frac{1}{8\pi} \int d\Omega \int_{line\ of\ sight} dl \rho^2(r(l,\psi)) \tag{2.29}$$

Of course, the J-factor suffers large uncertainties because we don't know the exact DM distribution. Besides DM density, when we study a particular amplifier we also have to take into account the potential background: for example, the galactic center is obviously the primary target for indirect searches, but we have to deal with the huge background which is not well understood yet; on the other hand, dwarf galaxies are much cleaner systems, although with a smaller J-factor.

But what should we observe? We don't know the particle output of WIMP

annihilation, but we can suppose two SM particles as final products; since WIMPs are very massive particles, many annihilation channels are theoretically allowed: quark-antiquark or lepton-antilepton pairs, as well as W and Z bosons or Higgs bosons. However, only some of these particles are stable, thus being able to travel up to the Earth to be detected: we can take a look, in particular, at what we expect in terms of photons and neutrinos. These particles, in fact, have the great advantage of being neutral: this means that they are not deflected by the galactic and intergalactic magnetic fields, so they are able to deliver information about the direction of the source.

Photons High energy photons can be detected with the use of the Imaging Atmosphere Cherenkov Telescope (IACT). As a photon enters the upper atmosphere, it generates an electromagnetic shower (a cascade of particles, mainly composed of photons, electrons and positrons): the charged particles in the shower are ultra-relativistic, so they emit Cherenkov radiation as they travel through the atmosphere. IACTs detect this radiation on the ground, and they are able to build an image of the shower, and therefore to reconstruct the properties of the primary photon (like its energy and direction).

The expected photon flux from WIMP annihilations in the direction ψ is given by:

$$\frac{d\Phi}{dE_\gamma}(E_\gamma, \psi) = \sum_i \frac{\langle \sigma_i v \rangle}{m_\chi^2} \frac{dN_i}{dE_\gamma} J \tag{2.30}$$

$\langle \sigma_i v \rangle$ and dN_i/E_γ are respectively the cross section and the number of photons of energy E_γ produced in the i^{th} annihilation channel.

The γ-ray spectrum produced by WIMP annihilations depends on the dominant annihilation channel (Fig. 2.5). For example, the direct production of two photons, $\chi\chi \to \gamma\gamma$, would produce a monochromatic line at $E_\gamma \simeq m_\chi$ (WIMPs are non-relativistic particles, so the available energy during the reaction is mostly given by their mass), that, if observed, would represent a smoking gun signature of WIMPs. However, this interaction usually can happen only at 1-loop order (otherwise WIMP would not be dark!), so it is heavily suppressed.

If, instead, WIMPs annihilate into quarks, leptons, or gauge bosons, photons are produced from the shower of their decay products: in this case, the energy spectrum does not have a distinctive shape, so we must search for a continuum excess over the background. This, of course, can be done only if the background is well understood, which is the task of many experiments making use of IACTs (like HESS, MAGIC and VERITAS).

Neutrinos Neutrinos are exploited as astrophysical messengers only in very recent times: their detection is already very challenging, so if we want to acquire

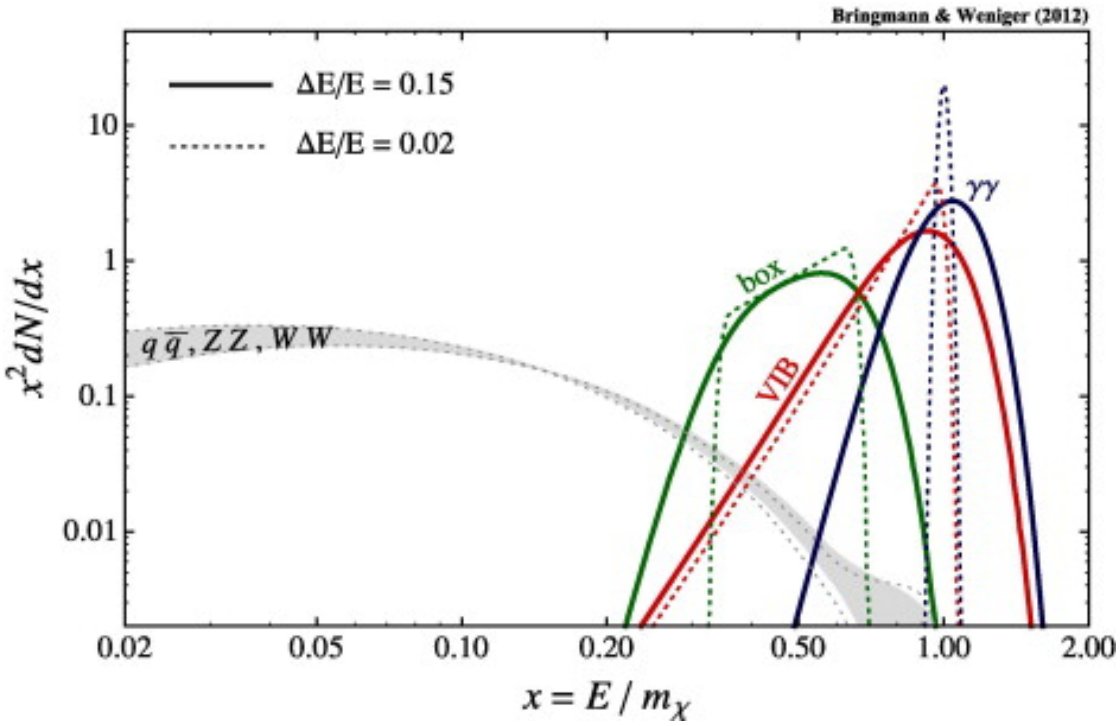

Figure 2.5: Various γ-ray spectra expected from DM annihilations. The blue line represents the direct annihilation into a $\gamma\gamma$ pair, the red line represents the radiation due to virtual internal bremsstrahlung (where the photons are radiated from charged virtual particles), while the green line is the box spectrum arising from the intermediate neutral state ($\chi\chi \to \phi\phi$) which then decay ($\phi \to \gamma\gamma$). The gray band represents the broad spectrum produced by quarks and gauge bosons final state. Solid and dotted lines compare two different energy resolutions. From [59].

enough statistics for a meaningful analysis of a neutrino source we need powerful detectors. The most promising one for high-energy neutrino astronomy is certainly IceCube, located at the South Pole, which aims to detect the Cherenkov radiation produced by the product of a neutrino collision in the ice (the principle is similar to the IACTs, but we need to go deep under the ice to be shielded from cosmic rays).

However, the low rate of interaction can also be considered one of neutrinos advantages: this means, in fact, that they are able to escape very dense regions (like the nucleus of the Sun) without interacting with the surrounding medium, thus delivering direct information about those regions. This is the reason why we search for high-energy neutrinos coming from the Sun. In fact, when WIMPs pass through the Sun, they may scatter and be slowed below the escape velocity; once

captured, they will settle in the center of the Sun, thus increasing their number density and therefore their annihilation rate. The only annihilation products able to escape from the Sun are exactly neutrinos.

If $C_\odot$ is the WIMP capture rate and $A_\odot = \langle\sigma v\rangle/V$ is the annihilation cross section per volume, then for N WIMPs in the Sun:

$$\dot{N} = C_\odot - A_\odot N^2 \tag{2.31}$$

Thus, the annihilation rate is:

$$\Gamma = \frac{1}{2} A_\odot N^2 = \frac{1}{2} C_\odot \tanh^2\left(\sqrt{C_\odot A_\odot} t_\odot\right) \tag{2.32}$$

$t_\odot$ is the age of the solar system. In many models, the Sun has already reached equilibrium ($\sqrt{C_\odot A_\odot} t_\odot \gg 1$), so $\Gamma \simeq C_\odot/2$. This is not true, instead, for the Earth, which is a far smaller target and provides a less deep gravitational well for capture. The neutrino flux expected on Earth must also take into account how neutrinos are produced from a single annihilation: despite this being a model-dependent feature, in the case in which the dominant annihilation mode is given by final states like $b\bar{b}$, $t\bar{t}$, $\tau^+\tau^-$, W^+W^-, the difference is not dramatic. In the end, the neutrino flux is almost completely determined by the capture rate $C_\odot$, so on the WIMP-proton cross section: the limits found by IceCube [60] for the spin-independent cross section are not competitive with the ones found from direct detection experiments (spin-independent cross section increases with the mass of the nucleus and the Sun is made up mostly by hydrogen), but they are important for spin-dependent cross section (as we can see from the right panel of Fig. 2.4).

Of course, neutrinos and photons are just the most convenient candidates to look for when we talk about indirect searches; but every other astrophysical particle could give a hint for DM annihilations. For example, for many years now an excess in the fraction of positrons over electrons in the 10 GeV to 1 TeV energy range has been observed by the PAMELA satellite [61]. This excess can be emitted by nearby astrophysical sources (like pulsars), but DM annihilations could also provide a reasonable motivation; the observed flux, however, requires a WIMP annihilation cross section far greater (a factor about 10 to 10^3) than the one predicted by the thermal relic density. An elegant solution to this problem is given by the so called Sommerfeld enhancement: supposing long-range interactions between WIMPs, through the exchange of a light force carrier ϕ, the cross section is enhanced by a factor:

$$S = \frac{\pi\alpha_X/v_{rel}}{1 - e^{-\pi\alpha_X/v_{rel}}} \tag{2.33}$$

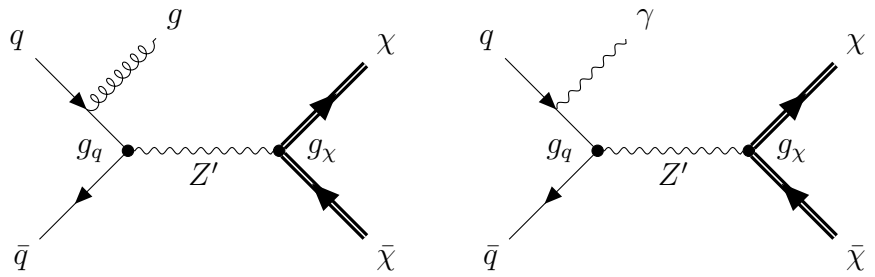

Figure 2.6: Diagrams for the pair production of WIMPs, with initial state radiation resulting in a jet (a) or monophoton final state (b).

2.3.3 Collider searches

If WIMPs have a non-vanishing annihilation cross section into SM particles, then the opposite reaction (SMSM $\rightarrow \chi\chi$) should also exist. This possibility is investigated in particle colliders: the Large Hadron Collider (LHC), in particular, can create proton collisions with energies up to 13.6 TeV in the center of mass, which, in principle, is more than enough to produce WIMPs.

If produced, WIMPs will not interact with the detector, but we can infer their presence from the missing energy and momentum we would observe from the final product of the collision: in this sense, they behave exactly like neutrinos, which, in turn, represent the main background for this type of search. The major sources of neutrinos are given by the decays of the Z boson ($Z \rightarrow \nu\bar{\nu}$) and the W boson ($W^{\pm} \rightarrow l^{\pm}\nu$), which are generally accounted for using Monte Carlo simulations. The neutrino background problem is very relevant for hadron colliders, for which the initial energy of the partonic collision cannot be fixed; as a result, an eventual DM signal would be practically undistinguishable [62]. For lepton colliders, on the other hand, the initial energy can be determined, and the beam can be polarized to further reduce the expected background [63].

The purely direct production of WIMPs, which do not leave visible tracks in the detector, would be unobservable. Fortunately, WIMP production can be generally accompanied by one or more SM particles. Experimental searches can be thus focused on events in which visible tracks from a SM particle recoil against missing energy from the WIMPs. These types of event are generally called "mono-X searches", where X is the accompanying SM particle produced in the final state (Fig. 2.6). For example, mono-jet and mono-photon searches are performed at LHC [64, 65].

The data analysis proceeds as follows: one takes into account only events in which a large missing transverse momentum is observed; these data are further pu-

rified by rejecting events with isolated energetic leptons (to reduce the background from W and Z decays) and applying a series of quality criteria on jets [66]; the number of events is compared with the prediction from SM interactions to search for an excess. No excess has been found yet [64, 65].

The results from this type of search can be translated into exclusion regions on WIMP pair production. The limits are obviously heavily model-dependent, but it's possible to get general conclusions using an effective field theory approach [67], where the interaction between the SM particles and DM is modeled by:

$$\mathcal{L}_{int} = \frac{g_q g_\chi}{M_{Z'}^2} \left[\bar{\chi}\Gamma^\chi \chi\right] \left[\bar{q}\Gamma^q q\right] \tag{2.34}$$

Γ_i denotes the type of interaction (scalar, pseudoscalar, vector, axial vector, tensor) while g_q and g_χ are the coupling constants with the massive intermediate vector boson Z'. This theoretical framework, however, is valid only when the mass $M_{Z'}$ of the mediator is much larger than the energy of the collision (which is a non-trivial assumption, given the high energies reached by the LHC). The limits for vector and axial-vector mediators found by ATLAS [64] and CMS [65] are reported in Fig. 2.7.

Another possibility is that DM might appear as a decay product of some SM particles. Most of the SM particle decays are well known, however some room for new physics is still available in the branching ratios of the Z boson and the Higgs boson [68]. The SM already predicts an invisible decay width (into neutrinos) for the Z boson, but this complication is not present for the Higgs boson; moreover, its decay rate to invisible particles is still weakly constrained (the branching ratio is about 20 % [68]), therefore the Higgs can still have non-negligible couplings to invisible new particles with mass lighter than about $m_h/2 \simeq 63\,\text{GeV}$ (that's why we talk about "Higgs-portal" models for DM). In the simple case in which the invisible decay width of the Higgs is all given by a unique DM particle, the constraints provided by LHC are stronger than the ones given by direct detection experiments like XENON [69].

In any case, we must be aware of the fact that the potential discovery of a new particle in colliders does not mean that the DM puzzle is solved: further studies will be needed to constrain the properties of this new particle and to see if it is indeed a good DM candidate. The relic density must be computed, and other experimental strategies can be exploited to verify the cosmological abundance and to test properties that cannot be seen at colliders. In this sense, direct, indirect and collider searches are complementary to each other.

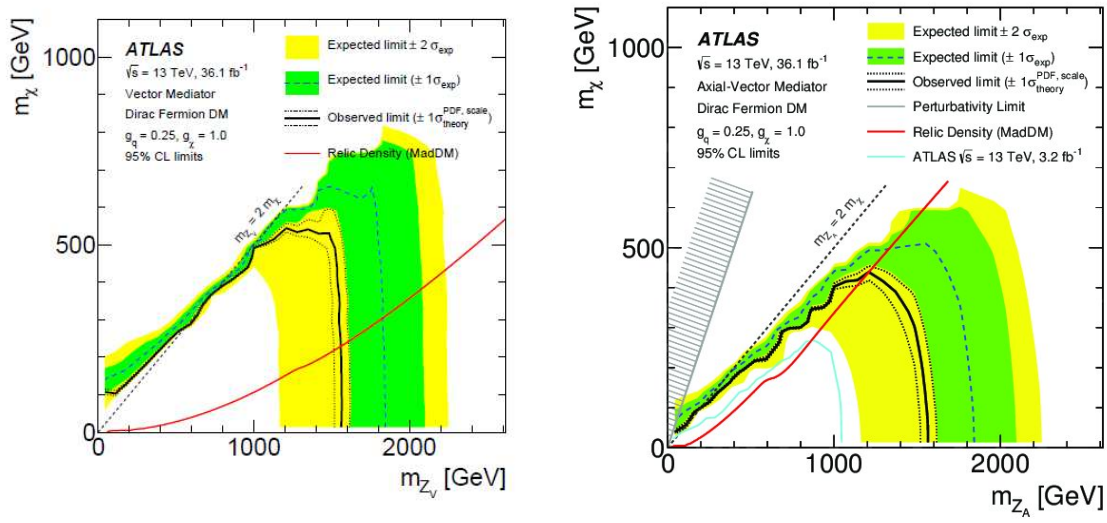

(a)

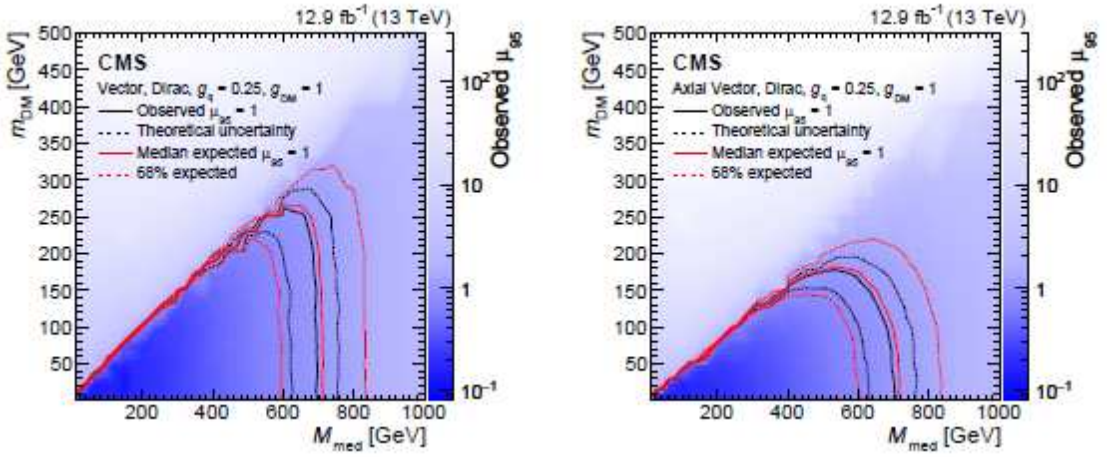

(b)

Figure 2.7: The exclusion regions at 95% CL for vector and axial-vector interactions in the $m_{Z'} - m_{\chi}$ parameter plane from ATLAS [64] monojet searches (a) and CMS [65] monophoton searches (b). The regions below the observed contours are excluded.

Chapter 3

Z' physics

A particular set of models that are well suited for the WIMP paradigm revolves around the extension of the SM gauge group with an additional abelian gauge symmetry, which is broken at an energy scale higher than the electroweak one. This new $U(1)'$ gauge symmetry is associated with a massive gauge boson Z' that, besides mediating a new type of interaction between SM particles, could also provide a portal toward the dark sector. Additional $U(1)'$ gauge symmetries arise from several motivated extensions of the SM [70, 71]: Grand Unified Theories (GUT), for example, work with a much larger gauge symmetry group with respect to the SM gauge group G_{SM}; the breaking of this symmetry group often results in the survival of $G_{SM} \times U(1)'^{n}$ at the electroweak energy scale. We will limit ourselves to the case $n = 1$.

The $U(1)'$ gauge symmetry can be of various nature; some of the most studied models are:

- Sequential Standard Model: the new Z' gauge boson couples to the SM fermions in the same way as the SM Z boson [72];
- $U(1)_B$: the baryon number of the SM is promoted to a gauge symmetry spontaneously broken at low scale [73];
- $U(1)_{B-L}$: as for $U(1)_B$, the difference between baryon and lepton number is gauged [71, 74].

Together with the new gauge boson, a new scalar is generally introduced to provide mass for the new mediator through the Higgs mechanism; in certain models, this new particle could turn out to be particularly relevant for phenomenology [74].

3.1 Theoretical framework

There is a great variety of models involving an additional $U(1)'$ gauge symmetry, each one of them addressing different issues besides being able to include a viable DM candidate (a useful review can be found in [71]); however, we can discuss some common features among them.

3.1.1 Kinetic mixing

The most general kinetic term for an additional $U(1)'$ gauge symmetry is:

$$\mathcal{L}_{kin} = -\frac{1}{4}\hat{B}_{\mu\nu}\hat{B}^{\mu\nu} - \frac{1}{4}\hat{Z'}_{\mu\nu}\hat{Z'}^{\mu\nu} - \frac{1}{2}s_{Z'}\hat{B}_{\mu\nu}\hat{Z'}^{\mu\nu} \tag{3.1}$$

where $\hat{B}_{\mu\nu}$ and $\hat{Z'}_{\mu\nu}$ are the field strengths for the $U(1)_Y$ and $U(1)'$ gauge bosons $\hat{B}_\mu$ and $\hat{Z'}_\mu$ respectively. The last term in the Lagrangian shows the mixing between $\hat{B}_\mu$ and $\hat{Z'}_\mu$, which is parametrized by $s_{Z'} = \sin\theta_{Z'}$ (since the $U(1)$ gauge groups are abelian, this term doesn't spoil the gauge invariance). Even if $\theta_{Z'} = 0$, an effective coupling between $\hat{B}_\mu$ and $\hat{Z'}_\mu$ can be generated by loop effects of particles that are simultaneously charged under both gauge groups [75]. We can diagonalize the kinetic term via the following non-unitary transformation ($c_{Z'} = \cos\theta_{Z'}$ and $t_{Z'} = \tan\theta_{Z'}$):

$$\begin{pmatrix}\hat{B}_\mu \\ \hat{Z'}_\mu\end{pmatrix} = \begin{pmatrix}1 & -t_{Z'} \\ 0 & 1/c_{Z'}\end{pmatrix}\begin{pmatrix}B_\mu \\ Z'_\mu\end{pmatrix} \equiv G(\theta_{Z'})\begin{pmatrix}B_\mu \\ Z'_\mu\end{pmatrix} \tag{3.2}$$

The advantage of the above transformation is to eliminate the dependence on the mixing angle inside the Lagrangian and transfer its effects directly into the coupling constants; if J'_μ is the fermionic current coupled to the Z' boson, then its coupling strength is modified by:

$$J'_\mu \to -t_{Z'}J^Y_\mu + \frac{1}{c_{Z'}}J'_\mu \tag{3.3}$$

where j^Y_μ is the hypercharge current.

3.1.2 Scalar sector

Besides the SM Higgs field, a new scalar S is usually introduced to break the additional $U(1)'$ gauge symmetry:

$$\mathcal{L}_{scalar} = (D_\mu H)^\dagger (D^\mu H) + (D_\mu S)^\dagger (D^\mu S) - V(H,S) \tag{3.4}$$

$$\begin{aligned} V(H,S) =& \lambda_h \left(H^\dagger H - \frac{v_h^2}{2} \right)^2 + \lambda_s \left(S^\dagger S - \frac{v_s^2}{2} \right)^2 \\ &+ \lambda_{hs} \left(H^\dagger H - \frac{v_h^2}{2} \right) \left(S^\dagger S - \frac{v_s^2}{2} \right) \end{aligned} \tag{3.5}$$

Expanding the fields around their respective vevs:

$$H = \frac{1}{\sqrt{2}} \begin{pmatrix} 0 \\ v_h + h \end{pmatrix} \tag{3.6}$$

$$S = \frac{v_s + s}{\sqrt{2}} \tag{3.7}$$

We get the following mass matrix for the two physical Higgs bosons:

$$V(H,S) \supset \frac{1}{2} \begin{pmatrix} h & s \end{pmatrix} \begin{pmatrix} 2\lambda_h v_h^2 & \lambda_{hs} v_h v_s \\ \lambda_{hs} v_h v_s & 2\lambda_s v_s^2 \end{pmatrix} \begin{pmatrix} h \\ s \end{pmatrix} \equiv \frac{1}{2} \begin{pmatrix} h & s \end{pmatrix} M_{\text{scalar}} \begin{pmatrix} h \\ s \end{pmatrix} \tag{3.8}$$

The mixing between H and S leads to a non-diagonal mass matrix M_{scalar}. This matrix needs to be positive definite, so that the potential $V(H,S)$ is bounded from below; this corresponds to the requirement:

$$\det(M_{\text{scalar}}) > 0 \quad \rightarrow \quad \lambda_{hs} < 2\sqrt{\lambda_h \lambda_s} \tag{3.9}$$

Together with the perturbativity condition, this bound constrains the scalar couplings of the scalar potential (see [76] for details), and, consequentially, the mass of the physical Higgs bosons, which can be found diagonalizing M_{scalar} with a unitary rotation:

$$\begin{pmatrix} h \\ s \end{pmatrix} = \begin{pmatrix} c_\alpha & s_\alpha \\ -s_\alpha & c_\alpha \end{pmatrix} \begin{pmatrix} h_{mass} \\ s_{mass} \end{pmatrix}, \qquad t_{2\alpha} = -\frac{\lambda_{hs} v_h v_s}{\lambda_h v_h^2 - \lambda_s v_s^2} \tag{3.10}$$

The masses of the gauge bosons, instead, come from the kinetic term of the Higgs fields. Usually, the new scalar S is assumed to be neutral under the SM gauge group; if g' is the coupling constant associated with the Z' boson and z_s is the $U(1)'$ charge of S, then its covariant derivative reads:

$$D_\mu S = (\partial_\mu - i g' z_s Z'_\mu) S \tag{3.11}$$

A similar expression applies to the covariant derivative of the SM Higgs boson H. In models with multiple Higgs fields, the resulting mass matrix for the neutral gauge bosons will be of the form $M = \frac{1}{2} M^2_{\alpha\beta} Z_{\alpha,\mu} Z^{\mu}_{\beta}$, where:

$$M^2_{\alpha\beta} = g_\alpha g_\beta \sum_i z_{\alpha i} z_{\beta i} v_i^2 \tag{3.12}$$

where g_α is the coupling constant associated with the $U(1)_\alpha$ gauge symmetry group, and $z_{\alpha i}$ is the $U(1)_\alpha$ charge of the i-esim Higgs field with vev v_i.

The mass matrix for the neutral gauge bosons $(W^3_\mu, \hat{B}_\mu, \hat{Z'}_\mu)$ reads:

$$M^2_{W^3,\hat{B},\hat{Z'}} = \frac{v_h^2}{4} \begin{pmatrix} g^2 & -g_Y g & -2gg' z_h \\ -g_Y g & g_Y^2 & 2g_Y g' z_h \\ -2gg' z_h & 2g_Y g' z_h & \frac{4g'^2}{v_h^2}(z_h^2 v_h^2 + z_s^2 v_s^2) \end{pmatrix} \tag{3.13}$$

At this point, we can apply two different rotations in order to obtain the following change of basis:

$$\begin{pmatrix} W^3_\mu \\ \hat{B}_\mu \\ \hat{Z}'_\mu \end{pmatrix} \xrightarrow{\theta_{Z'}} \begin{pmatrix} W^3_\mu \\ B_\mu \\ Z'_\mu \end{pmatrix} \xrightarrow{\theta_W} \begin{pmatrix} A_\mu \\ Z_\mu \\ Z'_\mu \end{pmatrix} \tag{3.14}$$

The first rotation is due to the kinetic mixing term, while the second one is the usual mixing between the neutral SM gauge bosons parametrized by the Weinberg angle θ_W. In this way, the first row and column of $M^2_{W^3,\hat{B},\hat{Z'}}$ result vanishing, giving the eigenvalue $m_\gamma = 0$ for the photon A_μ. Therefore, we are left with the simpler diagonalization of the 2x2 lower right block; considering $z_h = 0$ for simplicity, we can write it as:

$$M^2_{Z,Z'} = \frac{v_h^2}{4} \begin{pmatrix} g_Z^2 & t_{Z'} g_Y g_Z \\ t_{Z'} g_Y g_Z & t_{Z'}^2 g_Y^2 + \frac{4g'^2}{c^2_{Z'} v_h^2} z_s^2 v_s^2 \end{pmatrix} \tag{3.15}$$

where $g_Z^2 = g^2 + g_Y^2$ is the coupling constant associated with the Z boson.

The mixing angle between the Z and Z' mass eigenstates can be expressed as:

$$\tan 2\beta = \frac{2 c_{Z'} s_{Z'} v_h^2 g_Y g_Z}{c^2_{Z'} g_Z^2 v_h^2 (1 - s_W^2 t^2_{Z'}) - 4g'^2 z_s^2 v_s^2} \tag{3.16}$$

Electro Weak Precision Tests [77] require this angle to be very small, $\beta \lesssim 10^{-3}$. Defining:

$$a = \frac{4g'^2}{c^2_{Z'} v_h^2} z_s^2 v_s^2, \tag{3.17}$$

the resulting mass eigenvalues are therefore:

$$m^2_{Z,Z'} = \frac{v_h^2}{8}\left[g_Z^2 + t^2_{Z'}g_Y^2 + a \pm \sqrt{(g_Z^2 + t^2_{Z'}g_Y^2 + a)^2 - 4ag_Z^2}\right]$$

$$= \begin{cases} \dfrac{g_Z^2 v_h^2}{4}\left(1 - \dfrac{v_h^2}{v_s^2}\dfrac{s^2_{Z'}g_Y^2}{4g'^2 z_s^2}\right) + \mathcal{O}\left(\dfrac{v_h^6}{v_s^4}\right) \\ \dfrac{g'^2 z_s^2 v_s^2}{c^2_{Z'}} + \dfrac{v_h^2}{4}t^2_{Z'}g_Y^2 + \mathcal{O}\left(\dfrac{v_h^4}{v_s^2}\right) \end{cases} \tag{3.18}$$

The results are approximate for $v_s > v_h$, motivated by the expectation $m_{Z'} > m_Z$.

3.1.3 Dark sector

The UV-completion of additional $U(1)'$ gauge symmetries commonly requires at least one new fermion χ which, if stable, could play the role of our DM candidate. New *exotic fermions* are predicted in the context of anomaly cancellation: all triangle anomalies involving the new Z' boson must vanish, as it already happens for the other gauge bosons of the SM (see Appendix A). Among the many different conditions coming from the mixing between the Z' boson and the SM ones, two of them must always be satisfied:

$$\sum_f z_f^3 = 0 \tag{3.19}$$

$$\sum_f z_f = 0 \tag{3.20}$$

Here, the z_f are the dark charges of the fermion f and we are working in a basis in which all fermions are left-handed Weyl spinors (right-handed fermions f_R are traded with their conjugate f^c, so their charges are flipped, $z_{f^c} = -z_{f_R}$). The (3.19) comes from the cancellation of the triangle diagram with 3 external Z', while the (3.20) comes from the mixed gauge-gravitational anomaly. An evident feature we can appreciate from the above equations is that the addition of a vector-like fermion pair ($z_f = -z_{f^c}$) does not affect the anomaly conditions.

The solution to these two Diophantine equations gives the set of charges for an arbitrary number of exotic fermions. The two equations are homogeneous and symmetric under charge permutations, thus a solution is given, without loss of generality, by a coprime set of charges that satisfy the following condition:

$$z_1 \geq |z_2| \geq \cdots \geq |z_n| \geq 1 \tag{3.21}$$

It is possible to demonstrate [78] that a general solution of the anomaly equations can be generated starting from two vector-like sets of fermions $\{\vec{x}\} = \{x_1, \ldots, x_n\}$ and $\{\vec{y}\} = \{y_1, \ldots, y_n\}$ through the following operation:

$$\{\vec{x}\} \oplus \{\vec{y}\} = \left(\sum_{i=1}^{n} x_i y_i^2\right)\{\vec{x}\} - \left(\sum_{i=1}^{n} x_i^2 y_i\right)\{\vec{y}\} \tag{3.22}$$

In particular, the solution for even n is generated by the sets ($m = n/2 - 1$):

$$\begin{aligned} \{\vec{v}_+\} &= \{l_1, k_1, \ldots, k_m, -l_1, -k_1, \ldots, -k_m\} \\ \{\vec{v}_-\} &= \{0, 0, l_1, \ldots, l_m, -l_1, \ldots, -l_m\} \end{aligned} \tag{3.23}$$

While for odd n we have ($m = (n-3)/2$):

$$\begin{aligned} \{\vec{u}_+\} &= \{0, k_1, \ldots, k_{m+1}, -k_1, \ldots, -k_{m+1}\} \\ \{\vec{u}_-\} &= \{l_1, \ldots, l_m, k_1, 0, -l_1 \ldots, -l_m, -k_1\} \end{aligned} \tag{3.24}$$

Thus, for any number n of chiral fermions, the set of dark charges can be parametrized by $n - 2$ integers.

Usually, the new exotic particles are taken to be chiral under the $U(1)'$ gauge symmetry, since vector current interactions are significantly constrained by direct detection experiments; on the other hand, they need to be non-chiral under the SM gauge group, in order to reduce the sensitivity to electroweak precision constraints. With these assumptions, the solution to the anomaly equations requires at least 3 new exotics [79]. The stability of the lightest one is a mandatory requirement, which is usually satisfied by some ad hoc discrete symmetry.

3.2 Models

We can describe in more detail some relevant models in the literature.

3.2.1 Sequential Dark Z'

One of the simplest models in the context of additional $U(1)'$ gauge symmetries is given by the so-called sequential dark Z' [72], in which the couplings of the Z' boson to SM fermions are the same of the SM Z boson. If we consider a Majorana fermion χ as our DM candidate, coupled with the Z' boson, the relevant part of the Lagrangian is then:

$$\mathcal{L}^S \supset \left[-g_\chi \overline{\chi}\gamma^\mu\gamma^5\chi - \sum_{f\in SM} \overline{f}\gamma^\mu(g_V^f + g_A^f\gamma^5)f\right] Z'_\mu \tag{3.25}$$

	Q_L^i	u_R^i	d_R^i	L_L^i	e_R^i	N_R^j	χ	H	S
$U(1)_{B-L}$	1/3	1/3	1/3	-1	-1	-1	-1	0	2
Z_2	$+$	$+$	$+$	$+$	$+$	$+$	$-$	$+$	$+$

Table 3.1: Particle content in the B-L model ($i = 1, 2, 3$ runs over the 3 SM generations, while N_R^j, $j = 1, 2$ and χ are the 3 right-handed neutrinos), with their respective dark charges and parity assignment.

where g_χ, g_V^f and g_A^f are the couplings associated respectively with the dark fermion χ (which, being a Majorana fermion, can only have axial-vector couplings), and the vector and axial-vector currents of each SM fermion f. The SM fermion couplings are given by:

$$g_V^f = \frac{e}{2c_W s_W}\left(T_3^f - 2s_W^2 Q^f\right) \tag{3.26}$$

$$g_A^f = \frac{e}{2c_W s_W} T_3^f \tag{3.27}$$

In this way, the number of free parameters is reduced to only three, being the DM and Z' boson masses m_χ and $m_{Z'}$ and the coupling g_χ. This model does not provide a UV-complete theory (the cross section of the annihilation $\chi\chi \to Z'Z'$ is in fact proportional to s, thus breaking perturbativity at relatively low energy), but it is nevertheless a simple and predictable setup which can be a useful reference when comparing constraints from different sources.

3.2.2 Majorana dark matter in B-L model

We give the general features of a DM scenario in which the SM gauge symmetry is extended with a $B - L$ gauge symmetry [80]; the theory is anomaly-free thanks to the introduction of 3 right-handed Majorana neutrinos and a supplementary Higgs field to break the $U(1)_{B-L}$ gauge symmetry. This theoretical setup has the great advantage of automatically implementing the seesaw mechanism for neutrino masses. Moreover, a Z_2 discrete symmetry is introduced to ensure the stability of one of the right-handed neutrinos, so that it is a viable DM candidate.

The Lagrangian in this model is very similar to the Lagrangian of the Sequential Dark Z' in Eq. (3.25), with just one difference: the axial-vector coupling of the SM fermions g_A^f is set to zero since in this case Z'_μ is associated to baryon and lepton numbers, which do not care about chirality.

The right-handed neutrinos gain their mass through Yukawa couplings:

$$\mathcal{L}^{B-L}_{Yuk} \supset \sum_{i=1}^{3}\sum_{j=1}^{2} y^{(\nu)}_{ij}\overline{L}^{i}_{L}\tilde{H}N^{j}_{R} - \frac{1}{2}\sum_{k=1}^{2} y^{M}_{k} S\overline{N^{kC}}_{R}N^{k}_{R} - \frac{1}{2}y^{M}_{\chi} S\overline{\chi^{C}}\chi + h.c. \tag{3.28}$$

where N^{i}_{R}, $i = 1, 2$ are the 2 Z_2-even neutrinos and χ is the Z_2-odd neutrino (which is also our DM candidate). $y^{(\nu)}_{ij}$ and y^{M}_{i} are respectively the Dirac and Majorana Yukawa coupling constants; because of its Z_2 oddity, χ cannot couple with the other leptons (all other particles are Z_2-even). After the spontaneous symmetry breaking of $U(1)_{B-L}$ and the electroweak symmetry breaking, Majorana and Dirac mass terms are generated for the neutrinos:

$$m^{D}_{ij} = \frac{y^{(\nu)}_{ij} v_h}{\sqrt{2}} \tag{3.29}$$

$$M^{M}_{k} = \frac{y^{M}_{k} v_s}{\sqrt{2}} \tag{3.30}$$

$$M_{\chi} = \frac{y^{M}_{\chi} v_s}{\sqrt{2}} \tag{3.31}$$

Thus, the neutrino mass matrix (excluding χ) reads:

$$M_{\nu} = \begin{pmatrix} 0 & m^{D} \\ (m^{D})^{T} & M^{M} \end{pmatrix} \tag{3.32}$$

In this way, the seesaw mechanism comes into play for the 2 N^{i}_{R}. Assuming $|m^{D}_{ij}| \ll M^{M}_{k}$, if we consider only one generation, we obtain one light and one heavy mass eigenvalues:

$$\begin{aligned} m_l &\simeq \frac{(m^{D})^2}{M^{M}} \\ m_h &\simeq M^{M} \end{aligned} \tag{3.33}$$

3.2.3 $U(1)_X$ for right-handed fermions

The introduction of a new $U(1)_X$ gauge symmetry to the SM gauge group is a possible way to explain the discrepancies between predictions and measurements of the muon anomalous magnetic moment [81, 82]. In this case, the Z' boson carrying the new interaction has flavor non-universal couplings to the SM fermions: in particular, we choose to charge only the second generation of right-handed fermions to minimize the number of free parameters needed [83].

The anomaly conditions are very important to determine the possible set of X charges: besides the (3.19) and (3.20), the anomaly equations involve also

	Q_L^i	L_L^i	u_R^2	d_R^2	e_R^2	χ_R	H	Φ	S
$U(1)_X$	0	0	-1	1	1	-1	0	-1	1

Table 3.2: Particle content and dark charges in the $U(1)_X$ model with charged second generation fermions. The remaining right-handed fields are neutral are uncharged. H and Φ have the same SM charges as the regular SM Higgs field, while S is a SM gauge singlet.

the mixing between $U(1)_X$ and the SM gauge groups $U(1)_Y$ and $SU(3)$; since only right-handed fields are charged under $U(1)_X$, the mixing with $SU(2)_L$ is not relevant. These equations are solved per generation, delivering the following solution:

$$X_{d_R} = 2X_{Q_L} - X_{U_R} \qquad X_{L_L} = -3X_{Q_L} \tag{3.34}$$

$$X_{e_R} = -2X_{Q_L} - X_{u_R} \qquad X_{\chi_R} = X_{u_R} - 4X_{Q_L} \tag{3.35}$$

It's immediate to check that the charges in Table 3.2 satisfy the above equations.

A fundamental consequence of the anomaly condition is that in order to build a consistent flavor non-universal theory, we need at least two Higgs doublets: H, which has Yukawa couplings with all fermions except for the ones charged under $U(1)_X$, and Φ, which is the one coupled with the second generation of right-handed fermions. A scalar singlet S is always needed to break the $U(1)_X$ gauge symmetry. Thus, the mass matrix (3.13) is slightly modified, but the rotation from flavor to mass basis is carried out in the same way we described in Section 3.1.2 (see [83] for detailed calculations).

The interaction between SM fermions and the mass eigenstate Z'_μ can be written as:

$$\begin{aligned}\mathcal{L}^X \supset & \left[g_U^f \sum_f (\overline{f}_R \gamma^\mu f_R + \overline{f}_L \gamma^\mu f_L)\right] Z'_\mu \\ & - c_\beta g' \left[\sum_{f=u,d,e} \overline{f}_R \mathbb{F}^f \gamma^\mu f_R\right] Z'_\mu + c_\beta g' \overline{\chi}_R \gamma^\mu \chi_R Z'_\mu\end{aligned} \tag{3.36}$$

In the above equation, we have separated the flavor universal and non-universal contributions to the coupling between SM fermions and Z'_μ. In fact, we have defined:

$$g_U^f = s_\beta g_Z + c_\beta t_{Z'} g_Y Y_f \tag{3.37}$$

where the angles β and $\theta_{Z'}$ are defined in (3.16) and (3.1) and Y_f is the hypercharge of the fermion f. The second term, instead, is non-diagonal in the flavor space, thanks to the matrix:

$$\mathbb{F}^f = \mathbb{R}_f^\dagger \mathbb{X}^f \mathbb{R}_f, \qquad \mathbb{X}^f_{ij} = X^f \delta_{2i}\delta_{2j} \tag{3.38}$$

The matrices $\mathbb{R}_f$ are the ones that rotate the SM fermions from flavor to mass basis (in the SM, they appear mainly in the CKM matrix). The matrices $\mathbb{F}^f$ enclose the amount of flavor non-universality of the model, thus being very important when analyzing flavor violating processes.

Chapter 4

Phenomenology

In this chapter, we describe some particular models involving DM particle candidates which interact via an additional Z' gauge boson.

We begin with a deeper analysis of the benchmark model presented in [79]. In this model, the main features of the new exotic fermions are guided by anomaly cancellation: we require, in fact, that all anomalies between the newly introduced $U(1)'$ gauge group and the usual SM gauge group $G_{SM} = SU(3)_c \times SU(2)_L \times U(1)_Y$ vanish. These conditions lead to the following relation:

$$\sum_{i=1}^{n} \left(z_{\chi_i}\right)^3 = \frac{1}{9}\left(\sum_{i=1}^{n} z_{\chi_i}\right)^3 \tag{4.1}$$

This equation is valid for any number n of dark fermions (a general solution can be found in [78]); we choose to analyze the simple case with 3 dark fermions χ_i with equal charges $z_{\chi_i} = 1$. The new $U(1)'$ gauge symmetry is mediated by the gauge boson V_μ and it is spontaneously broken at high energy by the non-vanishing vacuum expectation value of a dark Higgs field S. The exotic fermions are SM gauge singlets, which acquire mass thanks to a Majorana mass term with the dark Higgs field. Thus, the dark sector can be described by the following Lagrangian:

$$\mathcal{L} = -g'\left[\sum_{i=1}^{3} z_{\chi_i}\overline{\chi}_i\gamma^\mu\gamma^5\chi_i + \sum_{f\in SM}\left(z_L^f\overline{f}_L\gamma^\mu f_L + z_R^f\overline{f}_R\gamma^\mu f_R\right)\right]V_\mu \tag{4.2}$$

Being Majorana spinors, the χ_i can only have axial-vector couplings with Z'. The dark charges of the SM fermions are not totally free, since they also need to satisfy the anomaly cancellation conditions and the gauge invariance of the Yukawa sector; considering flavor universal charges, we can choose them to be:

$$\{z_{Q_L}, z_{u_R}, z_{d_R}, z_{L_L}, z_{e_R}\} = \{0, -1, 1, 0, 1\} \tag{4.3}$$

	Q_L^i	u_R^i	d_R^i	L_L^i	e_R^i	χ_i	H	S
$U(1)'$	0	-1	1	0	1	-1	-1	1

Table 4.1: Dark charges for the benchmark model of [79].

The dark charges of the Higgs bosons are instead:

$$z_h = -1, \qquad z_s = 1 \tag{4.4}$$

The Higgs sector consists of the SM Higgs field H and of the dark Higgs S which is also a SM gauge singlet. The Lagrangian is the same exposed in Eq. (3.4), from which we report the most relevant part for the processes we are going to study:

$$\mathcal{L}_{Higgs} \supset \frac{(v_h + h)^2}{2}\left(\frac{g_Z}{2} Z_\mu^{(SM)} + g' V_\mu\right)^2 \tag{4.5}$$

The mass eigenstates for the neutral and the Higgs bosons are given by the following rotations:

$$\begin{pmatrix} h \\ s \end{pmatrix} \to \begin{pmatrix} c_\alpha & s_\alpha \\ -s_\alpha & c_\alpha \end{pmatrix} \begin{pmatrix} h \\ s \end{pmatrix} \tag{4.6}$$

$$\begin{pmatrix} Z_\mu^{(SM)} \\ V_\mu \end{pmatrix} \to \begin{pmatrix} c_\beta & s_\beta \\ -s_\beta & c_\beta \end{pmatrix} \begin{pmatrix} Z_\mu \\ Z'_\mu \end{pmatrix} \tag{4.7}$$

In this case, we are neglecting the kinetic mixing between the neutral gauge bosons V_μ and $Z_\mu^{(SM)}$ (since it is loop suppressed); the mass mixing angles of the two rotations are (we can notice the difference with Eq. (3.16) in which we considered $z_h = 0$):

$$\tan 2\alpha = -\frac{\lambda_{hs} v_h v_s}{\lambda_h v_h^2 - \lambda_s v_s^2} \tag{4.8}$$

$$\tan 2\beta = \frac{4 g_Z g' z_h v_h^2}{4 g'^2 (z_h^2 v_h^2 + z_s^2 v_s^2) - g_Z^2 v_h^2} \tag{4.9}$$

Due to the strict experimental limits [77] on the neutral bosons mixing angle ($\beta \lesssim 10^{-3}$), in the following calculations we will take the limit $\beta \simeq 0$. The Higgs-dark Higgs mixing angle α is constrained by the observed Higgs signal strength: the mass-independent upper limit can be set to be $\alpha < 0.34$ at 95% CL [84, 85].

Finally, the Yukawa sector for the χ_i reads:

$$\mathcal{L}_{Yuk} = -\frac{1}{2} y_{\chi_i} S \overline{\chi_i^C} \chi_i \overset{SSB}{=} -\frac{1}{2} m_{\chi_i} \overline{\chi_i^C} \chi_i - \frac{y_{\chi_i}}{2\sqrt{2}} s \overline{\chi_i^C} \chi_i \tag{4.10}$$

where the DM mass is:

$$m_{\chi_i} = \frac{y_{\chi_i} v_s}{\sqrt{2}} \tag{4.11}$$

Altogether, the Lagrangian gives rise to the following Feynman rules for the Z' and s bosons:

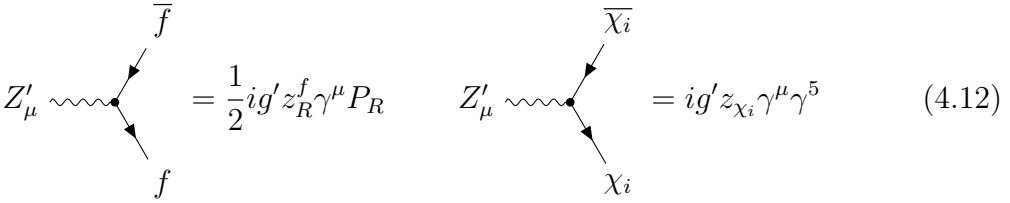

(4.12)

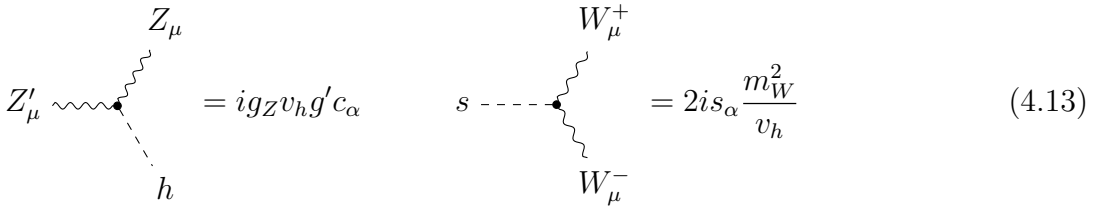

(4.13)

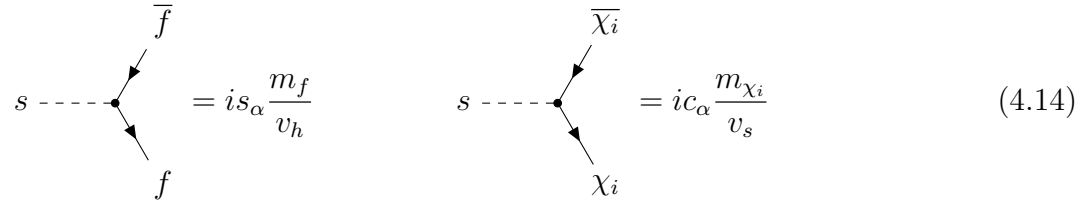

(4.14)

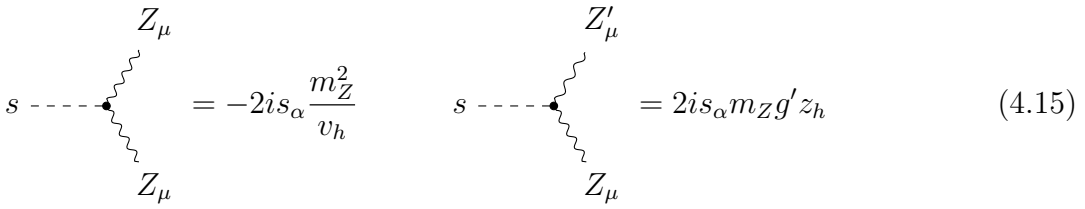

(4.15)

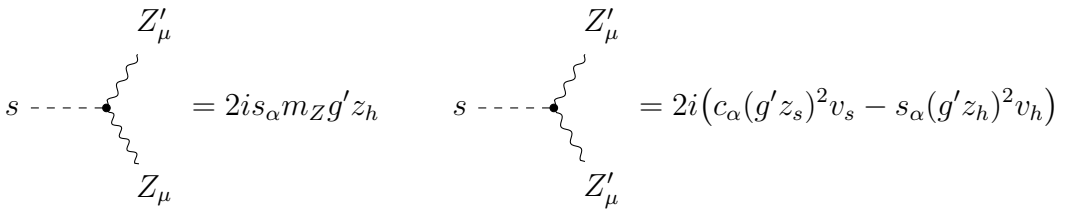

(4.16)

Notice that all left-handed fields are neutral under $U(1)'$, thus the coupling with the Z' boson only involves right-handed fermions.

4.1 Decay rates

Before entering the calculation on the cross section, we need to calculate the decay width of the two new mediators Z'_μ and s.

The allowed decay channels for the Z'_μ boson are into $\overline{f}f$, $\overline{\chi_i}\chi$ and Zh. As an example, we can explicitly calculate the Feynman amplitudes for the decay into a fermion pair thanks to the Feynman rules obtained before.

$$\mathcal{M}(Z' \to \overline{f}f) = \quad = \frac{1}{2} i g' \overline{u}(p_1) \left[z_R^f \gamma^\mu P_R \right] v(p_2) \epsilon_\mu \tag{4.17}$$

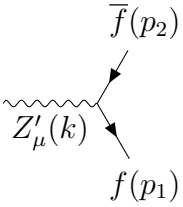

Averaging over the initial spin polarizations of the particle, we get the following squared Feynman amplitude:

$$|\overline{\mathcal{M}}|^2 = \frac{2(g' z_R^f)^2 N_c^f}{3} \left(m_{Z'}^2 - m_f^2 \right) \tag{4.18}$$

where N_c^f is the color multiplicity of the final fermions (which is equal to 3 for quarks and 1 for leptons). Thus the decay rate is given by:

$$\Gamma(Z' \to \overline{f}f) = \frac{1}{16\pi} \left[1 - \frac{4m_f^2}{m_{Z'}^2} \right]^{\frac{1}{2}} \frac{2(g' z_R^f)^2 N_c^f}{3 m_{Z'}} \left(m_{Z'}^2 - m_f^2 \right) \tag{4.19}$$

The decay rates for the remaining channels assume a very similar form. We show the Z' branching ratios on the left panel in Fig. 4.1: we can see that the rate is dominated by the decay into a SM fermion pair (in particular quarks, due to their color multiplicity), even when the $\chi\chi$ channel is kinematically allowed.

The s boson has more decay channels due to its non-zero mixing with the h boson (right panel ofFig. 4.1): however, decay rates into SM particles are suppressed by the Higgs mixing angle α; as a result, the rate is dominated by the decay into $\chi\chi$ and $Z'Z'$.

4.2 Cross section

We can define the cross section in the center of mass frame for the annihilation of two particles in the following way:

$$\sigma I = \frac{1}{16\pi^2} \frac{|\vec{k}|}{\sqrt{s}} \int \overline{|\mathcal{M}|}^2 d\Omega \tag{4.20}$$

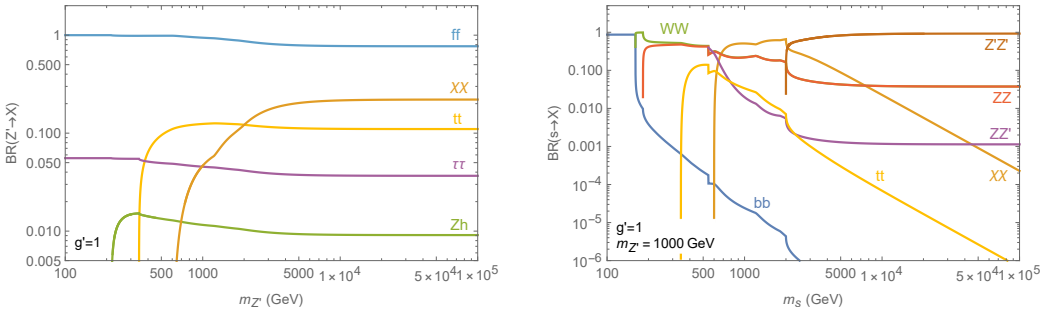

Figure 4.1: Branching ratios for the Z' gauge boson (left) and the dark Higgs s boson (right). For both calculations, we took into consideration 3 DM particles with mass $m_\chi = 300$, 600 and 900 GeV.

where $I = 4g^2\sqrt{(p_1 \cdot p_2)^2 - m^4} = 4g^2|\vec{p}|\sqrt{s}$ is the covariant flux factor (g is the number of degrees of freedom of the incoming particles with momenta p_1 and p_2) and $\vec{k}$ is the outgoing 3-momentum; s is the Mandelstam variable $(p_1 + p_2)^2$.

It is useful to expand the expression (4.20) in the low-velocity limit, since we need the annihilation cross section at freeze-out times, when DM particles were already non-relativistic. σI is a function of s, which in turn can be expanded as:

$$s = m_{\chi_i}^2(4 + v^2) + \mathcal{O}(v^4) \tag{4.21}$$

This means that the cross section will contain only even powers of the velocity v; therefore, we can always expand the annihilation cross section in the following way:

$$\sigma I \simeq a + bv^2 \tag{4.22}$$

a and b are respectively the s-wave and p-wave components of the annihilation cross section.

4.2.1 Z' mediated processes

DM can communicate with the SM particles either through the Z' boson or the s boson, but the freeze-out is mainly dominated by Z' mediated processes; in this section, we discuss the most relevant annihilation channels involving this mediator, like the annihilation into SM fermions (which represents the dominant contribution) and the annihilation into a Z and an h boson (which is, instead, a sub-dominant process). Other processes are suppressed by the neutral bosons mixing angle β.

The Feynman amplitude for the $\overline{\chi_i}\chi_i \to Z' \to \overline{f}f$ process can be written in

the following way:

$$\mathcal{M}(\overline{\chi_i}\chi_i \to Z' \to \overline{f}f) = \quad = \quad \begin{aligned} &= \overline{v}(p_2)(ig' z_{\chi_i}\gamma^\mu\gamma^5)u(p_1)\left(-\eta_{\mu\nu} + \frac{q_\mu q_\nu}{m_{Z'}^2}\right)\frac{i}{q^2 - m_{Z'}^2 + i\Gamma_{Z'}m_{Z'}}\times \\ &\qquad \times\overline{u}(k_2)\frac{1}{2}ig'\left[z_R^f\gamma^\mu P_R\right]v(k_1) \end{aligned} \tag{4.23}$$

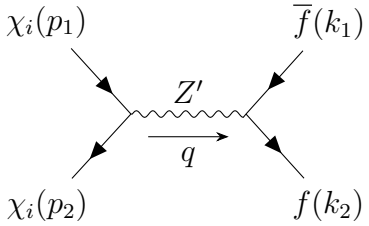

The $q_\mu q_\nu/m_{Z'}^2$ term gives a contribution proportional to $m_\chi m_f/m_{Z'}^2$: in the low energy limit($q^2 = s \gtrsim 4m_\chi^2$), we can neglect this contribution.

$$\begin{aligned} \overline{|\mathcal{M}|}^2_{\chi\chi\to ff} = &\frac{8(g' z_{\chi_i})^2(g' z_R^f)^2 N_c^f}{(s - m_{Z'}^2)^2 + \Gamma_{Z'}^2 m_{Z'}^2}\times \\ &\times\left[\frac{s^2}{4} + 4\left(\frac{s}{4} - m_{\chi_i}^2\right)\left(\frac{s}{4} - m_f^2\right)\cos^2\theta - m_{\chi_i}^2 s + 2m_{\chi_i}^2 m_f^2\right] \end{aligned} \tag{4.24}$$

θ is the angle between the 2 outgoing particles. The cross section can now be easily calculated using Eq. (4.20); then, expanding in the low-velocity limit, we obtain the following results for the a and b coefficients:

$$\begin{cases} a = \dfrac{2}{\pi}(g' z_{\chi_i})^2(g' z_R^f)^2 N_c^f \dfrac{\sqrt{1-\phi^2}}{(4\xi^2-1)^2 + \Gamma_{Z'}^2/m_{Z'}^2}\dfrac{m_{\chi_i}^2 m_f^2}{m_{Z'}^4} \\ b = \dfrac{1}{2\pi}(g' z_{\chi_i})^2(g' z_R^f)^2 N_c^f \dfrac{\sqrt{1-\phi^2}}{(4\xi^2-1)^2 + \Gamma_{Z'}^2/m_{Z'}^2}\times \\ \quad\times\left[\dfrac{8m_{\chi_i}^4}{3m_{Z'}^4} + \dfrac{m_{\chi_i}^2 m_f^2}{m_{Z'}^4}\left(-\dfrac{2}{3} + \dfrac{\phi^2}{2(1-\phi^2)} - \dfrac{8\xi^2(4\xi^2-1)}{(4\xi^2-1)^2 + \Gamma_{Z'}^2/m_{Z'}^2}\right)\right] \end{cases} \tag{4.25}$$

where we have defined the quantities $\phi = m_f/m_{\chi_i}$ and $\xi = m_{\chi_i}/m_{Z'}$.

The same procedure is applied to the annihilation into a Z and an h boson:

$$\begin{aligned} \overline{|\mathcal{M}|}^2_{\chi\chi\to Zh} = &\frac{4(g' z_{\chi_i})^2(g' g_Z z_h v_h)^2}{(s - m_{Z'}^2)^2 + \Gamma_{Z'}^2 m_{Z'}^2}\left[\frac{s}{2} - 4m_{\chi_i}^2 + \right. \\ &\left. + \frac{2}{m_Z^2}\left(\frac{s}{4}(m_Z^2 + |\vec{k}|^2) - \left(\frac{s}{4} - m_{\chi_i}^2\right)|\vec{k}|^2\cos^2\theta\right)\right] \end{aligned} \tag{4.26}$$

Here, $|\vec{k}|^2$ is the modulus of the 3-momentum of the outgoing particles in the center of mass frame. The final result in the low-velocity limit is:

$$\begin{cases} a = \dfrac{1}{8\pi}(g' z_{\chi_i})^2 (g' g_Z v_h)^2 \dfrac{1}{m_{Z'}^4} \dfrac{1}{(4\xi^2-1)^2 + \Gamma_{Z'}^2/m_{Z'}^2} \dfrac{\tilde{m}^{3/2}}{8 m_Z^2 m_{\chi_i}^2} \\ b = \dfrac{1}{8\pi}(g' z_{\chi_i})^2 (g' g_Z v_h)^2 \dfrac{\tilde{m}^{1/2}}{m_{Z'}^4 m_{\chi_i}^2} \left[\dfrac{1}{(4\xi^2-1)^2 + \Gamma_{Z'}^2/m_{Z'}^2} \times \right. \\ \quad \times \left(m_{\chi_i}^2 + \dfrac{\tilde{m}}{48 m_Z^2} + \dfrac{m_{\chi_i}^4}{2 m_Z^2} + \dfrac{m_{\chi_i}^2}{8 m_Z^2}(m_Z^2 + m_h^2) - \dfrac{(m_Z^2 - m_h^2)^2}{16 m_Z^2} \right) - \\ \quad \left. - \dfrac{\tilde{m}}{8 m_Z^2} \dfrac{1}{m_{Z'}^4} \dfrac{2\xi^2(4\xi^2-1)}{\left((4\xi^2-1)^2 + \Gamma_{Z'}^2/m_{Z'}^2\right)^2} \right] \end{cases} \tag{4.27}$$

where we have defined:

$$\tilde{m} = \left(m_Z^2 + m_h^2\right)^2 - 2 m_h^2 (m_Z^2 + 4 m_\chi^2) + m_h^4 \tag{4.28}$$

4.2.2 s mediated processes

DM annihilations into the SM sector can also be mediated by the dark Higgs boson s. The s boson, however, does not directly couple with SM particles: interactions with the SM particles can occur only due to the Higgs bosons mixing (Eq. (4.6)). For this reason, the cross section for this type of processes is suppressed by the Higgs-dark Higgs mixing angle α; in any case, these processes can become relevant in resonant scenarios.

The Feynman amplitude for the annihilation into a pair of SM fermions is the following:

$$\mathcal{M}(\overline{\chi_i}\chi_i \to s \to \overline{f} f) =$$

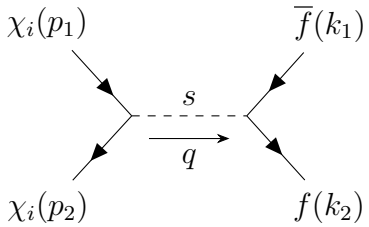

$$= c_\alpha \frac{m_{\chi_i}}{v_s} \overline{v}(p_2) u(p_1) \frac{-i}{q^2 - m_s^2 + i\Gamma_s m_s} s_\alpha \frac{m_f}{v_h} \overline{u}(k_2) v(k_1) \tag{4.29}$$

$$\overline{|\mathcal{M}|}^2_{\chi\chi \to ff} = \frac{16 N_c^f c_\alpha^2 s_\alpha^2}{(s - m_s^2)^2 + \Gamma_s^2 m_s^2} \frac{m_{\chi_i}^2 m_f^2}{v_s^2 v_h^2} \left(\frac{s}{2} - 2 m_{\chi_i}^2\right) \left(\frac{s}{2} - 2 m_f^2\right) \tag{4.30}$$

In the low-velocity limit, we obtain:

$$\sigma_{\chi\chi\to ff} I = \frac{2}{\pi} N_c^f c_\alpha^2 s_\alpha^2 \frac{m_{\chi_i}^2 m_f^2}{v_s^2 v_h^2} \frac{m_{\chi_i}^4 (1-\phi^2)^{3/2}}{(4m_{\chi_i}^2 - m_s^2)^2 + \Gamma_s m_s^2} v^2 \tag{4.31}$$

The other relevant annihilation channel mediated by the s boson is the production of two W bosons, for which we have:

$$\overline{|\mathcal{M}|}^2_{\chi\chi\to WW} = \frac{16 c_\alpha^2 s_\alpha^2}{(s-m_s^2)^2 + \Gamma_s^2 m_s^2} \frac{m_{\chi_i}^2 m_W^4}{v_s^2 v_h^2} \left(\frac{s}{2} - 2m_{\chi_i}^2\right)\left(3 - \frac{s}{m_W^2} + \frac{s^2}{4m_W^4}\right) \tag{4.32}$$

$$\sigma_{\chi\chi\to WW} I = \frac{1}{\pi} c_\alpha^2 s_\alpha^2 \frac{m_{\chi_i}^4}{v_s^2 v_h^2} \frac{(1-\phi^2)^{3/2}}{(4m_{\chi_i}^2 - m_s^2)^2 + \Gamma_s m_s^2} \left(3m_W^4 - 4m_{\chi_i}^2 m_W^2 + 4m_{\chi_i}^4\right) v^2 \tag{4.33}$$

Notice that s mediated annihilations are p-wave, thus they are further suppressed with respect to the Z' mediated processes described in the previous section. In any case, we can also notice that the cross sections 4.31 and 4.33 are enhanced in correspondence with the resonance $m_s \simeq 2m_{\chi_i}$, therefore their contribution cannot be neglected.

4.2.3 Searches at colliders

Signals for the existence of an additional neutral vector boson are actively searched for at colliders (in particular at the LHC): even at the highest collision energies, no deviation from the SM predictions has been found yet [86, 87]. In any case, the collected data can be used to put bounds on our model.

The strongest bounds on the mass of the Z' boson come from the search for dilepton resonances at the LHC [86]: the process $h_1 h_2 \to Z' + X \to l^+ l^- + X$ provides two very clean channels to look for ($l = e, \mu$), for which the irreducible background is dominated by the well-understood SM Drell-Yan process (Fig. 4.2).

The cross section for the $q\bar{q} \to Z' \to l^+ l^-$ process reads [88]:

$$\sigma(q\bar{q} \to Z' \to l^+ l^-) = \frac{g'^4}{(Q^2 - m_{Z'}^2)^2 + m_{Z'}^2 \Gamma_{Z'}^2} \frac{1}{9\pi} \frac{Q^2}{16} (z_R^q)^2 (z_R^l)^2 \tag{4.34}$$

To obtain the cross section for the Drell-Yan process, we need to convolute the hard quark scattering with the parton distribution functions (PDFs):

$$\begin{aligned} &\sigma(h_1 h_2 \to Z' + X \to l^+ l^- + X) = \\ &= \sum_{q=u,d} \int_0^1 dx_1 \int_0^1 dx_2 \left[f_{q/h_1}(x_1) f_{\bar{q}/h_2}(x_2) + f_{\bar{q}/h_1}(x_1) f_{q/h_2}(x_2) \right] \sigma(q\bar{q} \to Z' \to l^+ l^-) \end{aligned} \tag{4.35}$$

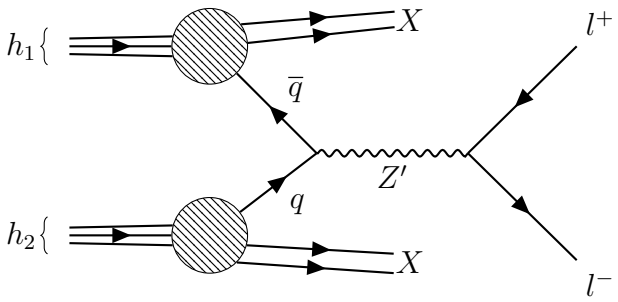

Figure 4.2: The Drell-Yan process mediated by a Z' boson.

In narrow width approximation, we can write this cross section as:

$$\sigma(h_1 h_2 \to Z' + X \to l^+ l^- + X) = \frac{\pi}{6s}\left[c_u w_u(s, m_{Z'}^2) + c_d w_d(s, m_{Z'}^2)\right] \tag{4.36}$$

here, $s = (p_1 + p_2)^2$, where p_i is the 4-momentum of h_i, and the quantities c_q and w_q are defined in the following way:

$$c_q = g'^2 (z_R^q)^2 \,\mathrm{BR}(Z' \to l^+ l^-), \quad \mathrm{BR}(Z' \to l^+ l^-) = \frac{\Gamma_{Z'}(Z' \to l^+ l^-)}{\Gamma_{Z'}} \tag{4.37}$$

$$w_q(s, m_{Z'}^2) = \int_0^1 dx_1 \int_0^1 dx_2 \left[f_{q/h_1}(x_1) f_{\bar{q}/h_2}(x_2) + f_{\bar{q}/h_1}(x_1) f_{q/h_2}(x_2)\right] \delta\left(\frac{m_{Z'}^2}{s} - x_1 x_2\right) \tag{4.38}$$

In this way, we managed to separate the model-dependent part of the cross section (encompassed in c_q) from the PDFs in w_q. Equation (4.36) can therefore be used to search for resonances in the dilepton spectrum of pp collisions, thus putting bounds on the free parameter of the theory if no excess of events is detected.

4.3 Relic density

From the low-velocity limit of the cross section, it is easy to get the following formula for the thermally averaged cross section (see Appendix B for the details):

$$\langle \sigma v \rangle = \frac{1}{4 g^2 m_{\chi_i}^2}\left(a + \frac{3(16b - a)}{8x}\right) \tag{4.39}$$

where g is the number of degrees of freedom of the DM particle and $x = m_{\chi_i}/T$. Inserting this expression in the Boltzmann equation, we can find a numerical solution to be compared to the experimental limits (the plots in the following pages are obtained employing `Mathematica`).

The free parameters that characterize our model are the following: the dark coupling constant g', the Higgs-dark Higgs mixing α and the masses of the new particles of our model, namely $m_{Z'}$, m_s and m_{χ_i}. Imposing that a given set of parameters reproduces the observed relic abundance $\Omega_\chi h^2 = 0.12$, we can get a better understanding of the relevance of the various constraints. The analysis of the relic density of just one DM particle species can already give a lot of information: in Fig. 4.3 we can see that the curve that reproduces the correct relic abundance lies well within the region excluded by the ATLAS experiment (the limits were extracted by [86]); even in correspondence of the s resonant region ($m_s = 2m_\chi$), the relic density is not able to evade the ATLAS limits. It's interesting to note that, on the left panel of Fig. 4.3, the variation of the Higgs-dark Higgs mixing angle doesn't really affect the final relic density: in fact, in this case the dominant contribution comes from the Z' channel, in particular from the annihilation into SM fermions, since the s mediated channels are suppressed by s_α. This behavior changes for heavy Z' masses $m_{Z'} > 4\,\text{TeV}$: at this point, the Z' mediated channels are heavily disfavoured (since the cross section is proportional to $1/m_{Z'}^4$), thus the s mediated ones become more relevant. A different behavior is observed on the right panel: since, in this case, $m_s = 2m_\chi$, the cross section of the s mediated processes is greatly enhanced, thus becoming the dominant contribution to the relic density.

The above analysis suggests that, in this model, a relic abundance compatible with the actual experimental limits can only be achieved nearby the mediator resonances (if we don't consider the $m_{Z'} > 6\,\text{TeV}$ region, for which we have no experimental limits yet). This feature is even clearer if we look at the bottom panel of Fig. 4.3. As a consequence, the existence of 3 different exotic fermions represents a great tuning problem, since, for the same reason explained above, all of their masses should be tuned to the mass of the Z' or the s boson. The 3 different χ_i, in fact, do not mix with each other, thus they are all stable and they all contribute to the final relic density. At the top of Fig. 4.4, for example, we show the parameter values for 3 DM particles with mass $2, 3$ and $4\,\text{TeV}$ for two different values of the s boson mass: in these cases, there is always at least one fermion outside the resonant regions, which therefore gives the dominant contribution to the relic density. As a result, large values of the dark coupling g' (around the unity) are required for any range of the Z' or the s boson masses. On the other hand, we can look at the extremely degenerate case in which all the 3 exotic fermions have the same mass $m_\chi = 2m_s$ (bottom panels of Fig. 4.4): in these cases, the relic density is able to peak outside the ATLAS excluded region (for $m_{Z'} \simeq m_s$).

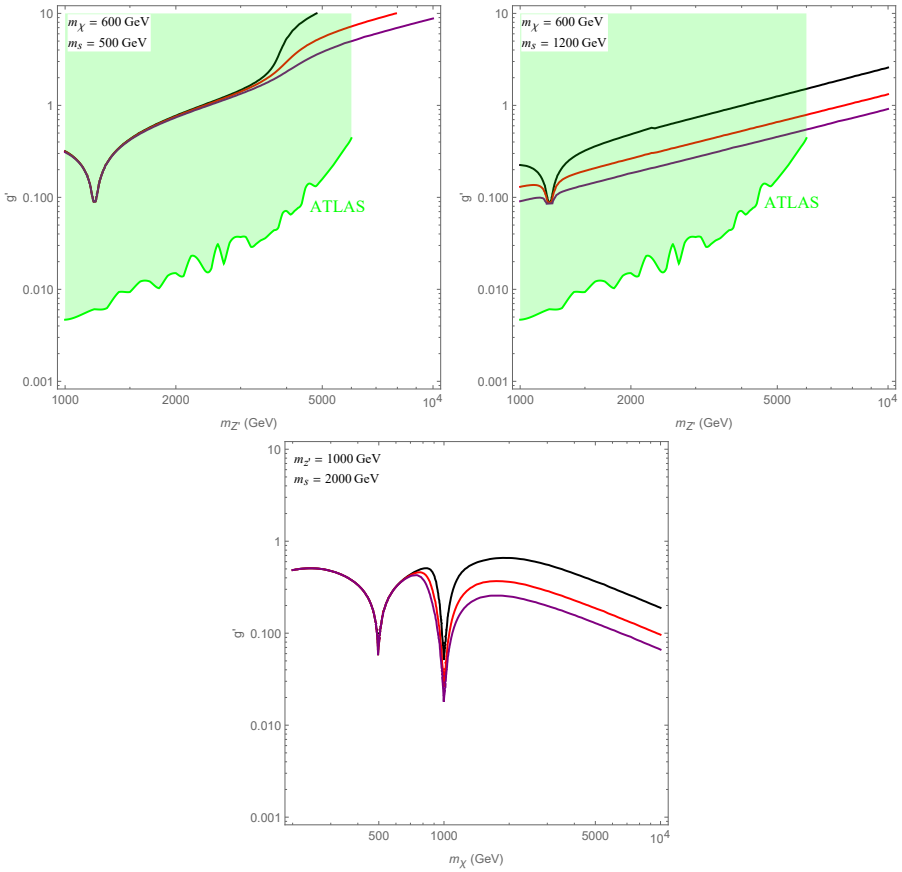

Figure 4.3: At the top, parameter values for which $\Omega_\chi h^2 = 0.12$ in the $m_{Z'} - g'$ plane.The green shaded region is excluded by ATLAS [86]. At the bottom, the constraints are shown in the $m_\chi - g'$ plane. The black, red and purple lines correspond to different values of the Higgs-dark Higgs mixing ($\alpha = 0.1, 0.2, 0.3$ respectively).

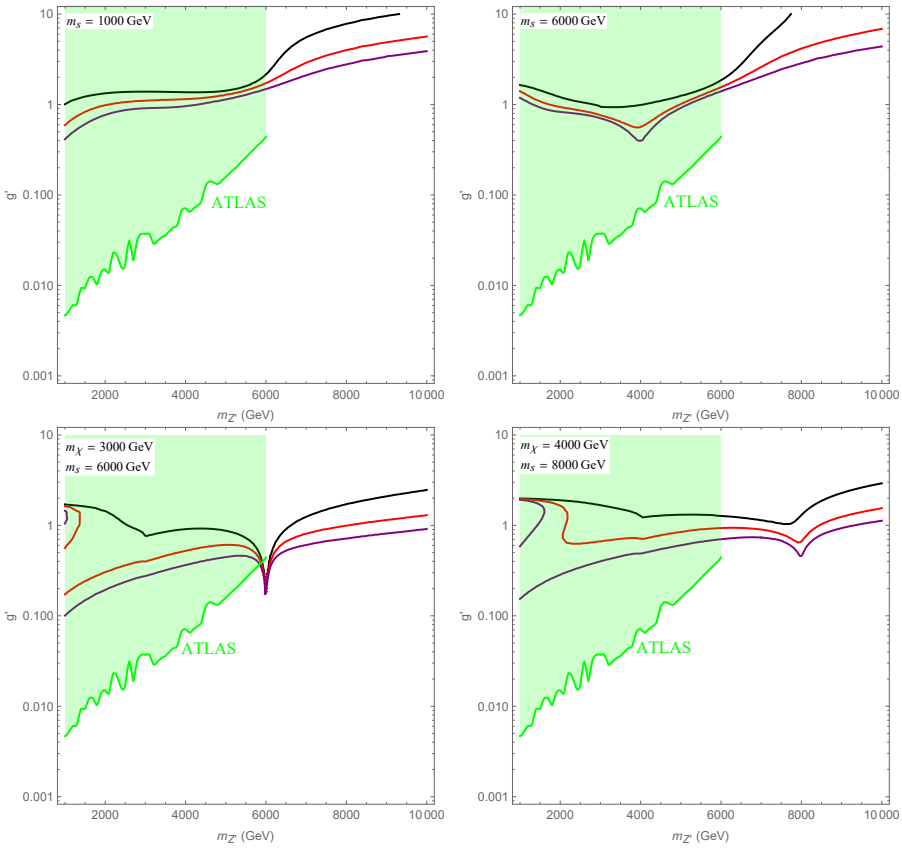

Figure 4.4: At the top, parameter values for which $\Omega_\chi h^2 = 0.12$ for 3 dark fermions with masses $m_\chi = 2, 3, 4\,\text{TeV}$ in the $m_{Z'} - g'$ plane, for dark Higgs masses $m_s = 1\,\text{TeV}$ and $m_s = 6\,\text{TeV}$ respectively. At the bottom, the relic density for the degenerate cases in which all the 3 dark fermions share the same mass ($m_\chi = 3\,\text{TeV}$ and $m_\chi = 4\,\text{TeV}$ respectively) and $m_s = 2m_\chi$. The green shaded region is excluded by ATLAS [86]. The black, red and purple lines correspond to different values of the Higgs-dark Higgs mixing ($\alpha = 0.1, 0.2, 0.3$ respectively).

4.4 Conclusions

In conclusion, we can say that the predictions from this model of production of DM by thermal freeze-out do not evade the actual experimental limits for sub-TeV masses of the 3 exotic fermions and the two mediators; only resonant scenarios can accommodate the relic abundance with the bounds imposed by ATLAS, although a high degree of degeneracy is required. In any case, further investigation is needed to test the multi-TeV spectrum of the theory, which is in the reach of future colliders (like FCC [89] or a Muon Collider [90]).

Chapter 5

Conclusions

In this thesis, we took a deep dive into Dark Matter physics, exploring the so-called vector portal models in an anomaly-free theoretical framework and studying their phenomenology in order to exploit the experimental constraints coming from particle colliders.

In Chapter 1 we recalled the main evidence for the existence of invisible matter in the universe, which does not interact with light and which actually represents the major component of the matter content of the universe. Thanks to cosmological observations, we recognized this type of matter as being of non-baryonic origin, thus requiring beyond-the-Standard-Model physics to explain it; a list of the most popular particle candidates is provided in Section 1.5.

Among them, we chose to focus around the leading paradigm of WIMPs, which is one of the best known in the literature due to its simplicity and large number of motivated candidates. In Chapter 2 we outlined both the theoretical features that describe their phenomenology (namely the freeze-out mechanism) and the different experimental strategies employed to find a WIMP signal.

Next, in Chapter 3 we explored in more detail the vector portal WIMP models, a theoretical framework in which Dark Matter is connected to the Standard Model by the means of a new vector boson Z', mediator of a newly introduced $U(1)$ gauge symmetry group; particular emphasis has been put on the anomaly cancellation, a mandatory requirement for a self-consistent theory, that drives the set of charges of the different particles.

Finally, in Chapter 4 is located the original part of this thesis: we studied a rather general model which involves the introduction of 3 exotic fermions in the dark sector, a new neutral vector boson Z' and a dark Higgs s; we described the main annihilation channels of the dark fermions and how they impact the final relic density through the Boltzmann equation; the results were then compared to the most recent experimental bounds. We found out that the predicted relic density lies in a region of the parameter space excluded by ATLAS measurements

on the Drell-Yan process for sub-TeV masses of the 3 exotic fermions. Nevertheless, the multi-TeV spectrum of the theory can still deliver signals for a new massive particle, especially in resonant scenarios; this opens up new exciting possibilities for future experiments, which will be able to tackle the high energies required to explore this field in the following years.

Appendix A

Standard Model

In this appendix, we present a quick review of the Standard Model (SM) of particle physics (this chapter is based on [91], on which a much more extensive approach can be found).

The SM is a gauge theory based on the following gauge group:

$$G_{SM} = SU(3)_c \times SU(2)_L \times U(1)_Y \tag{A.1}$$

Thanks to the Higgs potential, the group is spontaneously broken into:

$$G_{SM} \to G_{SM}^{SSB} = SU(3)_c \times U(1)_{em} \tag{A.2}$$

Each factor of G_{SM} describes a different type of interaction, and brings a number of gauge bosons equal to the number of generators of that symmetry group. The resulting number of gauge bosons counts:

- 8 gluons for $SU(3)_c$ color interactions; this symmetry group is conserved after the SSB, so gluons stay massless;
- 4 gauge bosons for the $SU(2)_L \times U(1)_Y$ electroweak interactions, which after the SSB are rearranged in three massive weak bosons ($W^{\pm}$, Z) and one massless photon γ.

The only other boson present in the SM is the Higgs boson h, which is also the only known scalar particle: it was the last missing piece to be added to the SM, discovered only in 2012 [92].

Finally, the particle content of the SM is completed by fermions, which are denoted hereafter:

$$Q_L^i = \left\{ \begin{pmatrix} u_L \\ d_L \end{pmatrix}, \begin{pmatrix} c_L \\ s_L \end{pmatrix}, \begin{pmatrix} t_L \\ b_L \end{pmatrix} \right\} \qquad L_L^i = \left\{ \begin{pmatrix} \nu_{e,L} \\ e_L \end{pmatrix}, \begin{pmatrix} \nu_{\mu,L} \\ \mu_L \end{pmatrix}, \begin{pmatrix} \nu_{\tau,L} \\ \tau_L \end{pmatrix} \right\}$$
$$u_R^i = \{u_R, c_R, t_R\} \qquad e_R^i = \{e_R, \mu_R, \tau_R\}$$
$$d_R^i = \{d_R, s_R, b_R\}$$

On the left, **quarks** are displayed: these particles are charged under the $SU(3)_c$ gauge group, and for this reason, they also possess three further color indices (which are not expressed to keep the notation simple). They come in three different generations for a total of six flavors: up, down, charm, strange, top and bottom. Left-handed quarks are also charged under $SU(2)_L$, and that's why they appear as doublets. In the same way, on the right, there are six flavors of **leptons**: electron, muon, tau and the corresponding neutrinos. Interestingly enough, no right-handed neutrinos have been found yet.

Given all these particles, we can study how they interact with each other via the SM Lagrangian:

$$\mathcal{L}_{SM} = \mathcal{L}_{YM} + \mathcal{L}_H + \mathcal{L}_f + \mathcal{L}_{Yuk} \tag{A.3}$$

A.1 Yang-Mills sector

The Yang-Mills sector includes all the kinetic terms for gauge bosons, together with their non-Abelian interactions:

$$\mathcal{L}_{YM} = -\frac{1}{4} G^{A,\mu\nu} G^A_{\mu\nu} - \frac{1}{4} W^{I,\mu\nu} W^I_{\mu\nu} - \frac{1}{4} B^{\mu\nu} B_{\mu\nu} \tag{A.4}$$

Each field strength takes the following form:

$$G^A_{\mu\nu} = \partial_\mu G^A_\nu - \partial_\nu G^A_\mu + g_s f^{ABC} G^B_\mu G^C_\nu \tag{A.5}$$
$$W^I_{\mu\nu} = \partial_\mu W^I_\nu - \partial_\nu W^I_\mu + g f \epsilon^{IJK} G^J_\mu G^K_\nu \tag{A.6}$$
$$B_{\mu\nu} = \partial_\mu B_\nu - \partial_\nu B_\mu \tag{A.7}$$

The indices A and I run over the number of generators of the respective gauge groups (so $A = 1, \dots, 8$ for $SU(3)_c$ and $I = 1, 2, 3$ for $SU(2)_L$), f^{ABC} and ϵ^{IJK} are the structure constants of the associated Lie algebra and g_s g are the strong and weak coupling constant.

After the SSB, the field rotation A.16 mixes the electroweak kinetic terms, giving birth to a pletora of new interactions between the weak and electromagnetic gauge bosons. From these interactions, we can identify a relation between the electric charge and the couplings g and g_Y:

$$e = g s_W = g_Y c_W = \frac{g g_Y}{\sqrt{g^2 + g_Y^2}} \tag{A.8}$$

A.2 Higgs sector

The Higgs sector contains the kinetics of the Higgs field H (which is a doublet in the fundamental representation of $SU(2)_L$) and its potential:

$$\mathcal{L}_H = (D_\mu H)^\dagger (D^\mu H) - V(H^\dagger H) \tag{A.9}$$

$$V(H^\dagger H) = -\mu^2 H^\dagger H + \lambda (H^\dagger H)^2 \tag{A.10}$$

$$D_\mu H = \left(\partial_\mu - ig\frac{\sigma^I}{2} W_\mu^I - ig_Y Y_H B_\mu\right) H \tag{A.11}$$

g and g_Y are the $SU(2)_L$ and $U(1)_Y$ couplings respectively, $Y_H = 1/2$ is the hypercharge of the Higgs field and the σ^I are the Pauli matrices ($T_I = \sigma_I/2$ are the generators of $SU(2)_L$).

The Higgs potential A.10 has an infinite number of minima that correspond to non-vanishing vacuum expectation values (vev) for the Higgs field. We choose the following vacuum:

$$\langle H \rangle = \frac{1}{\sqrt{2}} \begin{pmatrix} 0 \\ v \end{pmatrix}, \qquad v = \frac{\mu}{\sqrt{\lambda}} \tag{A.12}$$

This choice spontaneously breaks the $SU(2)_L \times U(1)_Y$ gauge symmetry; we can check that the residual symmetry is $U(1)_{em}$, and its generator is given by a combination of the original gauge group generators:

$$Q = T_3 + Y \tag{A.13}$$

The Eq. (A.13) expresses the relation between electric charge, weak isospin and hypercharge.

At this point, we can expand the Higgs field in terms of fluctuations over its vacuum:

$$H = \exp\left(i\frac{\pi^I \sigma^I}{v}\right) \cdot \frac{1}{\sqrt{2}} \begin{pmatrix} 0 \\ v + h \end{pmatrix} \tag{A.14}$$

The π^I are the three Goldstone bosons born from the breaking of the three generators of $SU(2)_L \times U(1)_Y$ (Goldstone theorem). With a particular gauge choice (the unitary gauge) we can get rid of these unphysical degrees of freedom (basically setting $\pi^I = 0$). The real scalar field h is the only physical degree of freedom remaining, and it is called the Higgs boson. In the unitary gauge, $\mathcal{L}_H$ reads:

$$\begin{aligned} \mathcal{L}_H = {} & \frac{1}{2}(\partial_\mu h)(\partial^\mu h) - \frac{1}{2} m_h^2 h^2 + \frac{(v+h)^2}{4} g^2 W_\mu^+ (W^-)^\mu \\ & + \frac{(v+h)^2}{2} \frac{g^2 + g_Y^2}{4} Z_\mu Z^\mu - \lambda v h^3 - \frac{\lambda}{4} h^4 \end{aligned} \tag{A.15}$$

Where we have defined the fields:

$$\begin{cases} W_\mu^\pm = \dfrac{W_\mu^1 \mp W_\mu^2}{\sqrt{2}} \\ Z_\mu = c_W W_\mu^3 - s_W B_\mu \\ A_\mu = c_W B_\mu - s_W W_\mu^3 \end{cases} \qquad \begin{cases} c_W = \cos\theta_W = \dfrac{g}{\sqrt{g^2+g_Y^2}} \\ s_W = \sin\theta_W = \dfrac{g_Y}{\sqrt{g^2+g_Y^2}} \end{cases} \tag{A.16}$$

In Eq. (A.16) we have performed a rotation of the fields W_μ^3 and B_μ by an angle θ_W (Weinberg angle): in this way, we have obtained a diagonal mass matrix for the new fields $W^\pm$ and Z, which are the massive mediators of the weak force. Their masses are given by [68]:

$$m_W = \frac{gv}{\sqrt{2}} = 80.377 \pm 0.012\,\text{GeV}$$
$$m_Z = \frac{v\sqrt{g^2+g_Y^2}}{\sqrt{2}} = 91.1876 \pm 0.0021\,\text{GeV}$$

This is a fundamental consequence of SSB: gauge bosons are able to acquire mass without breaking the gauge invariance. The photon field A_μ, instead, does not appear in $\mathcal{L}_H$: as expected, it stays massless after the SSB.

Besides mass terms, the kinetic term of the Higgs field gives interactions terms between the Higgs boson and the new gauge bosons; from the potential $V(H^\dagger H)$, instead, we obtain cubic and quartic terms for the Higgs boson, together with its mass [68]:

$$m_h = \sqrt{2\lambda v^2} = 125.25 \pm 0.17\,\text{GeV}$$

Looking at its very large mass, we can understand why the discovery of the Higgs boson took so long to be accomplished.

A.3 Fermion sector

The fermion sector contains the kinetic terms for quarks and leptons and their couplings to gauge bosons:

$$\mathcal{L}_f = \sum_i \left[\overline{Q_L^i} i \not{D} Q_L^i + \overline{u_R^i} i \not{D} u_R^i + \overline{d_R^i} i \not{D} d_R^i + \overline{L_L^i} i \not{D} E_L^i + \overline{e_R^i} i \not{D} e_R^i \right] \tag{A.17}$$

The covariant derivative for fermions is:

$$D_\mu \psi = (\partial_\mu - i g_s \frac{\lambda^A}{2} G_\mu^A - i g \frac{\sigma^I}{2} W_\mu^I - i g_Y Y_\psi B_\mu)\psi \tag{A.18}$$

λ^A are the Gell-Mann matrices (the generators of $SU(3)_c$) and Y_ψ is the hypercharge of the associated fermion (to be more specific, Y_ψ should be multiplied by the identity matrix $\mathbb{1}_n$, where n is the dimension of the representation space chosen for ψ).

It is useful to rewrite $\mathcal{L}_f$ by its current interactions:

$$\begin{aligned}\mathcal{L}_f = &\sum_{f=u,d,c,s,t,b} \left[\overline{f}_L i\partial\!\!\!/ f_L + \overline{f}_R i\partial\!\!\!/ f_R\right] - \frac{g}{\sqrt{2}}(W^-_\mu J^\mu_+ + W^+_\mu J^\mu_-) \\ &- \frac{g}{c_W} Z_\mu J^\mu_Z - eA_\mu J^\mu_{em}\end{aligned} \tag{A.19}$$

Where (the index i runs over the three generations of quarks and leptons):

$$J^+_\mu = \sum_i \overline{d}^i_L \gamma_\mu u^i_L + \overline{e}^i_L \gamma_\mu \nu^i_{e,L} \tag{A.20}$$

$$J^-_\mu = \sum_i \overline{u}^i_L \gamma_\mu d^i_L + \overline{\nu}^i_{e,L} \gamma_\mu e^i_L \tag{A.21}$$

$$J^{em}_\mu = \sum_f \left[\overline{f}_L \gamma_\mu f_L + \overline{f}_R \gamma_\mu f_R\right] Q_f \tag{A.22}$$

$$J^Z_\mu = J^{3L}_\mu - s^2_W J^{em}_\mu = \sum_f \left[\overline{f}_L g^f_L \gamma_\mu f_L + \overline{f}_R g^f_R \gamma_\mu f_R\right] \tag{A.23}$$

Charged current interactions happen only for left-handed fields: this follows from the fact that the W bosons are combinations of the original $SU(2)_L$ gauge bosons only; On the other hand, neutral current and electromagnetic current interactions also affect right-handed fields, since the Z boson and the photon are combinations of W^3 and B, and the last one interacts with both chiralities. In particular, the electromagnetic interactions are symmetric in the 2 chiralities (QED is a *vector-like* theory), while the Z boson couples differently to left- and right-handed fields:

$$g^f_L = T^3_f - s^2_W Q_f \tag{A.24}$$

$$g^f_R = -s^2_W Q_f \tag{A.25}$$

A.4 Yukawa sector

The Yukawa sector describes the interactions between fermions and the Higgs field, and provides mass terms for the fermion fields:

$$\mathcal{L}_{Yuk} = -\sum_{i,j} \left[y^{(u)}_{ij}\, \overline{Q}^i_L \tilde{H} u^j_R + y^{(d)}_{ij} \overline{Q}^i_L H d^j_R + y^{(e)}_{ij} \overline{L}^i_L H e^j_R\right] + h.c. \tag{A.26}$$

Where we have defined:

$$\tilde{H} = i\sigma_2 H^* \tag{A.27}$$

We can check that $\mathcal{L}_{Yuk}$ is actually invariant under $SU(2)_L \times U(1)_Y$. The Yukawa matrices $y^{(f)}$ are general 3×3 complex matrices, so Yukawa interactions, at this point, are the only term that can mix different generations of fermions. Moreover, Yukawa interactions are the only ones in the SM that can mix left and right chiralities; this is particularly relevant for neutrinos, for which a right-handed chirality does not exist (or, at least, it has not been discovered yet). For this reason, neutrinos in the SM are massless. However, there is strong evidence (i.e. the neutrino oscillation) that neutrino masses should be non-vanishing; although this problem has not been solved yet, many solutions have been put forward (for example, the seesaw mechanism). In any case, the neutrino mass problem remains one of the best hints for the need for physics beyond the Standard Model (together with dark matter of course!).

After SSB, in the unitary gauge:

$$\mathcal{L}_{Yuk} = -\sum_{i,j} \frac{v+h}{\sqrt{2}} \left[\overline{u}^i_L y^{(u)}_{ij} u^j_R + \overline{d}^i_L y^{(d)}_{ij} d^j_R + \overline{e}^i_L y^{(e)}_{ij} e^j_R \right] + h.c. \tag{A.28}$$

Thus, we get non-diagonal mass matrices of the form:

$$m_{ij} = \frac{y_{ij} v}{\sqrt{2}} \tag{A.29}$$

We can diagonalize the mass matrices performing a biunitary transformation on the left and right chiralities of the fermion fields; with an abuse of notation, we indicate the triplet of each fermion type by its first generation particle, so:

$$u_L = \begin{pmatrix} u_L \\ c_L \\ t_L \end{pmatrix} \quad d_L = \begin{pmatrix} d_L \\ s_L \\ b_L \end{pmatrix} \quad e_L = \begin{pmatrix} e_L \\ \mu_L \\ \tau_L \end{pmatrix} \quad \nu_L = \begin{pmatrix} \nu^e_L \\ \nu^\mu_L \\ \nu^\tau_L \end{pmatrix} \tag{A.30}$$

Thus, we can perform the following rotation:

$$\begin{cases} u_L = L_u u_L \\ u_R = R_u u_R \end{cases} \quad \begin{cases} d_L = L_d d_L \\ d_R = R_d d_R \end{cases} \quad \begin{cases} e_L = L_e e_L \\ e_R = R_e e_R \\ \nu_L = L_\nu \nu_L \end{cases} \tag{A.31}$$

In this way, the mass matrices become:

$$m^{(u)} = L_u^\dagger y^{(u)} R_u = \begin{pmatrix} m_u & 0 & 0 \\ 0 & m_c & 0 \\ 0 & 0 & m_t \end{pmatrix} \tag{A.32}$$

$$m^{(d)} = L_d^\dagger y^{(d)} R_d = \begin{pmatrix} m_d & 0 & 0 \\ 0 & m_s & 0 \\ 0 & 0 & m_b \end{pmatrix} \tag{A.33}$$

$$m^{(e)} = L_e^\dagger y^{(e)} R_e = \begin{pmatrix} m_e & 0 & 0 \\ 0 & m_\mu & 0 \\ 0 & 0 & m_\tau \end{pmatrix} \tag{A.34}$$

The value of each mass is reported in Tables A.2 and A.3: it's interesting to note how wide is the mass spectrum of SM fermions, which spans over nearly six orders of magnitude.

However, switching from the flavor basis to the mass basis comes with a price to pay: weak charged current interactions are not diagonal anymore. In fact, if we look at the effect of the rotation A.31 on the fermion sector, we can see that neutral and electromagnetic current interactions are not changed (they couple the same flavor, so for each term we get extra factors like $L_f^\dagger L_f \, (R_f^\dagger R_f) = 1$); on the other hand, the weak charged current interactions become:

$$\begin{aligned} \mathcal{L}_{c.c.}^{\text{mass basis}} = &- \frac{g}{\sqrt{2}} \left[\overline{u}_L V_{CKM} \not{W}^+ d_L + \overline{d}_L V_{CKM}^\dagger \not{W}^- u_L \right] \\ &- \frac{g}{\sqrt{2}} \left[\overline{\nu}_L U_{PMNS} \not{W}^+ e_L + \overline{e}_L U_{PMNS}^\dagger \not{W}^- \nu_L \right] \end{aligned} \tag{A.35}$$

$V_{CKM} = L_u^\dagger L_d$ is the Cabibbo-Kobayashi-Maskawa matrix and $U_{PMNS} = L_\nu^\dagger L_e$ is the Pontecorvo-Maki-Nakagawa-Sakata matrix. These matrices allow physical interactions between different generations of fermions. We can count the number of physical parameters for V_{CKM} (the discussion for U_{PMNS} is the same). Being a complex unitary matrix, V_{CKM} has nine real degrees of freedom, that we can organize in 3 mixing angle and 6 phases. However, we can always redefine the quark fields in order to get rid of 5 phases (if all quarks are rotated by the same phase, V_{CKM} remains invariant; this invariance corresponds to the conservation of the baryon number). Thus, we are left with three angles $(\theta_{12}, \theta_{23}, \theta_{13})$ and one phase (δ):

$$V_{CKM} = \begin{pmatrix} 1 & 0 & 0 \\ 0 & c_{23} & s_{23} \\ 0 & -s_{23} & c_{23} \end{pmatrix} \begin{pmatrix} c_{13} & 0 & s_{13} e^{i\delta} \\ 0 & 1 & 0 \\ -s_{13} e^{i\delta} & 0 & c_{13} \end{pmatrix} \begin{pmatrix} c_{12} & s_{12} & 0 \\ -s_{12} & c_{12} & 0 \\ 0 & 0 & 1 \end{pmatrix} \tag{A.36}$$

Where $c_{ij} = \cos\theta_{ij}$ and $s_{ij} = \sin\theta_{ij}$. The same is valid for U_{PMNS}, which depends on two more phases if neutrinos are Majorana particles. Values of the CKM and PMNS parameters can be found in [68].

A.5 Gauge anomalies in the Standard Model

A symmetry of a classical theory that is broken at the quantum level is said to be anomalous. Thanks to Noether's theorem, we know that every symmetry is associated with a conserved current, so, for an anomalous symmetry, this current will not be conserved when we include quantum effects. Quantum anomalies are physically interesting when we talk about global symmetries (for example, the baryon number in the SM is anomalous, and its non-conservation is a necessary condition to generate the matter-antimatter asymmetry in the early universe), but they can be extremely dangerous when we are dealing with gauge symmetries. A gauge symmetry, in fact, is just a redundancy in our description of the theory, and it is fundamental to build a consistent theory, since it is used to remove negative norm states from the spectrum: without gauge invariance, unphysical polarizations could be produced and unitarity would be violated.

In QED case, for example, to eliminate negative norm states from the Hilbert space we use the Gupta-Bleuler condition:

$$\partial^\mu A_\mu^+ |\Psi\rangle = 0 \tag{A.37}$$

where A_μ^+ is the positive frequency part. The separation:

$$\partial^\mu A_\mu = \partial^\mu A_\mu^+ + \partial_\mu A_\mu^- \tag{A.38}$$

is trivial in the free theory (since from the equation of motion $\Box A^\mu = 0$ we have also $\Box \partial_\mu A^\mu = 0$), but in the interacting theory:

$$\Box \partial_\mu A^\mu = \partial_\mu j_{em}^\mu \tag{A.39}$$

If the gauge symmetry is anomalous, then the electromagnetic current j_{em}^μ is not conserved, therefore we have troubles building a physical Hilbert space for the theory.

That's the reason why any consistent quantum field theory should be anomaly free (for gauge symmetries). In this section, we will simply demonstrate that the SM is indeed an anomaly free theory. Taking the perturbation theory approach, anomalies arise from triangle loop diagrams like in Fig. A.1, where each vertex is attached to a particular gauge boson.

The anomaly free condition equals to verify the validity of the Ward identity for any combination of external gauge boson. This means:

$$\partial^\mu \langle J_\mu^i J_\nu^j J_\rho^k \rangle = 0 \tag{A.40}$$

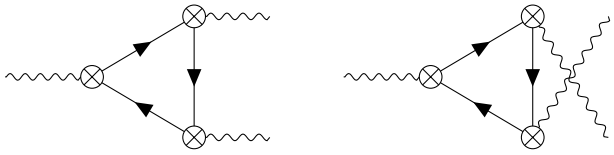

Figure A.1: Triangle diagrams giving rise to anomalies. We pictured a photon attached to each vertex, but any combination of gauge bosons is possible.

In the above expression, i, j, k represent the different currents coupled with the different gauge fields (for the SM, we can have $J_\mu^{QCD}, J_\mu^{\text{weak}}, J_\mu^Y$). For a generic non-Abelian gauge theory, this current can be expressed as:

$$J_\mu^a = \overline{\psi} T_R^a \gamma_\mu \psi \tag{A.41}$$

where T_R^a are the symmetry group generators in the representation R. This means that the triangle diagram picks up a factor T_R^a at each vertex and the whole contribution to the amplitude will be proportional to $Tr[T_R^a T_R^b T_R^c]$. Each diagram comes with a twin in which two bosons are exchanged (Fig. A.1): this means that the final amplitude must be proportional to the totally symmetric tensor:

$$Tr\left[T_R^a, \{T_R^b, T_R^c\}\right] = A(R) d^{abc} \tag{A.42}$$

$A(R)$ is the anomaly coefficient and depends on the representation, while d^{abc} is defined using the fundamental representation ($A(fund) = 1$). Left and right-handed fermions contribute to the anomaly with opposite signs, so the anomaly cancellation condition can be written as:

$$\left(\sum_{\text{left}} A(R_L) - \sum_{\text{right}} A(R_R) \right) d^{abc} = 0 \tag{A.43}$$

Where R_L and R_R are the representations in which left and right-handed fields transform. Now, we just need to check that any possible anomaly cancels in the SM:

- $SU(3)^3$: QCD is a non-chiral theory, so left and right-handed fields transform in the same representation; moreover, since we have the same number of left and right-handed quarks:

$$\sum_{\text{left}} A(\text{fund}) - \sum_{\text{right}} A(\text{fund}) = 0 \tag{A.44}$$

- $SU(3)^2 U(1)$: only quarks contribute to this anomaly. In the fundamental representation, the generators of $SU(3)$ are the Gell-Mann matrices, for

which $Tr\{\lambda^a, \lambda^b\} = \frac{1}{2}\delta^{ab}$, so:

$$\begin{aligned} Tr\big[\{\lambda^a, \lambda^b\}, Y\big] &= \Bigg(\sum_{\substack{\text{left}\\ \text{quarks}}} Y_L - \sum_{\substack{\text{right}\\ \text{quarks}}} Y_R\Bigg)\delta^{ab} \\ &= \delta^{ab}\big(6Y_{Q_L} - 3Y_{u_R} - 3Y_{d_R}\big) \end{aligned} \tag{A.45}$$

If we plug in the values in Table A.1, the above expression vanishes.

- $SU(3)U(1)^2$: the Gell-Mann matrices are traceless, so:

$$d^{abc} \propto Y^2 Tr[\lambda^a] = 0 \tag{A.46}$$

Since any generator of $SU(N)$ is traceless, the above argument can be applied any time we have just one factor of $SU(2)$ or $SU(3)$.

- $SU(2)^3$: in the fundamental representation, the generators of $SU(2)$ are half the Pauli matrices, for which $\{\sigma^a, \sigma^b\} = 2\delta^{ab}\mathbb{1}$; the Pauli matrices are traceless too, so:

$$d^{abc} = \frac{1}{2}\delta^{bc} Tr[\sigma^a] = 0 \tag{A.47}$$

- $SU(2)^2U(1)$: only left-handed fermions contribute to this anomaly:

$$Tr\big[\{\sigma^a, \sigma^b\}, Y\big] = 4\delta^{ab}\sum_{\text{left}} Y_L = 4\delta^{ab}(6Y_{Q_L} + 2Y_{L_L}) \tag{A.48}$$

Also in this case, the above equation vanishes for the hypercharges in Table A.1.

- $U(1)^3$: In this case we need to calculate:

$$\sum_{\text{left}} Y_L^3 - \sum_{\text{right}} Y_R^3 = 6Y_{Q_L}^3 + 2Y_{L_L}^3 - 3Y_{u_R}^3 - 3Y_{d_R}^3 - Y_{e_R}^3 = 0 \tag{A.49}$$

At last, a particular type of anomaly we need to account for is the one related to the graviton: in fact, if we couple the SM to gravity, it's possible to draw a triangular diagram with 2 graviton and one gauge boson. The cancellation of this anomaly results in the condition:

$$Tr[T_R^a] = 0 \tag{A.50}$$

This condition is trivially satisfied for $SU(2)$ and $SU(3)$, whose generators are traceless. For $U(1)$, instead, we get the condition:

$$\sum_{\text{left}} Y_L - \sum_{\text{right}} Y_R = 6Y_{Q_L} + 2Y_{L_L} - 3Y_{u_R} - 3Y_{d_R} - Y_{e_R} = 0 \tag{A.51}$$

All the SM gauge anomalies vanish. We make two final notes:

- The inclusion of a sterile right-handed neutrino doesn't spoil any of the above calculation, since they would be completely chargeless under any SM gauge group;
- The cancellation of the $SU(2)^2U(1)$ anomaly requires $3Y_{Q_L}+Y_{L_L}=0$ exactly: this is the reason why the proton and the electron must have the exact same charge.

	$SU(3)_c$	$SU(2)_L$	$U(1)_Y$	T_{3L}	$Q = T_{3L} + Y$
$\begin{pmatrix} u_L \\ d_L \end{pmatrix}$	**3**	**2**	$+1/6$	$\begin{pmatrix} +1/2 \\ -1/2 \end{pmatrix}$	$\begin{pmatrix} +2/3 \\ -1/3 \end{pmatrix}$
u_R	**1**	**1**	$+2/3$	0	$2/3$
d_R	**1**	**1**	$-1/3$	0	$-1/3$
$\begin{pmatrix} \nu_L \\ e_L \end{pmatrix}$	**1**	**2**	$-1/2$	$\begin{pmatrix} +1/2 \\ -1/2 \end{pmatrix}$	$\begin{pmatrix} 0 \\ -1 \end{pmatrix}$
e_R	**1**	**1**	-1	0	-1
$H = \begin{pmatrix} H^+ \\ H^0 \end{pmatrix}$	**1**	**2**	$+1/2$	$\begin{pmatrix} +1/2 \\ -1/2 \end{pmatrix}$	$\begin{pmatrix} +1 \\ 0 \end{pmatrix}$

Table A.1: Charges of the SM fermion and Higgs fields. Bold numbers indicate the dimension of the fundamental representation. Charges are the same for the three generations of fermions.

u	d	c	s	t	b
2.16 MeV	4.67 MeV	1.27 GeV	93.4 MeV	172.69 GeV	4.18 GeV

Table A.2: Quark mass spectrum, from [68].

e	μ	τ	$\sum \nu_L$
511 keV	105.66 MeV	1.777 GeV	< 1.1 eV

Table A.3: Lepton mass spectrum, from [68]. The neutrino limit is for the sum of the masses of the three neutrinos.

Appendix B

Boltzmann equation

The Boltzmann equation describes how the phase space distribution $f(\mathbf{x}, \mathbf{p}, t)$ of a DM particle evolves with time. The starting point of the Boltzmann equation is:

$$\mathbf{L}[f] = \mathbf{C}[f], \tag{B.1}$$

where $\mathbf{L}[f]$ is the Liouville operator, which depicts the evolution of f due to the geometry of space-time, and $\mathbf{C}[f]$ is the collision operator, which includes all the effects due to number changing processes (like scattering and decays).

In its most general form, the Liouville operator is:

$$\mathbf{L}[f] = \left[p^\mu \frac{\partial}{\partial x^\mu} - \Gamma^\mu_{\alpha\beta} p^\alpha p^\beta \frac{\partial}{\partial p^\mu} \right] f \tag{B.2}$$

where $\Gamma^\mu_{\alpha\beta}$ is the affine connection and p_μ is the four-momentum. We can specialize the above formula for the FRW metric:

$$ds^2 = dt^2 - a^2(t) \left[\frac{dr^2}{1 - kr^2} + r^2 d\Omega^2 \right] \tag{B.3}$$

Where a is the scale factor, $k = -1, 0, +1$ depends on the geometry of the universe and $d\Omega^2 = d\theta^2 + \sin^2\theta \, d\phi^2$. Imposing homogeneity and isotropy, we find:

$$\mathbf{L}[f] = E \frac{\partial f}{\partial t} - H(E^2 - m_\chi^2) \frac{\partial f}{\partial E} \tag{B.4}$$

E is the energy, H is the Hubble parameter and m_χ is the mass of the DM particle. In the following, we will need to integrate both sides of the equations over the phase space of the DM particle, in order to obtain more meaningful relations involving the number density of DM particles, which is defined as:

$$n_\chi = g_\chi \int f(E, t) \frac{d^3 p}{(2\pi)^3} \tag{B.5}$$

where g_χ is the number of internal degrees of freedom of χ. The integration of the Liouville operator gives:

$$g_\chi \int \mathbf{L}[f] \frac{d^3p}{E(2\pi)^3} = \frac{dn_\chi}{dt} + 3Hn_\chi \tag{B.6}$$

In absence of collisions ($\mathbf{C}[f] = 0$), the above equation shows that the evolution of the number density is only given by the dilution due to the expansion of the universe (we can check that, in this case, $na^3 = const.$).

We now turn our attention to the collision operator. If we consider scattering processes like $\chi b \leftrightarrow cd$, then it takes the form:

$$\begin{aligned}\mathbf{C}[f] = -\frac{1}{2} \int (2\pi)^4 \delta^4(p_\chi + p_b - p_c - p_d) d\Pi_b d\Pi_c d\Pi_d \\ \left[|M_{\chi b \to cd}|^2 f_\chi f_b (1 \pm f_c)(1 \pm f_d) - |M_{cd \to \chi b}|^2 f_c f_d (1 \pm f_\chi)(1 \pm f_b) \right]\end{aligned} \tag{B.7}$$

$M_{x \to y}$ is the matrix element for the reaction $x \to y$, the factors of the form $(1 \pm f)$ depend on the particle being a boson (plus sign) or a fermion (minus sign), the delta function enforces energy and momentum conservation and the phase-space factors are defined as:

$$d\Pi_i = g_i \frac{d^3p_i}{2E_i(2\pi)^3} \tag{B.8}$$

We now need to integrate the collision operator in the same way done for the Liouville operator. Before proceeding, we can make some general assumptions to simplify calculations:

- In the early universe we are away from degenerate conditions, so the Pauli blocking and Bose enhancement factors can be ignored: $1 \pm f_i \simeq 1$;
- We assume CP invariance, so that the squared matrix elements for direct and inverse reaction are equal $|M_{\chi b \to cd}|^2 = |M_{cd \to \chi b}|^2$
- Kinetic equilibrium is maintained:

$$f_i(E,t) = \frac{n_i(t)}{n_i^{eq}(t)} f_i^{eq}(E,t) \tag{B.9}$$

In this way, we obtain:

$$\begin{aligned} g_\chi \int \mathbf{C}[f] \frac{d^3p}{E(2\pi)^3} = -\int (2\pi)^4 \delta^4(p_\chi + p_b - p_c - p_d) d\Pi_\chi d\Pi_b d\Pi_c d\Pi_d \\ |M_{\chi b \to cd}|^2 (f_\chi f_b - f_c f_d) = -\langle \sigma v \rangle (n_\chi n_b - d n_c n_d) \end{aligned} \tag{B.10}$$

Where we have defined the thermally averaged cross section for the $\chi b \to cd$ process to be:

$$\langle \sigma v \rangle = \frac{\int d^3p_\chi d^3p_b \, \sigma v_{\text{Møl}} f_\chi^{eq} f_b^{eq}}{\int d^3p_\chi d^3p_b f_\chi^{eq} f_b^{eq}} \tag{B.11}$$

$v_{\text{Møl}}$ is the Møller velocity defined by:

$$v_{\text{Møl}} = \frac{\sqrt{(p_\chi p_b)^2 - m_\chi^2 m_b^2}}{E_\chi E_b} \tag{B.12}$$

All together, the Boltzmann equation now reads:

$$\dot{n}_\chi + 3Hn_\chi = -\langle \sigma v \rangle \left(n_\chi n_b - n_c n_d \right) \tag{B.13}$$

If we focus only on the annihilation reactions $\chi\chi \to \phi\phi$, where ϕ is a SM particle in equilibrium with the thermal bath, then the Eq. (B.13) assumes the form:

$$\dot{n}_\chi + 3Hn_\chi = -\langle \sigma v \rangle \left(n_\chi^2 - (n_\chi^{eq})^2 \right) \tag{B.14}$$

B.1 Low temperature approximation

The thermally averaged cross section $\langle \sigma v \rangle$ can be written as [93]:

$$\langle \sigma v \rangle = \frac{x}{8m^5} \frac{1}{K_2^2(x)} \int_{4m^2}^{\infty} \sigma_{ann}(s - 4m^2) \sqrt{s} K_1 \left(\frac{x\sqrt{s}}{m} \right) ds \tag{B.15}$$

where K_1 and K_2 are the modified Bessel function of first and second order. At low temperature we can express the Mandelstam variable s as a function of the velocity v in the center of mass frame:

$$s = m^2(4 + v^2) + \mathcal{O}(v^4) \tag{B.16}$$

Then, we perform the following change of variable in the integral:

$$v = \frac{1}{m}\sqrt{s - 4m^2} \quad \to \quad ds = 2m\sqrt{s - 4m^2} dv \tag{B.17}$$

Therefore we obtain:

$$\langle \sigma v \rangle = \frac{x}{8m^5} \frac{1}{K_2^2(x)} \int_0^{\infty} \frac{\sigma_{ann} I}{2g^2} 2m^3 v^2 K_1(x\sqrt{4 + v^2}) dv \tag{B.18}$$

At large x and low v, the Bessel functions can be expanded as:

$$K_1(x\sqrt{4+v^2}) \underset{\substack{x\to\infty \\ v\to 0}}{\simeq} e^{-2x} e^{-\frac{xv^2}{4}} \frac{\sqrt{\pi}}{2} \frac{1}{\sqrt{x}} \left(1 - \frac{1}{16} v^2\right) \tag{B.19}$$

$$K_2(x) \underset{x\to\infty}{\simeq} \sqrt{\frac{\pi}{2x}} e^{-x} \tag{B.20}$$

If we impose:

$$\sigma_{ann} I \simeq a + bv^2 \tag{B.21}$$

we can evaluate the integral, obtaining at the end:

$$\langle \sigma v \rangle = \frac{1}{4g^2 m^2} \left(a + \frac{3(16b - a)}{8x}\right) \tag{B.22}$$

Bibliography

[1] Gianfranco Bertone, Dan Hooper, and Joseph Silk. "Particle dark matter: Evidence, candidates and constraints". In: *Phys. Rept.* 405 (2005), pp. 279–390. DOI: 10.1016/j.physrep.2004.08.031. arXiv: hep-ph/0404175.

[2] Mariangela Lisanti. "Lectures on Dark Matter Physics". In: *Theoretical Advanced Study Institute in Elementary Particle Physics: New Frontiers in Fields and Strings*. 2017, pp. 399–446. DOI: 10.1142/9789813149441_0007. arXiv: 1603.03797 [hep-ph].

[3] A. Arbey and F. Mahmoudi. "Dark matter and the early Universe: a review". In: *Prog. Part. Nucl. Phys.* 119 (2021), p. 103865. DOI: 10.1016/j.ppnp.2021.103865. arXiv: 2104.11488 [hep-ph].

[4] Graciela B. Gelmini. "The Hunt for Dark Matter". In: *Theoretical Advanced Study Institute in Elementary Particle Physics: Journeys Through the Precision Frontier: Amplitudes for Colliders*. 2015, pp. 559–616. DOI: 10.1142/9789814678766_0012. arXiv: 1502.01320 [hep-ph].

[5] M. Milgrom. "A modification of the Newtonian dynamics as a possible alternative to the hidden mass hypothesis." In: *The Astrophysical Journal* 270 (July 1983), pp. 365–370. DOI: 10.1086/161130.

[6] Benoit Famaey and Stacy S. McGaugh. "Modified Newtonian Dynamics (MOND): Observational Phenomenology and Relativistic Extensions". In: *Living Reviews in Relativity* 15.1 (Sept. 2012). DOI: 10.12942/lrr-2012-10. URL: https://doi.org/10.12942%5C%2Flrr-2012-10.

[7] G. W. Angus, B. Famaey, and D. A. Buote. "X-ray group and cluster mass profiles in MOND: unexplained mass on the group scale". In: *Monthly Notices of the Royal Astronomical Society* 387.4 (July 2008), pp. 1470–1480. DOI: 10.1111/j.1365-2966.2008.13353.x. URL: https://doi.org/10.1111%5C%2Fj.1365-2966.2008.13353.x.

[8] Vera C. Rubin and Jr. Ford W. Kent. "Rotation of the Andromeda Nebula from a Spectroscopic Survey of Emission Regions". In: *The Astrophysical Journal* 159 (Feb. 1970), p. 379. DOI: 10.1086/150317.

[9] P. Salucci and A. Borriello. "The Intriguing Distribution of Dark Matter in Galaxies". In: (2002). DOI: 10.48550/ARXIV.ASTRO-PH/0203457. URL: https://arxiv.org/abs/astro-ph/0203457.

[10] Massimo Persic, Paolo Salucci, and Fulvio Stel. "The universal rotation curve of spiral galaxies I. The dark matter connection". In: *Monthly Notices of the Royal Astronomical Society* 281.1 (July 1996), pp. 27–47. ISSN: 0035-8711. DOI: 10.1093/mnras/278.1.27. eprint: https://academic.oup.com/mnras/article-pdf/281/1/27/30383982/281-1-27.pdf. URL: https://doi.org/10.1093/mnras/278.1.27.

[11] Giuseppina Battaglia et al. "The Radial velocity dispersion profile of the Galactic Halo: Constraining the density profile of the dark halo of the Milky Way". In: *Mon. Not. Roy. Astron. Soc.* 364 (2005). [Erratum: Mon.Not.Roy.Astron.Soc. 370, 1055 (2006)], pp. 433–442. DOI: 10.1111/j.1365-2966.2005.09367.x. arXiv: astro-ph/0506102.

[12] W. J. G. de Blok et al. "Mass density profiles of LSB galaxies". In: *Astrophys. J. Lett.* 552 (2001), pp. L23–L26. DOI: 10.1086/320262. arXiv: astro-ph/0103102.

[13] V. Springel et al. "The Aquarius Project: the subhaloes of galactic haloes". In: *Monthly Notices of the Royal Astronomical Society* 391.4 (Dec. 2008), pp. 1685–1711. DOI: 10.1111/j.1365-2966.2008.14066.x. URL: https://doi.org/10.1111%5C%2Fj.1365-2966.2008.14066.x.

[14] Julio F. Navarro, Carlos S. Frenk, and Simon D. M. White. "The Structure of cold dark matter halos". In: *Astrophys. J.* 462 (1996), pp. 563–575. DOI: 10.1086/177173. arXiv: astro-ph/9508025.

[15] Julio F. Navarro, Carlos S. Frenk, and Simon D. M. White. "The Structure of cold dark matter halos". In: *Astrophys. J.* 462 (1996), pp. 563–575. DOI: 10.1086/177173. arXiv: astro-ph/9508025.

[16] Alister W. Graham et al. "Empirical models for Dark Matter Halos. I. Nonparametric Construction of Density Profiles and Comparison with Parametric Models". In: *Astron. J.* 132 (2006), pp. 2685–2700. DOI: 10.1086/508988. arXiv: astro-ph/0509417.

[17] A. Burkert. "The Structure of dark matter halos in dwarf galaxies". In: *Astrophys. J. Lett.* 447 (1995), p. L25. DOI: 10.1086/309560. arXiv: astro-ph/9504041.

[18] Paul J. McMillan. "Mass models of the Milky Way". In: *Monthly Notices of the Royal Astronomical Society* 414.3 (Apr. 2011), pp. 2446–2457. DOI: 10.1111/j.1365-2966.2011.18564.x. URL: https://doi.org/10.1111%5C%2Fj.1365-2966.2011.18564.x.

[19] Riccardo Catena and Piero Ullio. "A novel determination of the local dark matter density". In: *JCAP* 08 (2010), p. 004. DOI: 10.1088/1475-7516/2010/08/004. arXiv: 0907.0018 [astro-ph.CO].

[20] Fabrizio Nesti and Paolo Salucci. "The Dark Matter halo of the Milky Way, AD 2013". In: *JCAP* 07 (2013), p. 016. DOI: 10.1088/1475-7516/2013/07/016. arXiv: 1304.5127 [astro-ph.GA].

[21] Sergey Mashchenko, James Wadsley, and H. M. P. Couchman. "Stellar Feedback in Dwarf Galaxy Formation". In: *Science* 319.5860 (Jan. 2008), pp. 174–177. DOI: 10.1126/science.1148666. URL: https://doi.org/10.1126%5C%2Fscience.1148666.

[22] Oleg Y. Gnedin et al. "Response of Dark Matter Halos to Condensation of Baryons: Cosmological Simulations and Improved Adiabatic Contraction Model". In: *The Astrophysical Journal* 616.1 (Nov. 2004), pp. 16–26. DOI: 10.1086/424914. URL: https://doi.org/10.1086%5C%2F424914.

[23] J. I. Read. "The Local Dark Matter Density". In: *J. Phys. G* 41 (2014), p. 063101. DOI: 10.1088/0954-3899/41/6/063101. arXiv: 1404.1938 [astro-ph.GA].

[24] F. Zwicky. "Republication of: The redshift of extragalactic nebulae". In: *General Relativity and Gravitation* 41.1 (Jan. 2009), pp. 207–224. DOI: 10.1007/s10714-008-0707-4.

[25] Alexandre Refregier. "Weak Gravitational Lensing by Large-Scale Structure". In: *Annual Review of Astronomy and Astrophysics* 41.1 (Sept. 2003), pp. 645–668. DOI: 10.1146/annurev.astro.41.111302.102207. URL: https://doi.org/10.1146%5C%2Fannurev.astro.41.111302.102207.

[26] Lin Wang et al. "SDSS J1640+1932: a spectacular galaxyquasar strong lens system". In: *Monthly Notices of the Royal Astronomical Society* 468.3 (Mar. 2017), pp. 3757–3763. DOI: 10.1093/mnras/stx733. URL: https://doi.org/10.1093%5C%2Fmnras%5C%2Fstx733.

[27] Douglas Clowe et al. "A direct empirical proof of the existence of dark matter". In: *Astrophys. J. Lett.* 648 (2006), pp. L109–L113. DOI: 10.1086/508162. arXiv: astro-ph/0608407.

[28] Planck Collaboration et al. "Planck 2018 results - VI. Cosmological parameters". In: *A&A* 641 (2020), A6. DOI: 10.1051/0004-6361/201833910. URL: https://doi.org/10.1051/0004-6361/201833910.

[29] Hsin-Chia Cheng and Ian Low. "TeV symmetry and the little hierarchy problem". In: *JHEP* 09 (2003), p. 051. DOI: 10.1088/1126-6708/2003/09/051. arXiv: hep-ph/0308199.

[30] James M. Overduin and P. S. Wesson. "Dark matter and background light". In: *Phys. Rept.* 402 (2004), pp. 267–406. DOI: 10.1016/j.physrep.2004.07.006. arXiv: astro-ph/0407207.

[31] Maxim Pospelov and Tonnis ter Veldhuis. "Direct and indirect limits on the electromagnetic form-factors of WIMPs". In: *Phys. Lett. B* 480 (2000), pp. 181–186. DOI: 10.1016/S0370-2693(00)00358-0. arXiv: hep-ph/0003010.

[32] Daniel Feldman, Zuowei Liu, and Pran Nath. "The Stueckelberg Z-prime Extension with Kinetic Mixing and Milli-Charged Dark Matter From the Hidden Sector". In: *Phys. Rev. D* 75 (2007), p. 115001. DOI: 10.1103/PhysRevD.75.115001. arXiv: hep-ph/0702123.

[33] Anne M. Green. "Primordial Black Holes: sirens of the early Universe". In: *Fundam. Theor. Phys.* 178 (2015), pp. 129–149. DOI: 10.1007/978-3-319-10852-0_5. arXiv: 1403.1198 [gr-qc].

[34] Bernard Carr, Florian Kuhnel, and Marit Sandstad. "Primordial Black Holes as Dark Matter". In: *Phys. Rev. D* 94.8 (2016), p. 083504. DOI: 10.1103/PhysRevD.94.083504. arXiv: 1607.06077 [astro-ph.CO].

[35] JiJi Fan et al. "Double-Disk Dark Matter". In: *Phys. Dark Univ.* 2 (2013), pp. 139–156. DOI: 10.1016/j.dark.2013.07.001. arXiv: 1303.1521 [astro-ph.CO].

[36] Michael Boylan-Kolchin, James S Bullock, and Manoj Kaplinghat. "Too big to fail? The puzzling darkness of massive Milky Way subhaloes". In: *Monthly Notices of the Royal Astronomical Society: Letters* 415.1 (2011), pp. L40–L44.

[37] Mark Vogelsberger, Jesus Zavala, and Abraham Loeb. "Subhaloes in self-interacting galactic dark matter haloes". In: *Monthly Notices of the Royal Astronomical Society* 423.4 (2012), pp. 3740–3752.

[38] Nilanjan Banik et al. "Novel constraints on the particle nature of dark matter from stellar streams". In: *JCAP* 10 (2021), p. 043. DOI: 10.1088/1475-7516/2021/10/043. arXiv: 1911.02663 [astro-ph.GA].

[39] Lawrence J. Hall et al. "Freeze-In Production of FIMP Dark Matter". In: *JHEP* 03 (2010), p. 080. DOI: 10.1007/JHEP03(2010)080. arXiv: 0911.1120 [hep-ph].

[40] C. A. Baker et al. "An Improved experimental limit on the electric dipole moment of the neutron". In: *Phys. Rev. Lett.* 97 (2006), p. 131801. DOI: 10.1103/PhysRevLett.97.131801. arXiv: hep-ex/0602020.

[41] Georg G. Raffelt. "Astrophysical axion bounds". In: *Lect. Notes Phys.* 741 (2008). Ed. by Markus Kuster, Georg Raffelt, and Berta Beltran, pp. 51–71. DOI: 10.1007/978-3-540-73518-2_3. arXiv: hep-ph/0611350.

[42] David J. E. Marsh. "Axion Cosmology". In: *Phys. Rept.* 643 (2016), pp. 1–79. DOI: 10.1016/j.physrep.2016.06.005. arXiv: 1510.07633 [astro-ph.CO].

[43] Scott Dodelson and Lawrence M. Widrow. "Sterile-neutrinos as dark matter". In: *Phys. Rev. Lett.* 72 (1994), pp. 17–20. DOI: 10.1103/PhysRevLett.72.17. arXiv: hep-ph/9303287.

[44] Takehiko Asaka, Mikko Laine, and Mikhail Shaposhnikov. "Lightest sterile neutrino abundance within the nuMSM". In: *JHEP* 01 (2007). [Erratum: JHEP 02, 028 (2015)], p. 091. DOI: 10.1088/1126-6708/2007/01/091. arXiv: hep-ph/0612182.

[45] Uros Seljak et al. "Can sterile neutrinos be the dark matter?" In: *Phys. Rev. Lett.* 97 (2006), p. 191303. DOI: 10.1103/PhysRevLett.97.191303. arXiv: astro-ph/0602430.

[46] Xiang-Dong Shi and George M. Fuller. "A New dark matter candidate: Non-thermal sterile neutrinos". In: *Phys. Rev. Lett.* 82 (1999), pp. 2832–2835. DOI: 10.1103/PhysRevLett.82.2832. arXiv: astro-ph/9810076.

[47] Stephen P. Martin. "A Supersymmetry primer". In: *Adv. Ser. Direct. High Energy Phys.* 18 (1998). Ed. by Gordon L. Kane, pp. 1–98. DOI: 10.1142/9789812839657_0001. arXiv: hep-ph/9709356.

[48] Gerard Jungman, Marc Kamionkowski, and Kim Griest. "Supersymmetric dark matter". In: *Phys. Rept.* 267 (1996), pp. 195–373. DOI: 10.1016/0370-1573(95)00058-5. arXiv: hep-ph/9506380.

[49] Jonathan L. Feng, Arvind Rajaraman, and Fumihiro Takayama. "Super-weakly interacting massive particles". In: *Phys. Rev. Lett.* 91 (2003), p. 011302. DOI: 10.1103/PhysRevLett.91.011302. arXiv: hep-ph/0302215.

[50] Andrea Marzo. "Infrared Production of Gravitinos". MA thesis. Università degli Studi di Padova, 2020. URL: http://hdl.handle.net/20.500.12608/22821.

[51] P. S. Bhupal Dev, Anupam Mazumdar, and Saleh Qutub. "Constraining Non-thermal and Thermal properties of Dark Matter". In: *Front. in Phys.* 2 (2014), p. 26. DOI: 10.3389/fphy.2014.00026. arXiv: 1311.5297 [hep-ph].

[52] Davide Racco. "Theoretical strategies for comparing dark matter searches". MA thesis. Università degli Studi di Padova, 2014. URL: http://hdl.handle.net/20.500.12608/18517.

[53] N. Wyn Evans, Ciaran A. J. O'Hare, and Christopher McCabe. *SHM^{++}: A Refinement of the Standard Halo Model for Dark Matter Searches in Light of the Gaia Sausage*. 2018. DOI: 10.48550/ARXIV.1810.11468. URL: https://arxiv.org/abs/1810.11468.

[54] Susana Cebrián. "Review on dark matter searches". In: *10th Symposium on Large TPCs for Low-Energy Rare Event Detection*. May 2022. arXiv: 2205.06833 [physics.ins-det].

[55] Laura Baudis. "DARWIN: dark matter WIMP search with noble liquids". In: *J. Phys. Conf. Ser.* 375 (2012). Ed. by Lothar Oberauer, Georg Raffelt, and Robert Wagner, p. 012028. DOI: 10.1088/1742-6596/375/1/012028. arXiv: 1201.2402 [astro-ph.IM].

[56] Laura Baudis. "WIMP Dark Matter Direct-Detection Searches in Noble Gases". In: *Phys. Dark Univ.* 4 (2014). Ed. by Frank Avignone and Wick Haxton, pp. 50–59. DOI: 10.1016/j.dark.2014.07.001. arXiv: 1408.4371 [astro-ph.IM].

[57] P. Cushman et al. "Working Group Report: WIMP Dark Matter Direct Detection". In: *Community Summer Study 2013: Snowmass on the Mississippi*. Oct. 2013. arXiv: 1310.8327 [hep-ex].

[58] R. Bernabei et al. "First results from DAMA/LIBRA and the combined results with DAMA/NaI". In: *Eur. Phys. J. C* 56 (2008), pp. 333–355. DOI: 10.1140/epjc/s10052-008-0662-y. arXiv: 0804.2741 [astro-ph].

[59] Torsten Bringmann and Christoph Weniger. "Gamma Ray Signals from Dark Matter: Concepts, Status and Prospects". In: *Phys. Dark Univ.* 1 (2012), pp. 194–217. DOI: 10.1016/j.dark.2012.10.005. arXiv: 1208.5481 [hep-ph].

[60] M. G. Aartsen et al. "Search for dark matter annihilations in the Sun with the 79-string IceCube detector". In: *Phys. Rev. Lett.* 110.13 (2013), p. 131302. DOI: 10.1103/PhysRevLett.110.131302. arXiv: 1212.4097 [astro-ph.HE].

[61] Oscar Adriani et al. "An anomalous positron abundance in cosmic rays with energies 1.5-100 GeV". In: *Nature* 458 (2009), pp. 607–609. DOI: 10.1038/nature07942. arXiv: 0810.4995 [astro-ph].

[62] Jonathan L. Feng, Shufang Su, and Fumihiro Takayama. "Lower limit on dark matter production at the large hadron collider". In: *Phys. Rev. Lett.* 96 (2006), p. 151802. DOI: 10.1103/PhysRevLett.96.151802. arXiv: hep-ph/0503117.

[63] Andreas Birkedal, Konstantin Matchev, and Maxim Perelstein. "Dark matter at colliders: A Model independent approach". In: *Phys. Rev. D* 70 (2004), p. 077701. DOI: 10.1103/PhysRevD.70.077701. arXiv: hep-ph/0403004.

[64] Morad Aaboud et al. "Search for dark matter and other new phenomena in events with an energetic jet and large missing transverse momentum using the ATLAS detector". In: *JHEP* 01 (2018), p. 126. DOI: 10.1007/JHEP01(2018)126. arXiv: 1711.03301 [hep-ex].

[65] Albert M Sirunyan et al. "Search for new physics in the monophoton final state in proton-proton collisions at $\sqrt{s} = 13$ TeV". In: *JHEP* 10 (2017), p. 073. DOI: 10.1007/JHEP10(2017)073. arXiv: 1706.03794 [hep-ex].

[66] "Selection of jets produced in 13TeV proton-proton collisions with the ATLAS detector". In: (July 2015).

[67] Maria Beltran et al. "Maverick dark matter at colliders". In: *JHEP* 09 (2010), p. 037. DOI: 10.1007/JHEP09(2010)037. arXiv: 1002.4137 [hep-ph].

[68] R.L. Workman et al. "Review of Particle Physics". In: (). to be published (2022).

[69] Abdelhak Djouadi et al. "Direct Detection of Higgs-Portal Dark Matter at the LHC". In: *Eur. Phys. J. C* 73.6 (2013), p. 2455. DOI: 10.1140/epjc/s10052-013-2455-1. arXiv: 1205.3169 [hep-ph].

[70] Thomas G. Rizzo. "Z' phenomenology and the LHC". In: *Theoretical Advanced Study Institute in Elementary Particle Physics: Exploring New Frontiers Using Colliders and Neutrinos*. Oct. 2006, pp. 537–575. arXiv: hep-ph/0610104.

[71] Paul Langacker. "The Physics of Heavy Z' Gauge Bosons". In: *Rev. Mod. Phys.* 81 (2009), pp. 1199–1228. DOI: 10.1103/RevModPhys.81.1199. arXiv: 0801.1345 [hep-ph].

[72] Giorgio Arcadi et al. "Dark sequential Z' portal: Collider and direct detection experiments". In: *Phys. Rev. D* 97.4 (2018), p. 043009. DOI: 10.1103/PhysRevD.97.043009. arXiv: 1708.00890 [hep-ph].

[73] Pavel Fileviez Pérez et al. "Anomaly-free dark matter models". In: *Phys. Rev. D* 100.1 (2019), p. 015017. DOI: 10.1103/PhysRevD.100.015017. arXiv: 1904.01017 [hep-ph].

[74] Martin Bauer et al. "Dark Matter in Anomaly-Free Gauge Extensions". In: *SciPost Phys.* 5.4 (2018), p. 036. DOI: 10.21468/SciPostPhys.5.4.036. arXiv: 1805.01904 [hep-ph].

[75] Bob Holdom. "Two U(1)'s and charge shifts". In: *Physics Letters B* 166.2 (1986), pp. 196–198. ISSN: 0370-2693. DOI: https://doi.org/10.1016/0370-2693(86)91377-8. URL: https://www.sciencedirect.com/science/article/pii/0370269386913778.

[76] Pavel Fileviez Pérez et al. "Leptophobic Dark Matter and the Baryon Number Violation Scale". In: *Phys. Rev. D* 99.3 (2019), p. 035009. DOI: 10.1103/PhysRevD.99.035009. arXiv: 1810.06646 [hep-ph].

[77] Jens Erler et al. "Improved Constraints on Z-prime Bosons from Electroweak Precision Data". In: *JHEP* 08 (2009), p. 017. DOI: 10.1088/1126-6708/2009/08/017. arXiv: 0906.2435 [hep-ph].

[78] Davi B. Costa, Bogdan A. Dobrescu, and Patrick J. Fox. "General Solution to the U(1) Anomaly Equations". In: *Phys. Rev. Lett.* 123.15 (2019), p. 151601. DOI: 10.1103/PhysRevLett.123.151601. arXiv: 1905.13729 [hep-th].

[79] Yanou Cui and Francesco D'Eramo. "Surprises from complete vector portal theories: New insights into the dark sector and its interplay with Higgs physics". In: *Phys. Rev. D* 96.9 (2017), p. 095006. DOI: 10.1103/PhysRevD.96.095006. arXiv: 1705.03897 [hep-ph].

[80] Satomi Okada. "Z' Portal Dark Matter in the Minimal $B-L$ Model". In: *Adv. High Energy Phys.* 2018 (2018), p. 5340935. DOI: 10.1155/2018/5340935. arXiv: 1803.06793 [hep-ph].

[81] T. Aoyama et al. "The anomalous magnetic moment of the muon in the Standard Model". In: *Phys. Rept.* 887 (2020), pp. 1–166. DOI: 10.1016/j.physrep.2020.07.006. arXiv: 2006.04822 [hep-ph].

[82] G. W. Bennett et al. "Final Report of the Muon E821 Anomalous Magnetic Moment Measurement at BNL". In: *Phys. Rev. D* 73 (2006), p. 072003. DOI: 10.1103/PhysRevD.73.072003. arXiv: hep-ex/0602035.

[83] F. C. Correia and Svjetlana Fajfer. "Light mediators in anomaly free U $(1)_X$ models. Part I. Theoretical framework". In: *JHEP* 10 (2019), p. 278. DOI: 10.1007/JHEP10(2019)278. arXiv: 1905.03867 [hep-ph].

[84] Michael Duerr et al. "How to save the WIMP: global analysis of a dark matter model with two s-channel mediators". In: *JHEP* 09 (2016), p. 042. DOI: 10.1007/JHEP09(2016)042. arXiv: 1606.07609 [hep-ph].

[85] *Measurements of the Higgs boson production and decay rates and constraints on its couplings from a combined ATLAS and CMS analysis of the LHC pp collision data at $\sqrt{s}$ = 7 and 8 TeV*. Tech. rep. Geneva: CERN, 2015. URL: http://cds.cern.ch/record/2052552.

[86] Georges Aad et al. "Search for high-mass dilepton resonances using 139 fb^{-1} of pp collision data collected at $\sqrt{s}$ =13 TeV with the ATLAS detector". In: *Phys. Lett. B* 796 (2019), pp. 68–87. DOI: 10.1016/j.physletb.2019.07.016. arXiv: 1903.06248 [hep-ex].

[87] Albert M Sirunyan et al. "Search for high-mass resonances in dilepton final states in proton-proton collisions at $\sqrt{s}$ = 13 TeV". In: *JHEP* 06 (2018), p. 120. DOI: 10.1007/JHEP06(2018)120. arXiv: 1803.06292 [hep-ex].

[88] Gil Paz and Joydeep Roy. "Remarks on the Z' Drell-Yan cross section". In: *Phys. Rev. D* 97.7 (2018), p. 075025. DOI: 10.1103/PhysRevD.97.075025. arXiv: 1711.02655 [hep-ph].

[89] A. Abada et al. "FCC Physics Opportunities: Future Circular Collider Conceptual Design Report Volume 1". In: *Eur. Phys. J. C* 79.6 (2019), p. 474. DOI: 10.1140/epjc/s10052-019-6904-3.

[90] D. Stratakis et al. "A Muon Collider Facility for Physics Discovery". In: (Mar. 2022). arXiv: 2203.08033 [physics.acc-ph].

[91] Matthew D Schwartz. *Quantum field theory and the standard model*. Cambridge University Press, 2014.

[92] Georges Aad et al. "Observation of a new particle in the search for the Standard Model Higgs boson with the ATLAS detector at the LHC". In: *Phys. Lett. B* 716 (2012), pp. 1–29. DOI: 10.1016/j.physletb.2012.08.020. arXiv: 1207.7214 [hep-ex].

[93] Paolo Gondolo and Graciela Gelmini. "Cosmic abundances of stable particles: Improved analysis". In: *Nucl. Phys. B* 360 (1991), pp. 145–179. DOI: 10.1016/0550-3213(91)90438-4.